TURUN
YLIOPISTO
UNIVERSITY
OF TURKU

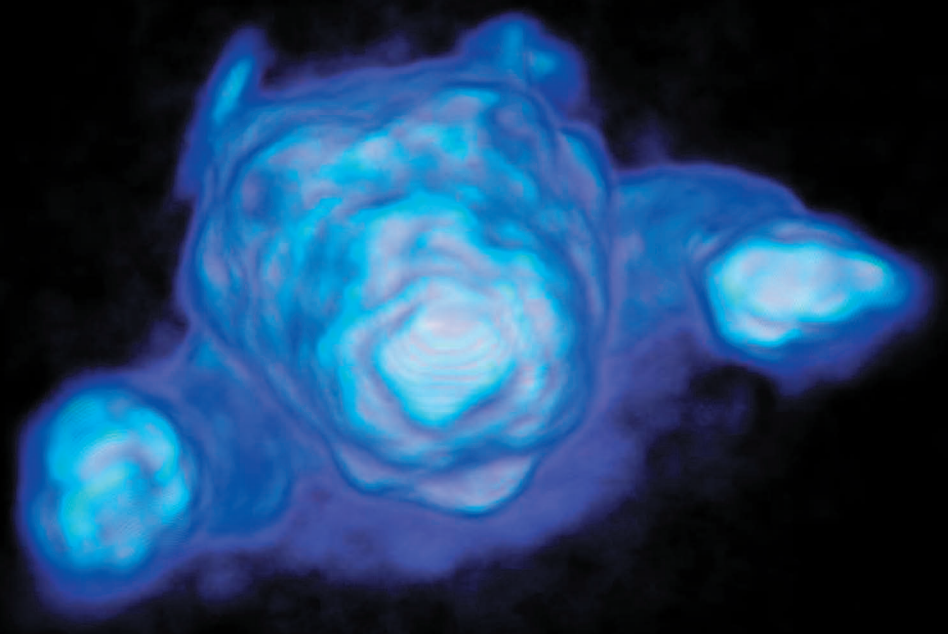

EXPERIMENTAL MODELS OF FOCAL NEUROINFLAMMATION

Efficacy Assessment of Pharmaceuticals of Multiple Sclerosis Using PET Imaging

Susanne Vainio

TURUN YLIOPISTON JULKAISUJA – ANNALES UNIVERSITATIS TURKUENSIS
SARJA – SER. D OSA – TOM. 1618 | MEDICA – ODONTOLOGICA | TURKU 2022

TURUN
YLIOPISTO
UNIVERSITY
OF TURKU

EXPERIMENTAL MODELS OF FOCAL NEUROINFLAMMATION

Efficacy Assessment of Pharmaceuticals of Multiple Sclerosis Using PET Imaging

Susanne Vainio

TURUN YLIOPISTON JULKAISUJA – ANNALES UNIVERSITATIS TURKUENSIS
SARJA – SER. D OSA – TOM. 1618 | MEDICA – ODONTOLOGICA | TURKU 2022

University of Turku

University of Turku
Faculty of Medicine
Clinical Neurosciences
Drug Research Doctoral Programme
Turku PET Centre
MediCity Research Laboratory

Supervised by

Adjunct Professor Merja Haaparanta-Solin, PhD
Turku PET Centre and
University of Turku
Turku, Finland

Professor Juha O. Rinne, MD, PhD
Turku PET Centre
Turku University Hospital and
University of Turku
Turku, Finland

Professor Laura Airas, MD, PhD
Turku University Hospital and
Department of Clinical Medicine
University of Turku
Turku, Finland

Reviewed by

Dr. Sylvie Chalon, PhD
Inserm U930
Imaging and Brain University of Tours
Tours, France

Assistant Professor Sandeep S. V. Golla, PhD
Amsterdam University Medical Center
Neuroscience – Brain Imaging
Amsterdam, The Netherlands

Opponent

Dr. Sabina Pappatà, MD, PhD
Institute of Biostructure and Bioimaging (IBB)
Consiglio Nazionale delle Ricerche (CNR)
Naples, Italy

The originality of this thesis has been checked in accordance with the University of Turku quality assurance system using the Turnitin OriginalityCheck service.

Cover Image: “Supermarsu” Susanne Vainio

ISBN 978-951-29-8799-3 (PRINT)
ISBN 978-951-29-8800-6 (PDF)
ISSN 0355-9483 (Print)
ISSN 2343-3213 (Online)
Painosalama, Turku, Finland 2022

To my family

UNIVERSITY OF TURKU
Faculty of Medicine
Department of Clinical Neurosciences
Turku PET Centre
SUSANNE VAINIO: Experimental models of focal neuroinflammation - Efficacy assessment of pharmaceuticals of multiple sclerosis using PET imaging
Doctoral Dissertation, 141 pp.
Drug Research Doctoral Programme
April 2022

ABSTRACT

Neuroinflammation (NI) is a key player in neurodegenerative diseases, such as multiple sclerosis (MS). Magnetic resonance imaging is the gold standard imaging method for diagnosis of MS, however, better diagnostic tools are needed for the follow-up of disease progression, earlier diagnosis, and assessment of patients' response to therapy. Positron emission tomography (PET) is a sensitive and selective functional imaging method for investigating mechanisms of diseases at a molecular level. NI can be visualised in PET by targeting the 18 kDa translocator protein (TSPO), which is upregulated during NI on the mitochondria of glial cells.

This study aimed to evaluate the properties of [^{18}F]GE-180, a 2nd generation TSPO PET radiotracer, in a unilateral model of acute NI and evaluate the efficacy of immunomodulatory drugs, anti-VLA-4 and dimethyl fumarate (DMF), in two different focal rat models of experimental autoimmune encephalomyelitis (EAE), the *f*DTH-EAE and *f*MOG-EAE models. The applied methods were *in vivo* PET imaging, digital autoradiography, and immunohistochemical (IHC) staining.

Study I indicated improved binding potential of [^{18}F]GE-180 over the 1st generation tracer [^{11}C]PK11195 and showed that the unilateral model of acute NI is suitable for the evaluation of novel PET tracers of NI. Study II indicated that anti-VLA-4 had no short-term treatment effects in the *f*DHT-EAE-rat model. However, discontinuation of the treatment caused a rebound that could be detected with [^{18}F]GE-180. Study III showed, that short-term, but not long-term, DMF treatment decreases uptake of [^{18}F]GE-180 in the *f*DTH-EAE rat model, and no rebound effect was detected after halting the treatment for 10 weeks. Nevertheless, the efficacy of DMF was detected using IHC for CD4$^+$ and CD8$^+$ cells. No DMF treatment effect was observed in the *f*MOG-EAE model.

In conclusion, focal animal models of NI are applicable for evaluating novel PET tracers. Furthermore, efficacy assessment of immunomodulatory drugs can be evaluated using TSPO PET when the tracer is binding to the same biomarker that the drug is affecting.

KEYWORDS: PET, TSPO, [^{11}C]PK11195, [^{18}F]GE-180, animal model, neuroinflammation, multiple sclerosis, LPS, EAE

TURUN YLIOPISTO
Lääketieteellinen tiedekunta
Kliiniset neurotieteet
Valtakunnallinen PET-keskus
SUSANNE VAINIO: Pesäkkeisen aivotulehduksen kokeelliset mallit – multippeliskleroosin lääkkeiden vaikuttavuuden arviointi käyttäen PET-kuvantamista
Väitöskirja, 141 s.
Lääketutkimuksen tohtoriohjelma
Huhtikuu 2022

TIIVISTELMÄ

Keskushermoston tulehdus on tila, joka ilmenee useissa hermorappeuma-sairauksissa, kuten pesäkekovettumataudissa (MS-tauti). MS-taudin kuvantamis-diagnostiikan ensisijainen menetelmä on magneettikuvaus, mutta uusia diagnostisia menetelmiä tarvitaan taudin mahdollisimman varhaiseksi toteamiseksi, etenemisen seuraamiseksi, ja uusien lääkehoitojen tehon arvioimiseksi. Positroniemissio-tomografia (PET) on kajoamaton kuvantamismenetelmä, jonka avulla on mahdollista seurata aivojen tulehdusreaktiota hyödyntämällä tulehduksen aikana yli-ilmentyvään translokaatioproteiiniin (TSPO) sitoutuvia PET-merkkiaineita.

Tämän tutkimuksen tavoitteena oli verrata TSPO-molekyyliin sitoutuvan toisen sukupolven PET-merkkiaineen ([^{18}F]GE-180) sekä jo käytössä olevan merkkiaineen ([^{11}C]PK11195) ominaisuuksia akuutin tulehduksen rottamallissa. Lisäksi tavoitteena oli arvioida immuunivastetta muokkaavien lääkkeiden, anti-VLA-4:n ja dimetyylifumaraatin, tehokkuutta lyhyt- ja pitkäaikaishoidossa *f*DTH-EAE- ja *f*MOG-EAE-malleissa, joissa rotille aiheutetaan pesäkkeinen autoimmuuni-enkefalomyeliitti. Tulehdusreaktiossa tapahtuvia muutoksia seurattiin hyödyntäen *in vivo* [^{18}F]GE-180-PET-kuvantamista, autoradiografiaa, sekä kudosvärjäyksiä.

Ensimmäisessä osatyössä [^{18}F]GE-180-merkkiaineen havaittiin soveltuvan [^{11}C]PK11195-merkkiainetta paremmin aivotulehduksen kuvantamiseen eläin-malleissa: aivojen tulehdusalue oli merkittävästi suurempi ja merkkiaineen sitoutumiskyky ja spesifisyys parempi. Toisessa osatyössä anti-VLA-4-lääkehoidon vaikutusta ei ollut mahdollista seurata [^{18}F]GE-180-PET-kuvantamisella *f*DTH-EAE-mallin kroonisen tulehduksen vaiheessa. Hoidon lopettamisen jälkeen ilmenevä voimakas tulehduksen uudelleenaktivoituminen oli kuitenkin mahdollista havaita PET-kuvauksella. Kolmannessa osatyössä dimetyylifumaraatin havaittiin hillitsevän tulehdusta *f*DTH-EAE-mallissa lyhytaikaishoidossa yhden viikon hoidon jälkeen, mutta ei enää myöhemmissä aikapisteissä, eikä *f*MOG-EAE-mallissa.

Tämä väitöskirjatutkimus osoitti, että pesäkkeisen tulehduksen rottamalleja voidaan hyödyntää uusien tulehdusta kuvantavien PET-merkkiaineiden, sekä immuunivastetta muokkaavien lääkkeiden tehokkuuden arvioinnissa.

AVAINSANAT: PET, TSPO, [^{11}C]PK11195, [^{18}F]GE-180, eläinmalli, aivo-tulehdus, multippeliskleroosi, lipopolysakkaridi, pesäkkeinen EAE

Table of Contents

Abbreviations

[^{11}C]-(R)-PK11195	[^{11}C]-N-butan-2-yl-1-(2-chlorophenyl)-N-methylisoquinoline-3-carboxamide
[^{11}C]TMSX	[7-methyl-[^{11}C]]-(E)-8-(3,4,5-trimethoxystyryl)-1,3,7-trimethylxanthine
[^{11}C]PiB	[^{11}C]Pittsburgh compound B
[^{18}F]GE-180	(S)-*N,N*-diethyl-9-(2-[^{18}F]fluoroethyl)-5-methoxy-2,3,4,9-tetrahydro-1*H*-carbazole-4-carboxamide
[^{18}F]FDG	2-deoxy-2-[^{18}F]fluoro-D-glucose
%IA/g	Percentage of injected activity per gram of tissue
Ab	Antibody
AD	Alzheimer's disease
AMS	Aggressive MS
ANOVA	Analysis of variance
ARG	Digital autoradiography
ARRIVE	Animal Research: Reporting of In Vivo Experiments
BBB	Blood-brain barrier
BCG	Bacillus Calmette-Guérin
BP_{ND}	Non-displaceable binding potential
CD	Cluster of differentiation
CIS	Clinically isolated syndrome
CNS	Central nervous system
CONFIRM	Efficacy and Safety Study of Oral BG-12 With Active Reference in Relapsing-Remitting Multiple Sclerosis
CT	Computed tomography
DAB	3,3' diaminobenzidine
DEFINE	Determination of the Efficacy and Safety of Oral Fumarate in Relapsing-Remitting MS
DMF	Dimethyl fumarate
DTH	Delayed-type hypersensitivity
DTI	Diffusion tension imaging
EAE	Experimental autoimmune encephalomyelitis
EDSS	Expanded Disability Status Scale

EU	European Union
*f*DTH-EAE	Focal delayed-type hypersensitivity experimental autoimmune encephalomyelitis
*f*MOG-EAE	Myelin oligodendrocyte glycoprotein experimental autoimmune encephalomyelitis
fMRI	Functional magnetic resonance imaging
FBP	Filtered-back projection
FOV	Field of view
GM	Grey matter
GE180	Non-radioactive GE180
GFAP	Glial fibrillary acidic protein
Gd	Gadolinium
HAE	Human autoimmune encephalomyelitis
HAMS	Highly active MS
Iba1	Ionised calcium-binding adapter molecule 1
IL	Interleukin
$LogD_{7.4}$	Distribution coefficient of a tracer at pH 7.4
LOR	Line of response
LPS	Lipopolysaccharide
mAb	Monoclonal antibody
MAP	Maximum *a posteriori*
MBP	Myelin basic protein
MHC	Major histocompatibility complex
MOA	Mechanism of action
MOG	Myelin oligodendrocyte glycoprotein
MR	Magnetic resonance
MRI	Magnetic resonance imaging
MS	Multiple sclerosis
NI	Neuroinflammation
NAGM	Normal appearing grey matter
NAMs	Non-animal models
NAWM	Normal appearing white matter
NEDA	No evident disease activity
Nrf2	Nuclear factor erythroid 2–related factor 2
OSEM3D	Ordered-subsets expectation maximisation algorithm in three dimensions
OX-42	CD11b clone Ab recognising integrin alpha-M
PB	Phosphate buffer
PBS	Phosphate buffered saline
PD	Parkinson’s disease

PET	Positron emission tomography
PK11195	Non-radioactive PK11195
PLP	Proteolipid protein
PML	Progressive multifocal leukoencephalopathy
PMT	Photomultiplier tube
PPMS	Primary progressive multiple sclerosis
PSL/mm^2	Photostimulated luminescence per square millimetre
PVE	Partial volume effect
RMS	Relapsing forms of MS
ROI	Region of interest
RRMS	Relapsing-remitting multiple sclerosis
S-D	Sprague-Dawley rat
SD	Standard deviation
SPMS	Secondary progressive multiple sclerosis
SUV	Standardised uptake value
T_1	Spin-lattice relaxation time
T_2	Spin-spin relaxation time
TB	Mycobacterium tuberculosis bacteria
TBI	Traumatic brain injury
TCR	T cell receptor
Th cell	T helper cell
TNF-α	Tumour necrosis factor alpha
TSPO	18-kDa translocator protein
VCAM-1	Vascular cell adhesion molecule
VOI	Volume of interest
WM	White matter

List of Original Publications

This dissertation is based on the following original publications, which are referred to in the text by their Roman numerals:

I Dickens AM, **Vainio SK**, Marjamäki P, Johansson J, Lehtiniemi P, Rokka J, Rinne JO, Solin O, Haaparanta-Solin M, Jones P, Trigg W, Anthony DC, Airas L. Detection of microglial activation in an acute model of neuroinflammation using positron emission tomography and radioligands [^{11}C]-(R)-PK11195 and [^{18}F]GE-180. *Journal of Nuclear Medicine*, 2014; 55:3.

II **Vainio SK**, Dickens AM, Tuisku J, Eskola O, Solin O, Löyttyniemi E, Anthony DC, Rinne J, Airas L, Haaparanta-Solin M. "Cessation of anti-VLA-4 therapy in a focal rat model of multiple sclerosis causes an increase in neuroinflammation". *European Journal of Nuclear Medicine and Molecular Imaging Research*, 2019; 9:38.

III **Vainio SK**, Dickens AM, Matilainen M, López-Picón F, Aarnio R, Eskola O, Solin O, Anthony DC, Rinne JO, Airas L, Haaparanta-Solin M. Dimethyl fumarate decreases short-term but not long-term inflammation in focal EAE model of neuroinflammation. *European Journal of Nuclear Medicine and Molecular Imaging Research*, 2022; 12:6.

In addition, some unpublished data are presented.

1 Introduction

Neuroinflammation (NI) is an event in which the immune system activates against the nervous system of the body. There are diseases where NI is thought to be the primary cause, such as multiple sclerosis (MS) or encephalitis, or diseases where NI occurs as a secondary response, such as Alzheimer's disease (AD), stroke or traumatic brain injury (TBI) (Naegele and Martin, 2014; Ritzel et al., 2019). The process involves both the resident glial cells within the brain parenchyma and immune cells from the periphery. The proceeding is highly variable according to the inflammatory signal, whether it being infection, mechanical damage, toxic metabolites, or autoimmunity (Yang and Zhou, 2018).

MS is a chronic disease with inflammatory, demyelinating, and neurodegenerative components, where both autoimmunity and infection are thought to play a role (Dobson and Giovannoni, 2019; Lassmann, 2018). Given that the exact pathomechanism remains unresolved, complex genetic and environmental interplay has been recognised as an almost certain purpose for pathology (Dobson and Giovannoni, 2019). The somewhat unknown aetiology of the disease provides challenges for both treatment and diagnostics. In the past two decades, remarkable progress has been made in the field of immunomodulatory treatment, which can reduce symptom relapses and partially also the progression of the disease (Hauser and Cree, 2020).

MS is a disease with an increasing female/male ratio with the onset ~30 years for females and ~40 years for males, with a latitude gradient and high prevalence in the Nordic countries (Pirttisalo et al., 2019; Westerlind et al., 2014). Because MS is common in young adults, and the disease causes only a modest reduction in life expectancy (Lunde et al., 2017), there is a lack of biopsies for research purposes from the early stage of the disease. Furthermore, because the disease path often conveys after 15-20 years of onset, animal models are needed to depict the different aspects of the disease especially in the early stage (Lassmann and Bradl, 2017). Considering that non-animal models (NAMs) for MS are scarce, there is a great number of animal models representing numerous aspects of the disease by applying various species and different methods to produce the condition (Burrows et al., 2018; Kipp et al., 2017; Procaccini et al., 2015). There are animal models, which are

induced by active immunisation using an antigen or a peptide, toxic models that induce demyelination, passive models caused by adoptive transfer, virus-induced models, and spontaneous, transgenic models (Bjelobaba et al., 2018). The mentioned models cause disseminated symptoms, which can be detected throughout the brain and spinal cord, i.e. the central nervous system (CNS). There are also models of focal inflammation, which are present at a predetermined area in the CNS (Matyszak and Perry, 1995).

There have been advances in diagnosing MS recently. While the neurological symptoms, lesions in magnetic resonance imaging (MRI), and cerebrospinal fluid (CSF) samples remain the gold standard for diagnosing MS (Brownlee et al., 2017), one possible approach to discover NI is positron emission tomography (PET) (de Paula Faria et al., 2014; van der Weijden et al., 2021). Rissanen et al. (2014) have shown that diffuse NI can be visualised by targeting the 18-kDa translocator protein (TSPO). The first generation TSPO PET tracer, [^{11}C]PK11195, has been successfully applied in clinical research (Rissanen et al., 2014), but it suffers from several drawbacks, such as poor signal-to-noise ratio. Thus, second generation TSPO tracers have been evolved to improve radiotracer qualities (Alam et al., 2017; Best et al., 2019). In MS studies, evaluation of abnormal TSPO expression has provided insight into the effect of immunomodulatory drugs (Ratchford et al., 2012).

The aim of this study was to identify, whether acute and chronic focal animal models can be applied for the evaluation of TSPO PET tracers and whether NI can be detected by the specific radiotracers (Figure 1; Studies I, II, III). In addition, the more chronic focal models (studies II and III) were applied in efficacy assessment of disease-modifying pharmaceuticals of MS, anti-VLA-4 and dimethyl fumarate (DMF), using TSPO PET imaging and immunohistochemistry (IHC).

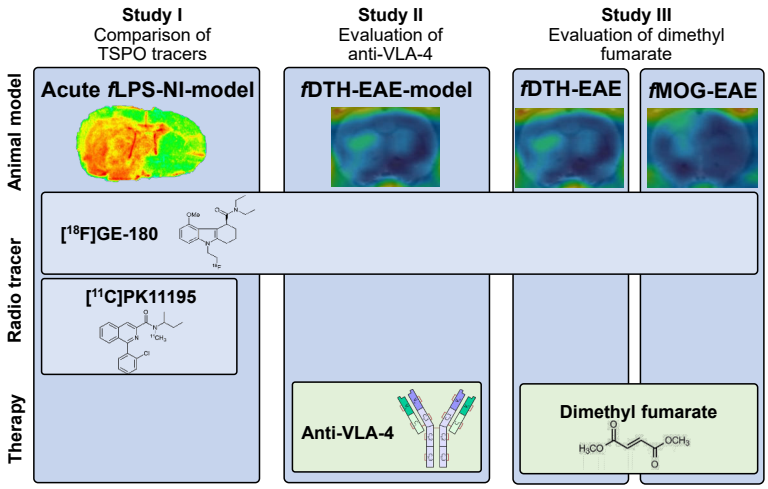

Figure 1. Outline of the thesis.

2 Review of the Literature

2.1 Neuroinflammation and multiple sclerosis

NI is an event that occurs in many neuropathological conditions of the CNS. NI is a key player in both CNS injury as well as neurodegenerative diseases, such as MS, AD, Parkinson's disease (PD), and amyotrophic lateral sclerosis (ALS) (Yang and Zhou, 2018). Previously it has been thought that the CNS is an immune-privileged organ based on the finding that allografts survived in the brain for longer periods than in the periphery. Other reasonings were, that neurons have a limited regeneration capacity, there is a low number of antigen-presenting cells (APCs) in the CNS, and the CNS was thought to lack a lymphatic system. Recent findings have shown that these statements were not completely accurate (Engelhardt et al., 2017; Negi and Das, 2018). When speaking about the CNS immune response, the special features, which are not detected in the peripheral nervous system, need to be considered. Firstly, anatomically the CNS is a closed structure protected by the blood-brain barrier (BBB) as well as the CSF barrier of the choroid plexus and the meninges. Secondly, there is indeed a special lymphatic system surrounding the dura mater, called the glymphatic system (Aspelund et al., 2015; Louveau et al., 2015; Stephenson et al., 2018). Thirdly, the antigen presenting cells are different to the periphery (Negi and Das, 2018).

The BBB consists of the tight junctions between the cerebrovascular endothelial cells and the glia limitans consisting of astrocytic feet and the parenchymal basement membrane. In the CNS, the neurovascular unit is an operating unit connecting the periphery with the parenchyma (Figure 2) (Kugler et al., 2021). The neurons are protected and nourished by the myelin sheath, which is produced by the oligodendrocytes (Ransohoff, 2018). Myelin consists primarily of myelin basic protein (MBP), the multilamellar structural myelin proteolipid protein (PLP), and myelin oligodendrocyte glycoprotein (MOG) on the superficial membrane (Ambrosius et al., 2020; Goverman et al., 1993). Astrocytes are maintaining homeostasis and refining synaptic connections by extending their processes to millions of synapses, and they have an active role in creating the BBB (Matejuk and Ransohoff, 2020). Microglia are contributing to homeostasis by removing synaptic elements by phagocytosis. Within the CNS, active immune surveillance is operated

by the glial cells, including microglia, astrocytes, oligodendrocytes, and oligodendrocyte progenitor cells (OPCs) (Negi and Das, 2018; Yang and Zhou, 2018). Because these are the first line of defence against pathogens in the CNS, they can be considered the innate immune system of the brain and spinal cord. After an inflammatory event, inflammatory mediators, such as $CD4^+$ and $CD8^+$ T lymphocytes, macrophages, and antibody (Ab) releasing B-lymphocytes enter the parenchyma. In addition, the endothelial cells play a key role in the inflammatory process (Lyman et al., 2014).

Other suggested entities modulating the neuroinflammatory processes are the human microbiome (Bell et al., 2018; Hänninen, 2017) and the toll-like receptor (TLR) activation by lipopolysaccharide (LPS), which is the main component of the outer membrane of gram-negative bacteria (Landén et al., 2016).

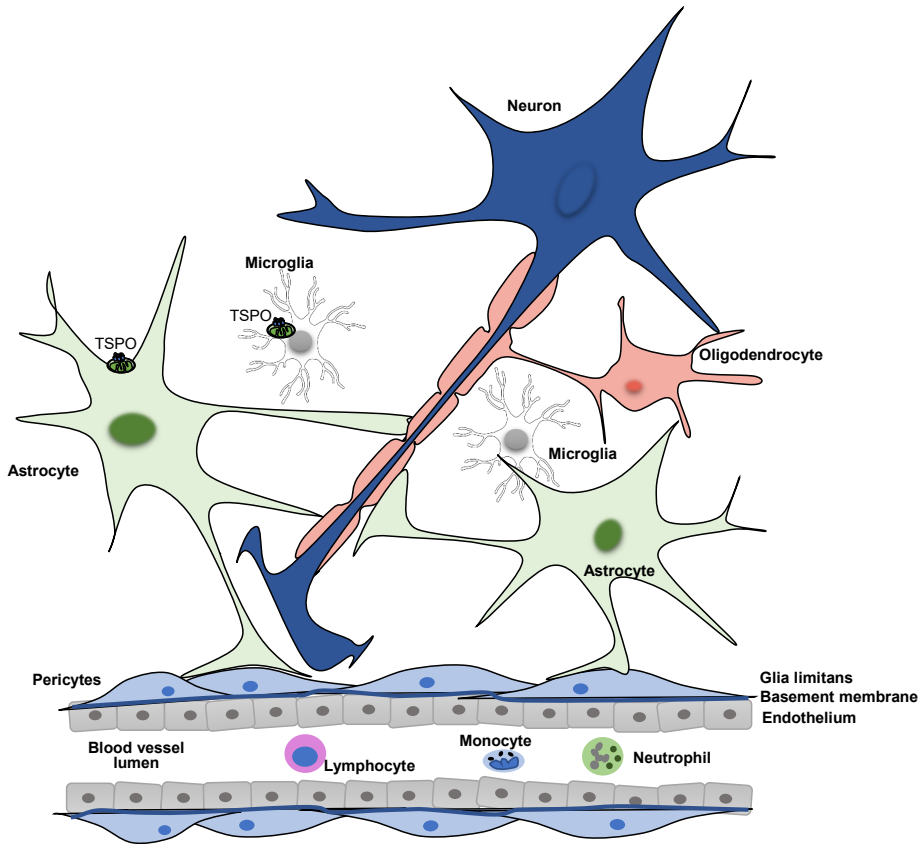

Figure 2. The neurovascular unit. The neurovascular unit in the CNS is an operating unit connecting the periphery, i.e. the blood circulation, with the parenchyma of the brain, in which the neurons are protected and nourished by the myelin sheath produced by the oligodendrocytes, astrocytes are maintaining homeostasis and refining synaptic connections, and microglia contribute to homeostasis by removing synaptic elements by phagocytosis.

2.1.1 The role of microglia in neuroinflammation

To detect neuroinflammation, a valid marker that reflects the inflammatory process must be identified (Calder et al., 2013). Currently, there is no consensus over which biomarkers would differentiate the events related to acute or chronic low-grade inflammation best. Microglia have been suggested as one of such biomarkers. Microglia are intrinsic cells of the brain and of myeloid origin differing significantly from peripheral macrophages. The expression transcripts that microglia are expressing are CD11b, CD40, CD45, CD80, CD86, CD68, F4/80, chemokine receptor CX_3CR_1, purinoceptors P_2Y_{12} and P_2Y_{13}, suppressor of cytokine signalling protein $SOCS_3$, triggering receptor $TREM_2$, transmembrane protein $TMEM_{119}$, G-protein-coupled receptor GPR_{34}, sialic-acid-binding immunoglobulin-like lectins SIGLEC, and spalt-like transcription factor $SALL_1$, which of $TMEM_{119}$, P_2Y_{12}, and $SALL_1$ are somewhat microglia specific (Matejuk and Ransohoff, 2020; Silvin and Ginhoux, 2018). It has recently been shown that adult microglia display remarkably similar transcriptomes despite their location (Matejuk and Ransohoff, 2020), while spatial and temporal heterogeneity has been suggested to occur both inter- and intraregionally (Silvin and Ginhoux, 2018). The post-natal microglia express developmental complexity demonstrated with genes associated with proliferation, metabolism, and motility (Matejuk and Ransohoff, 2020).

Microglia are local key players in NI, whereas in the normal state they promote homeostasis of the brain. In the normal state, the microglial phenotype appears as a small elliptical soma surrounded by branched processes, while in a disease state the cell bodies enlarge and processes retract showing a phagocytic appearance. Homeostasis is maintained during development by refining synaptic networks and pruning synapses, promoting developmental apoptosis, removing cell corpses, and promoting neuronal survival and their positioning. In the adult brain, microglia optimise network properties, produce antimicrobial peptides and increase synaptic plasticity, thus contributing to learning (Ransohoff, 2016). These findings have been established by preclinical observations using modern imaging and sequencing techniques (Hickman et al., 2013; Nimmerjahn et al., 2005; Zhang et al., 2014). Microglia are in contact with neurons by connecting their processes to neuronal somas, which in disease states can be disturbed, leading to a lack of stimuli from the injured neurons and exposure of the neurons to plasma proteins (Matejuk and Ransohoff, 2020; Ransohoff, 2016). Despite many efforts, no durable subset-categorisation for the microglia has been identified in the healthy brain (Burns et al., 2020), but the paradigm of microglial subsets is becoming more evident as opposed to microglia being described as a multitasking cell type that transforms its phenotype (Bisht et al., 2016; Tremblay, 2021).

In disease states, the microglia can become ‘activated’, in regards to the pathological state, and the morphology of the cell changes to a more amoeboid-like

structure (Guerrero and Sicotte, 2020; Yang and Zhou, 2018). In addition, during a neuroinflammatory state, the astrocytes become activated, which is referred to as astrogliosis.

2.1.2 Multiple sclerosis

Pathologist Jean-Martin Charcot was the first one to correlate clinical symptoms of MS to the pathological changes in tissues collected *post mortem* describing them as "la sclérose en plaques" that occur in the brain and spinal cord (Charcot, 1875; Kumar et al., 2011; Lubetzki, 2018). Currently, MS is described as an autoimmune disease with a strong neuroinflammatory component along with primary or secondary neurodegeneration. It causes demyelinating lesions primarily in the white matter (WM), but also diffuse neurodegeneration in the grey matter (GM) and normal-appearing white matter (NAWM). MS occurs typically at the age of 20–40 years and reduces life expectancy by some 7 years (Lunde et al., 2017).

The disease is classified into four categories: relapsing-remitting MS (RRMS), secondary progressive MS (SPMS), primary progressive MS (PPMS), and highly active MS (HAMS), sometimes referred to as aggressive MS (AMS), which is essentially a subcategory of RRMS with the rapid accumulation of deficits (Díaz et al., 2019). The majority of patients, some 80% of the cases (Compston and Coles, 2008), start with the relapsing forms of MS (RMS) (Figure 3), which later turns into slowly progressing SPMS some 10 to 15 years after disease onset (Lassmann, 2019). In a smaller subset of patients, the disease occurs as PPMS, the type which is dominating the patients with late-onset. The symptoms include spasticity and pain of limbs, fatigue, cognitive impairment, as well as sexual, bladder, and bowel dysfunction (Thompson et al., 2018b). These result in irreversible neurological decline with accumulating disability. While the exact pathomechanisms of the disease is unknown, multifactorial aetiology has been suggested.

Evidence suggests that the aetiology of MS is an interplay between many genetic and environmental factors. The biggest independent genetic risk factors have been identified to be the major histocompatibility complex (MHC) region and the human leukocyte antigen (HLA) DR15 serotypes (Harbo et al., 2013; Jelcic et al., 2018). The clinical concordance rate is some 25% for monozygotic twins compared to that of 5% for dizygotic twins (Compston and Coles, 2008). Considering that there is a clear latitude dependence in MS prevalence, risk factors increasing incidence are lack of vitamin D uptake (Munger et al., 2004), adolescent BMI of >27 (Manni et al., 2019), and Epstein-Barr virus (EBV) infection (Alfredsson and Olsson, 2019; Bjornevik et al., 2022). There is also circumstantial evidence of environmental factors contributing to the risk of MS, such as organic solvents and shift work (Mar et al., 2018), while reduced risk has been associated with nicotine, alcohol, and

coffee consumption (Alfredsson and Olsson, 2019). Interestingly, while the EBV infection has been identified universally in almost all MS patients, the cytomegalovirus infection has been suggested to have a protective role to MS (Alari-Pahissa et al., 2018). There is also an increasing female-to-male sex incidence ratio, currently being 2.5:1, or depending on the geographical location even up to 3.6:1, suggesting the role of sex hormones or the X-chromosome on MS incidence (Harbo et al., 2013; Magyari and Sorensen, 2019). Recently, the microbiome of the olfactory tract, oral cavity, and gut has been suggested to have a role in disease incidence (Bell et al., 2018) and cow milk casein has been shown to exacerbate symptoms in individuals with loss of tolerance to bovine casein (Chunder et al., 2022).

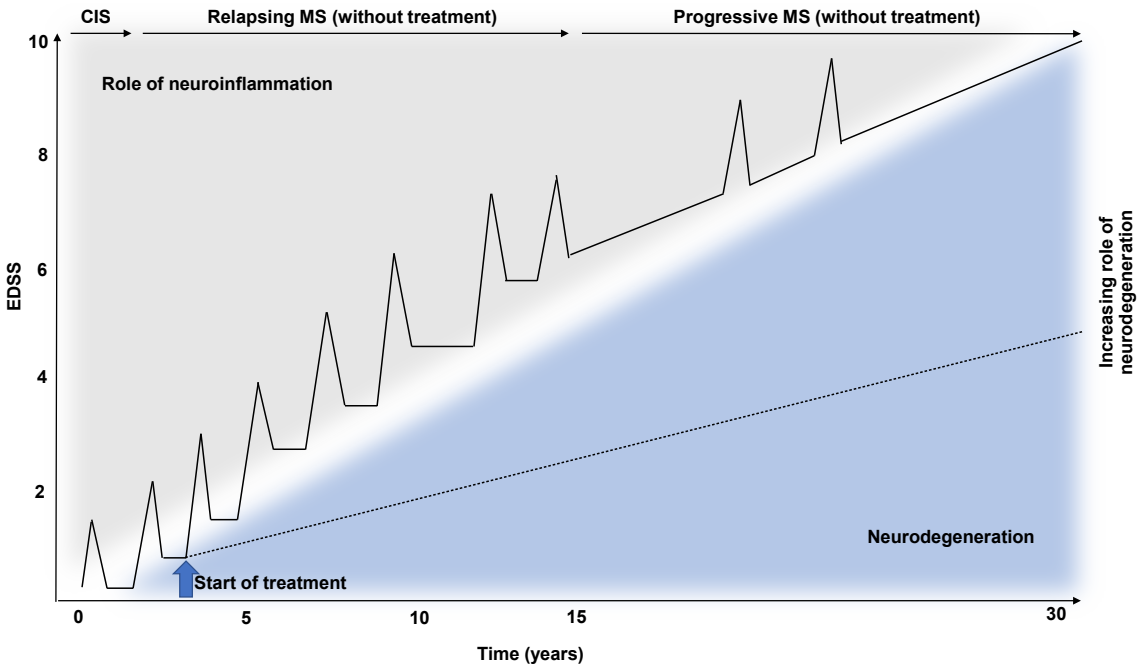

Figure 3. **The course of MS**. The black line illustrates the natural course of relapsing MS, which is the most common form of the disease. Here, the relapses are characterised by a neuroinflammatory component (grey background) and progression is related to neurodegeneration (blue background). The disease starts with the clinically isolated syndrome (CIS), and after the diagnosis of MS, relapses occur until the patient reaches the progressive phase with a gradual decline of physical abilities. EDSS score is indicated on the left. With the current effective disease-modifying therapies, the course of the disease can be dramatically different. After the start of treatment (blue thick arrow), relapses can be abolished totally, but silent progression (dashed line), which is independent of relapses, still occurs. After Hauser and Cree 2020 and Raffel et al. 2016.

2.1.2.1 Pathogenesis of multiple sclerosis

There is debate over whether MS is primarily a neuroinflammatory or neurodegenerative disease (Giovannoni et al., 2022; Trapp and Nave, 2008). Indisputably, there is a clear neuroinflammatory component from the adaptive immune system, indicating T and B cells as key players of the pathology. Since the disease is limited to the CNS and leaves the peripheral nervous system intact (Hauser and Cree, 2020), it appears that the T and B cells would be selectively recruited by autoantigens. Theories suggest either initiation of CNS antigen release into the periphery or, as the extrinsic model suggests, systemic infectious stimulus leading to an immune attack towards the CNS, both leading to release of antigens into the periphery exacerbating the attack towards the CNS (Thompson et al., 2018b). Also, innate immunity seems to play a role, while there is evidence of both the proinflammatory role of peripheral macrophages and the CNS resident microglial activation by secretion of cytokines, chemokines, free radicals, and glutamate (Thompson et al., 2018b). In the progressive phase of MS, the role of the compartmentalised immune response decreases (Figure 3) and the pathological events become more diffuse, manifesting as degeneration of demyelinated axons, astrogliosis, and microglial activation (Thompson et al., 2018b). Recent evidence shows that chronic active inflammation contributes to disability accumulation with patients who have slowly expanding, smoldering MS plaques (Absinta et al., 2019).

One of the hallmarks of MS is the concurrent demyelinated WM and GM lesions with preserved axons (Charcot, 1875) and destroyed oligodendrocytes (Babinski, 1885). Within the lesions, which are often located in the WM around the ventricles or the GM of the cortex, cerebellum, or the spinal cord, T and B lymphocytes as well as plasma cells can be observed around post-capillary venules (Jehna et al., 2015; Lassmann, 2018). Remyelination can occur at the site when OPC's are recruited. The stage of NI and axonal destruction can vary between patients but also within an individual between lesions, and NI changes accompanied by axonal damage can be detected in remyelinating or inactive lesions, or even in the NAWM (Kornek et al., 2000; Lassmann, 2018).

The pathogenesis of MS lesions can be divided into four patterns. The pattern I is characterised by T cells and macrophage driven damage. In Pattern II, the immune reaction against myelin is driven by B cells excreting antibodies and the complement. Patterns III and IV include oligodendrocyte atrophy. In pattern III, the damage resembles hypoxia-induced vascular or mitochondrial dysfunction, and pattern IV results in genetic susceptibility of oligodendrocytes to immune attacks. It appears that pattern II can be detected in almost all acute lesions, while the other patterns are less common (Compston and Coles, 2008; Lucchinetti et al., 2005).

MS lesions can be divided into active, inactive, and remyelinated lesions (shadow plaques). The first two are characterised by phagocytic activity in the rim,

possibly due to microglial activation, and reduced activity of phagocytic cells, mostly macrophages, in the core of the demyelinated lesion (Lassmann, 2019). In addition to the focal lesions, there is more diffuse neurodegeneration ongoing in the NAWM and the normal-appearing grey matter (NAGM). These account for the steady increase of brain and spinal cord atrophy, with the rate of 0.5–1.5% being more pronounced in the progressive phase (Lassmann, 2019; Thompson et al., 2018b). Thus, neurodegeneration and progression of the disease are not directly connected with the focal, neuroinflammatory component of MS (Giovannoni et al., 2022; Kipp et al., 2017).

Jelcic and colleagues (2018) discovered, that in patients with the HLA DR15 haplotype, self-reactive peripheral, myelin-specific $CD4^+$ T cells are elevated, and their proliferation is driven by memory B cells and production of IFN-γ, which in turn activates macrophages (Jelcic et al., 2018). They also recognised the protein RASGRP2 on the surface of B cells and in the parenchyma, which generates the autoproliferative response from the T cells. The inflammatory infiltrates in an emerging MS lesion consists mainly of $CD8^+$ T cells, while the $CD4^+$ T cells are sparse. This indicates, that the $CD4^+$ T cells may initiate the neuroinflammatory process in MS, but the effector cells in the lesions would be $CD8^+$ T cells and $CD20^+$ B cells, which mediate the demyelination (Lassmann, 2019).

Apparent qualitative differences in lesion pathology between PPMS and SPMS have not been detected (Lassmann, 2019). The microglia are present in all stages of MS lesions, having a role in both lesion expansion and remyelination (Guerrero and Sicotte, 2020). In addition, CD40 expressed on macrophages, but also B cells and monocytes, have been shown to play a crucial role in priming encephalitogenic T cells in autoimmune diseases (Aarts et al., 2019).

2.1.2.2 Diagnosis of multiple sclerosis

The diagnosis of MS is primarily based on the evaluation of clinical symptoms, visualisation of focal abnormalities using MRI, and laboratory testing of inflammatory markers in the CSF (Thompson et al., 2018a). A diagnosis requires dissemination in both time and space, meaning that there has to be damage on different days and in different areas of the brain (Raffel et al., 2016). A definite pathological diagnosis would require pathological samples, however, there is limited availability to biopsy tissue (Filippi et al., 2012). Therefore, less invasive methods are applied. MRI remains to be the gold standard imaging method for diagnostics of MS due to its ability to detect WM lesions (Galassi et al., 2016).

In Finland, diagnosis is founded on the McDonald criteria 2017, which describes the diagnostic parameters when defining MS (Käypä hoito, 2020; Thompson et al., 2018a). In the majority of patients, the disease begins with a clinically isolated

syndrome (CIS) lasting from 24 h to 1 month, which, in the case of incidental MRI findings, is often followed by a second episode. In addition, lesions that are not causing symptoms can be detected in MRI, and in this case, the diagnosis is called radiologically isolated syndrome (Käypä hoito, 2020).

The diagnosis route starts by assessing the clinical symptoms often using the EDSS (Expanded Disability Status Scale). The EDSS scores activities of daily living and ability to walk on an ordinal scale from 0–10, where 0–3.5 indicates impairment with no effect on mobility, 4–7.5 indicates impaired mobility, 8–9.5 indicates restriction to bed, and 10 indicates death due to MS. Being that EDSS is not the perfect measure of inability, due to its insensitivity to measure changes within an individual, it remains to be the most popular one in clinical settings (Chard and Trip, 2017). After clinical evaluation, the patient is directed to MR imaging where gadolinium (Gd) enhancing T_1-weighted lesions, or T_2-weighted lesions are observed. The laboratory testing of CSF samples can also be evaluated (Chard and Trip, 2017). Inflammatory activity due to demyelination can be detected from the CSF by elevated oligoclonal immunoglobulin G (IgG) bands (Raffel et al., 2016).

Predicting the course of the disease and therapeutic effect is difficult. Chung and colleagues (2020) suggested that the first year EDSS result (>3.5) and the radiological number of lesions, as well as their location, may be used as predictors (Chung et al., 2020). One possible tool that has been suggested is the "Universal Immune Simulator Framework" (UISS), to which personalised immunological parameters can be inserted to model MS dynamics in patients (Pappalardo et al., 2020).

2.1.2.3 Treatment of multiple sclerosis

There are currently 19 FDA-approved medications for MS (Goldschmidt and McGinley, 2021; Li et al., 2019). However, there is a great need to improve the therapy of MS since the disease is affecting young adults and no treatment is currently highly effective in the late progressive phase of MS. With effective disease-modifying treatment, the natural course of MS, illustrated in Figure 3, has been modified so that relapses have almost disappeared, but the silent progression is still occurring (Giovannoni et al., 2022; Hauser and Cree, 2020).

Pharmacotherapy of MS can be divided into acute treatment of relapses and immunomodulatory treatment aiming at reduced relapse frequency (Kipp et al., 2017). Historically, the treatment of relapses using corticosteroids was the only treatment of MS until 1993, when interferon-β was introduced. During the following decade, only glatiramer acetate came to the market, before natalizumab and the other immunomodulatory therapies were introduced. Despite the remarkable progress that has been made in the field of MS therapeutics, especially for the relapsing disease

during the past two decades, it is still a major goal for researchers to identify pathological processes behind the disease (Filippi et al., 2012). There is a vast number of potential medications approved by the United States Food and Drug Administration (FDA) and European Medicines Agency EMA to treat MS (Table 1). Disease-modifying treatment can be categorised into nine classes depending on the mechanism of action and the administration route (McGinley et al., 2021). These include the interferon β's and glatiramer acetate, which were the first injectables for MS. In addition, there is teriflunomide, sphingosine 1-phosphate modulators, fumarates, cladribine, and monoclonal Ab's.

The challenging treatment decision is performed by the physician and the patient, and is evaluated based on the disease type, patient needs, and preferences (Visser et al., 2020). Hauser and Cree (2020) suggest as the first therapy option, in the case of CIS or RMS, the oral medications fingolimod or DMF. In the unfavourable forms of CIS or RMS, the starting therapy can be ocrelizumab or natalizumab, whereas in the case of active SPMS, it can be siponimod. In the case of PPMS, the only alternative was suggested to be ocrelizumab (Hauser and Cree, 2020). This is due to alemtuzumab and mitoxantrone having toxic side effects.

In this thesis, the injectable monoclonal Ab (mAb), natalizumab (anti-VLA-4, TYSABRI), which affects the B cell populations (Kemmerer et al., 2020), and the oral treatment, DMF (Carrithers, 2014a; Carrithers, 2014b; Mrowietz et al., 2018; Prosperini and Pontecorvo, 2016), were applied. Natalizumab is more effective in the treatment of RRMS compared most available therapies. It is a humanised recombinant mAb binding to the very late activating antigen-4 (VLA-4), i.e. the α4-subunit of α4β1 and α4β7 integrins, which are expressed on the surface of all leukocytes excluding neutrophils. Thus, the drug inhibits the α4-mediated adhesion of leukocytes to their counterreceptors. These include the vascular cell adhesion molecule-1 (VCAM-1), expressed on activated vascular endothelium, and the mucosal addressin cell adhesion molecule-1 (MadCAM-1) present in the gastrointestinal tract on vascular endothelial cells. When this receptor interaction is disrupted, transmigration of leukocytes into the inflamed parenchyma is prevented (EMA, 2004). It was later discovered that compromising the immune system with natalizumab in people exposed to the John Cunningham virus (JVC) have an increased risk for progressive multifocal leukoencephalopathy (PML) (Goldschmidt and McGinley, 2021). Due to the risk of PML, natalizumab can only be prescribed via a restricted prescription program TOUCH® Prescribing Program (FDA, 2020). It was discovered in the clinical study, ASCEND, that anti-VLA-4 treatment slowed down the progression of upper extremity disability in SPMS, however, it did not hinder ambulatory disability or delay disease progression evaluated using the EDSS. This indicates that there is no efficacy at a chronic stage of the disease. Despite its

clinical efficacy in RRMS, natalizumab therapy often needs to be discontinued, causing a rebound effect in which pathology worsens (Giacomini, 2018).

DMF (BG-12), on the contrary, is an oral drug, which MOA is unclear, but has been indicated to reduce relapse rate and radiological signs of disease activity (Valencia-Sanchez and Carter, 2020). DMF has peripheral effects, which reduce short-term oxidative stress and activates antioxidant effects (Yadav et al., 2019). This is due to the activation of the transcription factor Nrf2, which is responsible for redox balance. An increase in oxidised isoprostanes, monocyte counts, and monocyte-derived oxidative processes have been observed when using DMF. In addition, after these events, changes in T cell numbers have been detected (Carlstrom et al., 2019). The central effects of DMF relate to the reduction of the T cell migration potential (Holm Hansen et al., 2020). The effect of DMF has been studied in several clinical settings: the CONFIRM (Efficacy and Safety Study of Oral BG-12 With Active Reference in Relapsing-Remitting Multiple Sclerosis); and DEFINE (Determination of the Efficacy and Safety of Oral Fumarate in Relapsing-Remitting MS).

Table 1. Therapies of MS.

	Drug	Indication	Proposed MOA	Administration	Approval (FDA)
Highly effective	**OCRELIZUMAB***	RMS, PPMS	mAb targeting **CD20** on B-cells resulting in Ab-dependent cytolysis of cells and complement-mediated lysis	*i.v.* initial two doses with 2-week intervals, after which every 6 mon	2017
	OFATUMUMAB	RMS	mAb targeting **CD20** on B-cells resulting in Ab-dependent cytolysis of cells and complement-mediated lysis	*s.c.* initial three doses with one-week intervals after which 1/month	2020
	NATALIZUMAB	RMS	mAb binding to the α4-subunit of α4β1 and α4β7 integrins on **leukocytes** inhibiting their adhesion to their counter-receptors	*i.v.* 1/month	2004
	ALEMTUZUMAB*	RMS	mAb targeting **CD52** present on T and B lymphocytes, natural killer cells, monocytes, and macrophages, resulting in antibody-dependent cellular cytolysis and complement-mediated lysis	*i.v.* initial 5-day regime 1/day, 12 months after this 3-day regime 1/day	2001
	MITOXANTRONE*	RMS, PPMS	DNA-reactive agent causing DNA crosslinks and strand breaks, interferes with RNA, and inhibits topoisomerase II (uncoils and repairs damaged DNA), leading to **inhibition of B cell, T cell, and macrophage proliferation**, impairing antigen presentation	*i.v.* 1/1–3 months	2000
Moderately effective	**FINGOLIMOD***	RMS	Sphingosine 1-phosphate (S_1P) receptor modulator blocking **lymphocyte egress** from the lymph nodes	*p.o.* 1/day	2010
	SIPONIMOD*	RMS	S_1P receptor 1 and 5 modulator blocking **lymphocyte egress** from the lymph nodes	*p.o.* initial doses with a 5-day titration regime after which 1/day	2019
	OZANIMOD	RMS	S_1P receptor 1 and 5 modulator blocking **lymphocyte egress** from the lymph nodes	*p.o.* initial doses with a 7-day titration regime after which 1/day	2020
	CLADRIBINE*	RMS	A prodrug that becomes active upon phosphorylation: cytotoxic effects on B and T cells by impairing DNA synthesis that results in **depletion of lymphocytes**	*p.o.* 1–2 tablets once daily over 4–5 days in 2 yearly treatment courses	2019

	DIMETHYL FUMARATE*	RMS	DMF and its metabolite, monomethyl fumarate (MMF), activate the **nuclear factor (erythroid-derived 2)-like 2 (Nrf2) pathway** *in vitro* and *in vivo* in animals and humans, which is involved in the cellular response to oxidative stress	*p.o.* 2/day, after the first 7 days, the dose is increased	2013
	DIROXIMEL FUMARATE	RMS	The active metabolite MMF activates **Nrf2**-pathway *in vitro* and *in vivo* in animals and humans, which is involved in the cellular response to oxidative stress	*p.o.* 2/day after the first 7 days the dose is increased	2013 (2019)
	MONOMETHYL FUMARATE	RMS	Activates **Nrf2**-pathway *in vitro* and *in vivo* in animals and humans, which is involved in the cellular response to oxidative stress, and is a nicotinic acid receptor agonist	*p.o.* 2/day after the first 7 days, the dose is increased	2013 (2020)
Modestly effective	**TERIFLUNOMIDE***	RMS	An immunomodulatory agent with anti-inflammatory properties, inhibits dihydroorotate dehydrogenase, which is a mitochondrial enzyme involved in *de novo* pyrimidine synthesis, which may involve a reduction of activated **lymphocytes** in the CNS	*p.o.* 1/day	2012
	GLATIRAMER ACETATE*	RMS	Immunomodulation by glatiramer acetate-specific **suppressor T cell induction,** which are peripherally activated	*s.c.* 1/1-3 days	1996
	INTERFERON-β-1A*	RMS	Cytokine that mediates antiviral, antiproliferative and **immunomodulatory** activities exerting interferon-induced gene products	*i.m.* 1/week	2002
	PEGINTERFERON-β-1A	RMS	**No** biochemical or physiological effect known to relate directly to the clinical effect	*s.c.* after a titration regime 2/month	2014
	INTERFERON-β-1B*	RMS	Induces expression of proteins responsible for pleiotropic bioactivities	*s.c.* 1 every other day	1993
n/a	**PONESIMOD**	RMS	S_1P_1 receptor modulator blocking **lymphocyte egress** from lymph nodes	*p.o.* initiation by dose titration during 2 weeks after which 1/day	2021
n/a	**AZATHIOPRINE**	RMS	Cytostatic immunosuppressive purine analogue depressing both **cellular and humoral immunity**	*p.o.* 1/day	1974
n/a	**DACLIZUMAB**	RMS	Ab binding to **CD25** blocking the interleukin-2 receptor	*s.c.* 1/month	2016**

*available in Finland; **withdrawn in 2018. References (EMA, 2021; FDA, 2021; Hauser and Cree, 2020; Massacesi et al., 2005; Neuhaus et al., 2007).
RMS = Relapsing forms of MS including CIS, RRMS, and active SPMS; PPMS = Primary progressive MS

2.2 Experimental models of neuroinflammation and demyelination

Non-animal models (NAMs), such as *in silico* modelling with computational techniques or in vitro cell models, can be applied, to some extent, to NI research (Cavalli et al., 2020; Lorenzetti et al., 2020; Mammana et al., 2018). MS disease dynamics and current treatments have been studied *in silico*, which can be applied to plan treatment strategies in the future (Pappalardo et al., 2020). However, data from NAMs can be accepted only when their outcome reliability can be confirmed and protection of human health can be achieved (Lorenzetti et al., 2020). This is why *in silico* and *in vitro* results are always confirmed by *in vivo* animal models, due to the complexity of immunological responses (Parravicini et al., 2020). An example of the complex nature of NI is the macrophage reactions, which are dependent on the tissue context and the activating stimuli, being consequently different *in vivo* and *in vitro* (Ransohoff, 2016).

Currently, all animal experiments are required to be performed according to "Animal Research: Reporting of In Vivo Experiments" (ARRIVE) 2.0 guidelines (Percie du Sert et al., 2020). The guidelines are applied to promote reproducible science by transparent reporting of studies (NC3R^S, 2021). ARRIVE checklist focuses on detailed reporting of experiments to allow others to reproduce the data. This checklist includes proper reporting of the study design, sample size, the inclusion and exclusion criteria, as well as whether randomisation and blinding were applied. Furthermore, the outcome measures, statistical methods, and results should be clearly described. In addition, a detailed description of the experimental animals and procedures performed on them is required. The responsibility of precise reporting lies on both the operating researcher as well as the journal editors and reviewers (Kilkenny et al., 2012; Percie du Sert et al., 2020).

There are multiple ways in which animal models of NI and demyelination can be induced, illustrated in Figure 4. The earliest reports of induced NI date back to the '30s (Rivers and Schwentker, 1935; Rivers et al., 1933), when acute disseminated encephalomyelitis (ADEM), a disease that had recently been discovered in humans, was attempted to be established in macaque monkeys. Rivers and Schwentker (1935) made repeated injections of alcohol-ether rabbit brain extracts in aqueous emulsions to the parenchyma of the monkeys and reported myelin destruction as well as symptoms related to CNS pathologies, such as ataxia, paralysis, and blindness. This disease is nowadays known as experimental autoimmune encephalomyelitis (EAE) (Billiau and Matthys, 2001). These findings were extended by others (Kabat et al., 1947; Morgan, 1947), but Jules Freund, after whom the immunoadjuvant Freund's adjuvant was named (Billiau and Matthys, 2001), wanted to induce the condition in guinea pigs, due to its profitable way of sensitisation of the skin and capacity to produce Ab's (Freund et al., 1947). Together with T. M. Pisani (1947), he was able

to induce aseptic encephalomyelitis and radiculitis after just one subcutaneous (*s.c.*) injection of rabbit brain extract and heat-killed Mycobacterium tuberculosis bacteria (TB) in a water-in-paraffin-oil emulsion.

Adjuvants are substances that turn non-antigenic substances into antigens and increase levels of circulating Ab's (White, 1967). Complete Freund's adjuvant (CFA), which contains heat-killed TB, and incomplete Freund's adjuvant (IFA), with no TB, are the most common ways to cause autoimmune diseases in experimental animals even nowadays (Billiau and Matthys, 2001). In the 1940s, EAE was, in some species, found to result from a single injection of brain extract. In mice and guinea pigs, CFA is always needed to create EAE, while some rat strains can be induced without it (White, 1967).

The features that the animal models are presenting while depicting MS, are inflammatory lesions dominated by $CD8^+$ T cells and B-cells, with a lesser contribution from $CD4^+$ T cells, since $CD4^+$ T cells are triggering the inflammatory cascade, but not dominant in an established lesion. Also, these inflammatory lesions are characterised by profound microglial activation and the contribution of astrocytes forming the glial scar (Lassmann and Bradl, 2017).

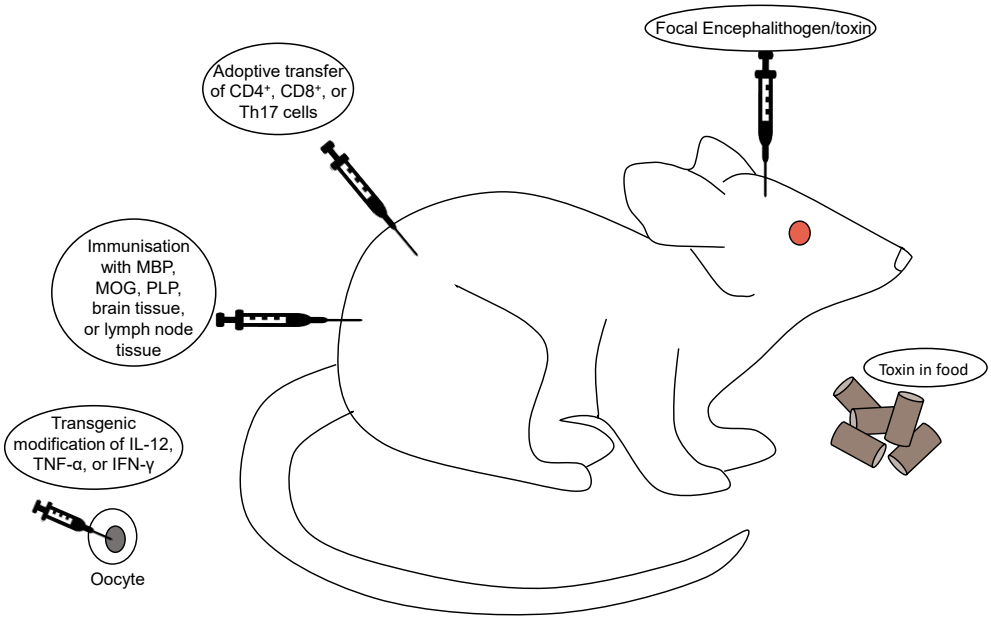

Figure 4. Different methods in which animal models of NI can be induced.

2.2.1 Disseminated models

MS is a disease, which has only been recognised in humans (Bjelobaba et al., 2018). Thus, there is no single experimental model to reproduce all pathological aspects of MS (Lassmann and Bradl, 2017). Depending on the research question, variable methods to create MS-like lesions exist (Table 2). Active immunisation using a CNS antigen, such as MOG, MBP, or PLP, together with a strong adjuvant, results in an acute or chronic inflammatory reaction mediated mainly by $CD4^+$ T cells resulting in axonal degeneration followed by secondary demyelination. Generally, it appears, that active immunisation of rats, guinea pigs, and primates with MOG resembles MS better than immunisation of mice (Lassmann and Bradl, 2017). The Marmoset EAE has been considered to have the closest resemblance to MS to other types of EAE models due to the high degree of homology with genes encoding myelin and immune cells resulting in similar lesion morphology and histology as in MS lesions (Pomeroy et al., 2005). The fundamental difference between the active immunisation models and MS pathology is, that when the antigen depot causing the inflammatory demyelination in the active models is removed, the disease subsides, reflecting a need for persistent stimulation from the periphery (Lassmann and Bradl, 2017).

Despite its flaws, EAE by active immunisation remains to be the most used model to depict multiple sclerosis, however, there are several other ways of inducing MS-like symptoms in animals (Figure 4) (Glatigny and Bettelli, 2018). In the viral models, inflammation and demyelination are induced by exposure to Theiler′s murine encephalomyelitis virus, the mouse hepatitis (corona) virus (MHV), or the canine distemper virus. An advantage regarding the viral models is the inflammatory demyelination without active immunisation using brain tissue, because it may be a more natural process in regards to the aetiology of MS in humans, even though there has been no direct virus identified as a causal factor for MS (Lassmann and Bradl, 2017).

Moreover, there is the passive EAE, i.e. the adoptive transfer models, in which T cells or pathogenic auto-Ab’s from previously immunised animals are transferred to naïve animals, acquiring a neuroinflammatory disease (Lassmann and Bradl, 2017). The animals from which the T cells are obtained, can be immunised with tissue extract from lymph nodes or myelin-specific proteins (Bjelobaba et al., 2018). These models are beneficial when studying the surveillance and entrance of T cells into the CNS (Lassmann and Bradl, 2017). However, the adoptive transfer might not be encephalitogenic enough to cause demyelination in the animal (Bjelobaba et al., 2018).

Furthermore, spontaneous EAE is achieved by using transgenic models, which express T cell or B cell receptors of encephalitogenic T cells (Lassmann and Bradl, 2017). Through transgenic methods or genetic ablation even humanised T cell receptor (TCR) models can be created (Ben-Nun et al., 2014).

Whereas the previously mentioned models readily induce NI, the toxin-induced disseminated models cause direct demyelination without axonal interference, contributing to oligodendrocyte death and OPC migration, following remyelination (Burrows et al., 2018). The toxins can be ethidium bromide, lysophosphatidylcholine, or cuprizone. There are also models combing active immunisation with toxin administration, resulting in a model of de- and remyelination with inflammatory components (Lassmann and Bradl, 2017).

2.2.2 Focal models

When considering the models of MS, the commonly used disseminated models form small focal lesions in the brain and spinal cord, which can be difficult to quantify by molecular imaging and to follow longitudinally, because the location of the lesions varies spatially in time. To create localised lesions, stereotactic injection of encephalitogens into the brain or spinal cord can be applied (Lassmann and Bradl, 2017). By using this method, many clinical pathologies with inflammatory, neoplastic, or neurodegenerative features can be induced, such as models of AD, PD, MS, gliomas, or epilepsy (Mori et al., 2000; Tetard et al., 2016). The specific location of the injection is determined by the target coordinates (Paxinos and Watson, 1986).

The focal models can be divided into acute and more chronic models. Injection of a toxin, such as LPS, unilateral acute NI occurs within a few hours of the injection (Montero-Menei et al., 1994). The inflammation emerges without killing the adjacent cells (Couch et al., 2011). Intracranial LPS binds to an LPS-binding protein (LBP) thus activating the immune system. The LBP merges with the toll-like receptor 4 (TLR4), which subsequently activates regulatory proteins, e.g. the NFκB, inducing transcription of pro-inflammatory genes and interferons (Alberts et al., 2008). The injection of LPS unilaterally leaves the contralateral hemisphere intact and free of inflammation (Couch et al., 2011).

In studies of MS, focal inflammatory demyelinating lesions can be induced when localisation of the lesion needs to be precise and reproducible (Lassmann and Bradl, 2017). Intracerebral injection of pro-inflammatory cytokines, such as TNF-α and IFN-γ into the GM, augment cortical inflammatory lesions after immunisation of the animal with spinal cord homogenates or myelin fragments, e.g. MOG (Merkler et al., 2006). Unlike the WM or spinal cord targeted persisting lesions, the cortical lesions created by stereotactic injection of cytokines on previously immunised animals creates a transient inflammatory infiltration followed by demyelination of the GM (Merkler et al., 2006). This *f*MOG-EAE resembles the MS lesion pathology of pattern II lesions described in 2.1.2.1, which are T cell and macrophage dominated lesions with IgG and complement depositions followed by demyelination and disintegration of the BBB (Serres et al., 2009a).

Another model, one depicting hallmarks of the pattern I lesions, is the focal delayed-type hypersensitivity (*f*DTH-EAE) model, where there is inflammatory infiltration of T cells and macrophages, but IgG and complement depositions are absent (Broom et al., 2005). The basis for this model comes from the discovery of Dienes in 1929, that a dermal hypersensitization after exposure to TB is of delayed-type rather than immediate-type allergenic reaction (Dienes, 1929). The *f*DTH-EAE model is created by intracerebral injection of heat-killed Bacillus Calmette-Guérin (BCG) and subsequent immunisation with CFA, after which a large, predictable lesion depicting hallmarks of MS lesions, such as monocyte recruitment, T cell infiltration, axonal and myelin damage, upregulation of matrix metalloproteinases, as well as microglial activation can be observed (Anthony et al., 1998; Matyszak and Perry, 1995). The intradermal sensitisation initiates a DTH lesion in the skin as well as at the site of the cerebral BCG deposit (Broom et al., 2005). Spatial localisation of the *f*DTH-EAE lesion is aimed at brain structures, such as the striata, which cause no overt clinical phenotype and therefore, no comorbidities or suffering for the animals (Broom et al., 2005). Previous studies applying the *f*DTH-EAE describe hyperintensity on a T_2 MRI in addition to Gd enhancement of the lesion, 2 weeks after peripheral immunisation, indicating BBB breakdown, which is resealed about 4 weeks after immunisation (Broom et al., 2005). The lesion evolves and enlarges over time creating a chronic state where axonal damage can be observed behind the resealed BBB (Broom et al., 2005). Without the peripheral activation of the lesion, BCG remains sequestered in the brain parenchyma for months (Matyszak and Perry, 1998; Matyszak et al., 1997) The T_2 MRI pattern in the *f*DTH-EAE and *f*MOG-EAE at day 14 are remarkably similar, despite their differences in histopathology (Serres et al., 2009a).

Table 2. Disseminated and focal models of NI and demyelination.

MODEL INDUCTION	LOCATION	ANIMAL SPECIES/ STRAIN	ENCEPHALITOGEN/ TOXIN/ENDOTOXIN (ADMINISTRATION)	PHENOTYPE	REFERENCE
ACTIVE IMMUNISATION	Disseminated	Guinea pig	Rabbit brain extract + CFA (*s.c.*)	Paralysis and lesions	(Freund et al., 1947)
	Disseminated	Rhesus monkey/ Common marmoset/ Macaque	CSF and CFA	Increase of T cells and IgG	(Kabat et al., 1951; Pomeroy et al., 2005)
	Disseminated	C57BL/6 mouse	Proteolipid protein (PLP) + TB	Limp tail, paralytic disease	(Tompkins et al., 2002)
	Disseminated	Lewis rat/ Dark Agouti rat/ BN rat	Myelin oligodendrocyte glycoprotein	Chronic relapsing or progressive, inflammation, demyelination, axonal loss	(Storch et al., 1998)
	Disseminated	Dog	Spinal cord + CFA	Varying disease course: ataxia, plegia	(Summers et al., 1984)
	Focal	Lewis rat	Heat-killed BCG (intracerebral) + CFA	*f*DTH-EAE with no overt phenotype	(Matyszak and Perry, 1995)
	Focal	Lewis rat	IFA *s.c.* + intracerebral TNF-α & IFN-γ	*f*MOG-EAE with no overt phenotype	(Merkler et al., 2006)
VIRUS INDUCED	Disseminated	SJL/J mouse	Theiler's murine encephalomyelitis virus	Chronic CD4+ T- and CD8+ T cell inflammation demyelination	(Njenga et al., 2004)
	Disseminated	Mouse	Mouse hepatitis (corona) virus (MHV)	Encephalitis, acute axonal damage demyelination, paralytic disease	(Bailey et al., 1949; Lassmann and Bradl, 2017)
	Focal, periventricular	Dog	Canine distemper virus	Non-inflammatory lesions, varying systemic symptoms: fever, lethargy	(Summers et al., 1984)

MODEL INDUCTION	LOCATION	ANIMAL SPECIES/ STRAIN	ENCEPHALITOGEN/ TOXIN/ENDOTOXIN (ADMINISTRATION)	PHENOTYPE	REFERENCE
ADOPTIVE TRANSFER	Disseminated	SJL/J mouse	Adoptive transfer of MBP reactive T cells + MBP and TB in IFA (*s.c.*)	Relapsing remitting EAE: limp tail, weakness, plegia	(Cross and Raine, 1990)
TOXIN INDUCED	Disseminated	Mouse	Cuprizone (*p.o.*)	De- and remyelination	(Kipp et al., 2009)
	Disseminated	Mouse	Cuprizone (*p.o.*) peripheral immunisation ($MOG_{35–55}$)	De- and remyelination, glial activation, axonal injury, paralysis, limp tail	(Lehto et al., 2017; Nack et al., 2019)
	Disseminated	Zebrafish	Lysophosphatidyl-choline (LPC)	Apoptotic neuronal death, demyelination	(Xu et al., 2016)
	Focal	57L/6 mouse	LPC (intracerebral) + peripheral immunisation ($MOG_{35–55}$)	De- and remyelination, immune & T cell activation, cytokine release	(Lamport et al., 2019)
	Focal	Lewis rat	Lipopolysaccharide (LPS; intracerebral)	Acute NI	(Montero-Menei et al., 1994)
	Focal	S-D rat	Ethidium bromide (intraventricular)	De- and remyelination	(Levine and Reynolds, 1999)
	Disseminated	SJL/J and BALB/c mice Lewis rat	Pertussigen, TB, & mouse spinal cord in CFA	Mononuclear and polymorphonuclear infiltration	(Munoz et al., 1984)
TRANSGENIC	Disseminated	C57BL/6xDBA/2	Expression of MBP specific TCR	encephalopathy with primary axonal injury	(Goverman et al., 1993)
	Disseminated	SJL/J	Expression of MOG specific TCR	MOG autoreactive B cells, demyelination	(Pöllinger et al., 2009)

2.3 Molecular imaging of neuroinflammation

The components of the innate immune system are adequate targets for several different imaging strategies (Dorward et al., 2012). These include ultrasound, MRI, computer tomography (CT), single-photon emission computed tomography (SPECT), PET, and optical imaging (Wu and Shu, 2018). The method of imaging depends on which aspect of a disease needs to be visualised, whether it being BBB breakdown, inflammation, WM/GM damage, or axonal loss (Nathoo et al., 2014).

In the '70s, CT was discovered by Hounsfield and Cormack, and used for the detection of MS lesions in the brain (Hershey et al., 1979). Later on, in the '80s, MRI was discovered, and it quickly became the gold standard to visualise MS pathology. However, linking MRI outcome and clinical EDSS scores is challenging (Chard and Trip, 2017). There are reports of worsening neurological symptoms in a patient while the number of Gd-enhancing lesions remained the same. This situation is called the clinico-radiological paradox (Barkhof, 2002; Chard and Trip, 2017), which has led to a need for more pathologically specific measures that indicate disease activity and the status of the lesions. One of the suggested methods to detect functional changes in the CNS has been PET imaging. While SPECT, that uses monoenergic radioisotopes that emit a single gamma photon, has been utilised in some studies of multiple sclerosis (Pozzilli et al., 1991), PET, that uses positron emitters, has become more popular during recent years (Airas et al., 2015b; Duncan, 1998). Multimodal imaging, in which two or more detection methods are combined, such as structural and functional imaging modalities, has provided a tool in which many parameters can be visualised simultaneously or consecutively (Coda et al., 2021; Wu and Shu, 2018).

2.3.1 Magnetic resonance imaging

Structural MRI is a method, which detects the physicochemical differences of tissues without ionising radiation that is applied in CT or PET. By applying a strong external magnetic field that affects the angular momentum of the nuclei of elements, an image in three planes can be created. This is achieved by measuring the variables nuclear spin density, T_1 relaxation time, T_2 relaxation time, flow shift, and spectral shift. When a low energy pulse is applied on a magnetised sample/nucleus, it absorbs some energy and tilts the magnetic moment causing precession in a specific frequency. A radio signal, called the Larmor frequency, in the same frequency as the precession, is emitted. This is unique for all substances and is applied when reconstructing the image by Fourier transform. After the energy pulse, the precession is aligned with the external magnetic field, a term called spin-lattice relaxation (T_1), and simultaneously the precession of the magnetic moment is dephased in spin-spin relaxation (T_2), contributing to the decay of the original radio signal (Hendee and Morgan, 1984a).

The imaging is divided into different sequences, where the variables are weighted according to the applied energy pulsation and time. The T_1 value varies from tissue to tissue regarding the solidity, with more liquid-like tissue having looser interatomic bonds thus resulting in shorter T_1 values shown as dark (hypointense) in the resultant image. In the T_2-weighted images, on the other hand, inhomogeneities in the surrounding magnetic field in a liquid have less molecular motion resulting in elongation of T_2, which is shown as white (hyperintense) in the MR image. In disease states, the water content of solid tissues is often increased resulting in increased T_2 times. One of the first applications of MRI was indeed MS (Hendee and Morgan, 1984a; Hendee and Morgan, 1984b). In such cases, where the BBB is broken, e.g. in active WM MS lesions, Gd enhancement of the T_2 image is applied.

To date, the diagnostic criteria using MRI rely on WM lesion activity (Filippi et al., 2012; Filippi et al., 2016). Evaluation of the pathological events using conventional MRI is not optimal, because lesions with different pathomechanisms, such as demyelination, stroke, or tumours, may appear the same in T_2-weighted images. Several methods applying MRI have been suggested to improve diagnostics, including: diffusion tension imaging (DTI) (Le Bihan et al., 2001), magnetization transfer, multiexponential T_2, and rotating-frame MRI methods (Lehto et al., 2017).

Functional MRI (fMRI) has also been suggested as a method of diagnosis for cortical changes. fMRI measures brain plasticity, which is altered during neuronal conditions, by measuring the changes between deoxyglucose, blood flow, and blood volume that attribute neuronal activity (De Stefano and Giorgio, 2017; Rocca and Filippi, 2007).

Gd-enhancing lesions are missing in progressive MS, indicating repaired BBB, while simultaneously pronounced inflammation is present in the SPMS and PPMS, in addition to the acute phase of RRMS (Frischer et al., 2009). As in RRMS, in the *f*DTH-EAE, the acute inflammation diminishes when the disease progresses, and diffuse pathology undetectable by conventional MRI remains prevalent (Broom et al., 2005). Thus, methodology to detect the diffuse inflammatory changes behind the sealed BBB, that can be observed in MS, are needed.

2.3.2 Positron emission tomography

PET is a relatively non-invasive technology that utilises short-lived positron (β^+) emitting isotopes produced in a cyclotron. The history of PET dates back to the 1950s when physicist Gordon Brownell and neurosurgeon William Sweet developed the first human positron imaging apparatus using sodium iodide scintillators to image brain tumours (Portnow et al., 2013). An improved scanner with multiple detectors in a hexagonal arrangement was introduced in mid-‘70s by nuclear physicist Michael Ter-Pogossian with his lab members Michael Phelps and Edward Hoffman (Phelps et al., 1975; Ter-Pogossian et al., 1975). Improved resolution and sensitivity were

obtained by using ring-shaped and cylindrical detectors in the 1980s (Portnow et al., 2013). The current PET detectors can consist of several different materials, e.g. lutetium oxyorthosilicate (LSO) or lutetium–yttrium oxyorthosilicate (LYSO) crystals, which are positioned in several rings and connected to photomultiplier tubes (PMTs) (Lewellen, 2008).

The radioisotopes applied in PET, commonly short-lived oxygen-15 [^{15}O], carbon-11 [^{11}C], nitrogen-13 [^{13}N], fluorine [^{18}F], gallium-68 [^{68}Ga], and zirconium-89 [^{89}Zr], account for the signal that is detected (Mitterhauser and Wadsak, 2014). Properties of the isotope that affect image quality are half-life ($T_{½}$) and energy of the positron (E) that accounts for the positron range (Conti and Eriksson, 2016). For instance, for [^{11}C], $T_{½}$=20.4 min and E=0.96 MeV, while for [^{18}F], the values are $T_{½}$=109.8 min and E=0.63 MeV, correspondingly (Ferrieri, 2003). In radiopharmaceuticals, the isotopes are attached to biologically active compounds, such as glucose or pharmaceuticals, which account for the *in vivo* interaction of the molecule (Mitterhauser and Wadsak, 2014). The radioactive compound is administered in tracer amounts, in micro- to picomolar concentrations, with no pharmaceutical effect to the patient. In the tissue, radioactive decay occurs, due to which positrons (β^+) are emitted. The positron travels shortly in the tissue (positron range, usually 0.5–3.00 mm) during which it loses kinetic energy until a point that it can interact (annihilate) with an electron (e^-) releasing two γ-quanta, i.e. coincidence photons of exactly 511 keV each, in opposite directions with a maximum deviation of 0.25° (Ziegler, 2011). The principle of PET is the coincidence detection of these paired photons along the line of response (LOR) by the multiple detectors around the study subject (Lewellen, 2008). Unpaired events resulting from scattering or random events are disregarded (Ziegler, 2011).

After the intravenous administration of the PET tracer, it travels in the body through the circulation to its target. A measure of the tracer that needs to be observed and standardised is the molar activity (MA, previously called specific activity), which describes the ratio of the radioactive and non-radioactive compound. If the MA is low, the non-radioactive compound will occupy target receptors leading to lower binding potential (Xi et al., 2011). Other important characteristics of the radiotracer are similar to pharmaceuticals: biocompatibility to avoid toxicity; bioavailability ensuring sufficient concentration reaching through the barriers of the body; the binding affinity of reversibly binding tracers, rapid equilibrium and wash-out for nonspecific binding; optimal lipophilicity ($logD_{7.4}$), which indicates the distribution of the compound in n-octanol/buffer at the physiological pH of 7.4; slow metabolism; as well as specificity and selectivity to the target (Patel and Gibson, 2008; Rudin, 2009). Non-specific binding of the tracer correlates directly with the lipophilicity of the tracer. Optimal entry through the BBB is observed for tracers with molecular weight less than 400 Da and moderately lipophilic tracers with $logD_{7.4}$ values between 2.0 and 3.5 (Pike, 2009; Zhang et al., 2021).

The data from the PMTs are reorganised into a 2D-sinogram, and by utilising reconstruction parameters, which estimate the integral of the tracer distribution, and by implementing Compton scatter and attenuation corrections, a digital image is processed (Ziegler, 2011). The spatial distribution of the tracer can be reconstructed by detecting all coincidence events along the possible LORs, even when the exact location of the annihilation is not known. When data are collected statically, information can be collected at specific time points, whereas dynamic imaging collects data throughout the imaging session, from which a time-activity curve (TAC) can be extracted for each individual voxel (Ziegler, 2011).

PET images are reconstructed using filtered-back projection (FBP), maximum *a posteriori* (MAP), or the ordered-subsets expectation maximization algorithm in two- or three dimensions (OSEM2D, OSEM3D) algorithms with special characteristics (Cheng et al., 2012). By using a fully 3D reconstruction algorithm, the high sensitivity, as well as the high spatial resolution, can be retained in the whole field of view (FOV) (Visser et al., 2009). Smoothing of data after each iteration in algorithm(s) is performed to reduce the effect of noise in the final image, however, at the cost of decreased image resolution. By determining the target resolution, the smoothing values are set for the reconstructed image to reach the target resolution (Siemens, 2014).

Quantification of preclinical PET studies is often expressed as a percentage of injected activity per unit mass (%IA/g) within a delineated region of interest (ROI) or a volume of interest (VOI) (Haubner and Decristoforo, 2011). In longitudinal studies, when the mass of the animal increases, the uptake must be standardised to the body mass, and thus the standardised uptake value (SUV) is applied. To accurately quantify PET scans, an input function is required. In clinical studies, the input function is typically acquired from the blood plasma, but in preclinical settings, it is less common due to the invasiveness of the procedure. Other approaches to obtain input function are image-derived, simplified reference tissue models (SRTM), or unsupervised and supervised clustering (Sridharan, 2016).

Currently, clinical use of PET in MS is restricted to clinical research, differential diagnosis, or determining the efficacy of immune-suppressive treatment (van der Weijden et al., 2021). Several targets for MS pathologies have been suggested, e.g. targeting myelin by applying the [^{11}C]Pittsburgh compound B [^{11}C]PiB (Bodini et al., 2016), quantitation of glucose metabolism depicting neuronal activity by using [^{18}F]FDG (Baumgartner et al., 2018), visualising astrocyte activity by using [^{11}C]Acetate (Takata et al., 2014), detecting an increase of adenosine, by using [^{11}C]TMSX ([7-methyl-[^{11}C]]-(E)-8-(3,4,5-trimethoxystyryl)-1,3,7-trimethylxanthine) (Rissanen et al., 2013), and evaluating expression of TSPO by using the tracer [^{11}C]PK11195 ([^{11}C]-N-butan-2-yl-1-(2-chlorophenyl)-N-methylisoquinoline-3-carboxamide) (Rissanen et al., 2014).

2.3.2.1 TSPO PET imaging

One of the prominent hallmarks of NI is the increase of the mitochondrial biomarker TSPO, previously called the peripheral benzodiazepine receptor (PBR), which is related to the rate-limiting step of cholesterol conversion to steroids (Daugherty et al., 2013; Zhang et al., 2021). In addition, TSPO has roles in immunomodulation, cell respiration, ion transport and many other functions (Zhang et al., 2021). Under physiological conditions, the expression of TSPO in the CNS parenchyma is low, but expression rises during pathological and neurodegenerative conditions (Lee et al., 2020). Thus, TSPO has even been suggested as a therapeutic target, however, the results have ended up controversial (Lee et al., 2020). Since the discovery of the TSPO PET tracer, [^{11}C]PK11195, in the mid-1980s (Camsonne et al., 1984), along with the other first-generation TSPO tracers, it has been applied as a marker in preclinical and clinical research of neuroinflammatory conditions (Alam et al., 2017; Pappata et al., 2000).

Since then, several 2nd generation TSPO tracers, some of which are listed in Table 3, such as [^{18}F]PBR06, [^{11}C]DPA713, [^{18}F]-DPA-714, and [^{18}F]PBR111, along with the novel tracer (at the start of this study), [^{18}F]GE-180, flutriciclamide, ((S)-*N,N*-diethyl-9-(2-[^{18}F]fluoroethyl)-5-methoxy-2,3,4,9-tetrahydro-1*H*-carbazole-4-carboxamide), have been developed. The 2nd generation TSPO tracers have led to the discovery of TSPO polymorphism in humans (Owen et al., 2012). The polymorphism of *TSPO* Ala147Thr in humans indicates high-affinity binders (HAB), mixed-affinity binders (MAB) and low-affinity binders (LAB) among humans. In clinical research, [^{11}C]PK11195 has been applied despite this (Rissanen et al., 2014), because no genotyping is needed due to its high lipophilicity ($logD_{7.4}$ = 4.58) that leads to its binding to structures containing fat within the CNS and thus, poor signal-to-noise ratio. Furthermore, it has been shown not to be extremely selective for TSPO (Ching et al., 2012).

Due to the TSPO gene polymorphism (rs6971), the use of 2nd generation tracers as clinical PET biomarkers have been restricted due to the need for genotyping of the subjects (Werry et al., 2019). However, HAB's, MAB's and LAB's have not been detected or described in animal models (Sridharan, 2016).

Studies of TSPO expression in MS patients using PET has brought up the issue of non-selectivity of the target and its inability to detect microglia with proinflammatory markers (Nutma et al., 2019), while the goal would be allowing longitudinal follow-up of diffuse NI (Airas et al., 2015b). Furthermore, [^{18}F]FEPPA was not able to detect chronic diffuse microglial activation in the WM using MHCII expression as a marker (Al-Khishman et al., 2020). This was possibly due to the difficulty of distinguishing WM in the rat brain and the low resolution of PET.

2.3.2.2 Other PET targets for neuroinflammatory diseases

Considering the limitations of TSPO PET, more cell-specific and functionally relevant biomarkers are needed (Jain et al., 2020). There are several other receptors, some of which are listed in Table 3, that can be targeted using PET (Jain et al., 2020). Purinoreceptors P_2X_7 and $P_2Y_{12}R$ have been extensively studied (Beaino et al., 2017). Adenosine A_{2A}, which is one of the four adenosine receptors expressed in the CNS, but also during NI, can be targeted with [^{11}C]TMSX (Mishina et al., 2007; Rissanen et al., 2013). The issue with many of these suggested targets is their selectivity, while many of the receptors are expressed on more than one cell types (Jain et al., 2020).

Table 3. Targets for NI and some of the available PET tracers.

Target	Tracer	Reference
TSPO	[^{11}C]PK11195	(Camsonne et al., 1984)
	[^{11}C]PBR28	(Owen et al., 2012)
	[^{11}C]DAC	(Xie et al., 2012)
	[^{18}F]FEMPA	(Varrone et al., 2015)
	[^{18}F]GE-180	(Jones et al., 2011)
	[^{18}F]DPA-713	(Endres et al., 2009)
	[^{18}F]DPA-714	(Coda et al., 2021; Vicidomini et al., 2015)
	[^{18}F]FEPPA	(Al-Khishman et al., 2020)
	[18F]GE387	(Qiao et al., 2019)
Cannabinoid receptor CB2	[^{11}C]A-836339	(Horti et al., 2010)
Adenosine A2A	[^{11}C]TMSX	(Rissanen et al., 2013)
Purinoceptor P_2X_7	[^{11}C]SMW139	(Hagens et al., 2020)
	[^{11}C]GSK1482160	(Jain et al., 2020)
	[^{11}C]JNJ717	(Zhang et al., 2021)
Purinoceptor P_2Y_{12}	[^{11}C]Ethyl 6-(3-(3-((5-chlorothiophen-2-yl)sulfonyl)ureido)azetidin-1-yl)-5-cyano-2-methylnicotinate	(Beaino et al., 2017; Villa et al., 2018)
COX1	[^{11}C]celecoxib	(Jain et al., 2020)
Colony stimulating factor 1 receptor CSF1R	[^{11}C]CPPC	(Horti et al., 2019)
Triggering receptor expressed on myeloid cells 1 (TREM1)	[^{64}Cu]TREM1-mAb	(Jain et al., 2020)
CD20	[^{64}Cu]rituximab	(Jain et al., 2020)
CD19	[^{64}Cu]CD19-mAB	(Jain et al., 2020)
Monoamine oxidase B MAO-B	SL25.1188	(Zhang et al., 2021)

3 Aims

The aim of this thesis was to evaluate the binding of TSPO PET radiopharmaceuticals in focal animal models of NI and to discover the effects of immunomodulatory drugs of MS in these animal models.

The following objectives were set:

1. To investigate the binding of the 2nd generation TSPO PET-tracer [^{18}F]GE-180 when compared to the gold standard 1st generation TSPO PET-tracer [^{11}C]PK11195, and to evaluate its applicability to small animal studies (**I**).
Study hypothesis: [^{18}F]GE-180 has superior properties over [^{11}C]PK11195.

2. To investigate the efficacy of the immunomodulatory drug, anti-VLA-4, in the *f*DTH-EAE-rat model using [^{18}F]GE-180 and IHC. Furthermore, the aim was to discover whether a rebound effect can be detected after halting the treatment (**II**).
Study hypothesis: anti-VLA-4 has anti-inflammatory effects in the *f*DTH-EAE-rat model.

3. To investigate the efficacy of DMF in two focal models of NI, the *f*DTH-EAE and the *f*MOG-EAE rat models using [^{18}F]GE180 and IHC, and to determine whether a rebound effect can be detected after halting the treatment (**III**).
Study hypothesis: DMF has anti-inflammatory effects in both the *f*DTH-EAE and *f*MOG-EAE rat models.

4 Materials and Methods

4.1 Experimental models

In this thesis, inbred Lewis rats were chosen for all studies except the metabolite analysis, in which outbred Sprague-Dawley (S-D) rats were used because of the availability of the animals at the time of the study. Lewis rat is an albino inbred strain of Rattus norwegicus (CharlesRiver, 2021). An inbred strain (LEW/Crl and LEW/HanHsd) was chosen for the majority of the studies to minimize eventual differences caused by individual responses, and in particular, because of the susceptibility of Lewis rats to autoimmune diseases.

To investigate the applicability of the novel tracer (at the time), [^{18}F]GE-180, in neuroinflammatory states, a rapidly inducible model of acute NI was applied (Study I & the metabolite study). However, in the efficacy assessment of immunomodulatory pharmaceuticals, focal models of EAE were applied, because the pathology of the lesions resemble MS Type I and Type II lesions. The induction timelines for the rat models used in this thesis are illustrated in Figure 5. The acute LPS-NI model started as a pilot experiment since it was not known whether such inflammation can be detected by TSPO PET. After promising results, the animal number was added up.

Animal experiments received ethical approval from the Finnish National Animal Experiment Board, nowadays called the Project Authorisation Board, under the licence ESAVI/6360/04.10.03/2011. The experiments were carried out according to the animal welfare instructions in the Treaty of Amsterdam for the European Union (EU) and reported along with the ARRIVE 2.0 guidelines (Percie du Sert et al., 2020). Rats were housed in pairs or threes in 12 h light-dark cycles in temperature of 21(1.3) ºC and air humidity at 55(15)% (values are indicated as mean(SD)). Pellet food (CRM[E], Special diet services, Witham, United Kingdom) and tap water were provided *ad libitum*.

The age of the rats that were applied in this research was set to rats over 8 weeks. At this age, we estimated that the brain and skull of the rats have reached the size of a mature rat (Sengupta, 2013).

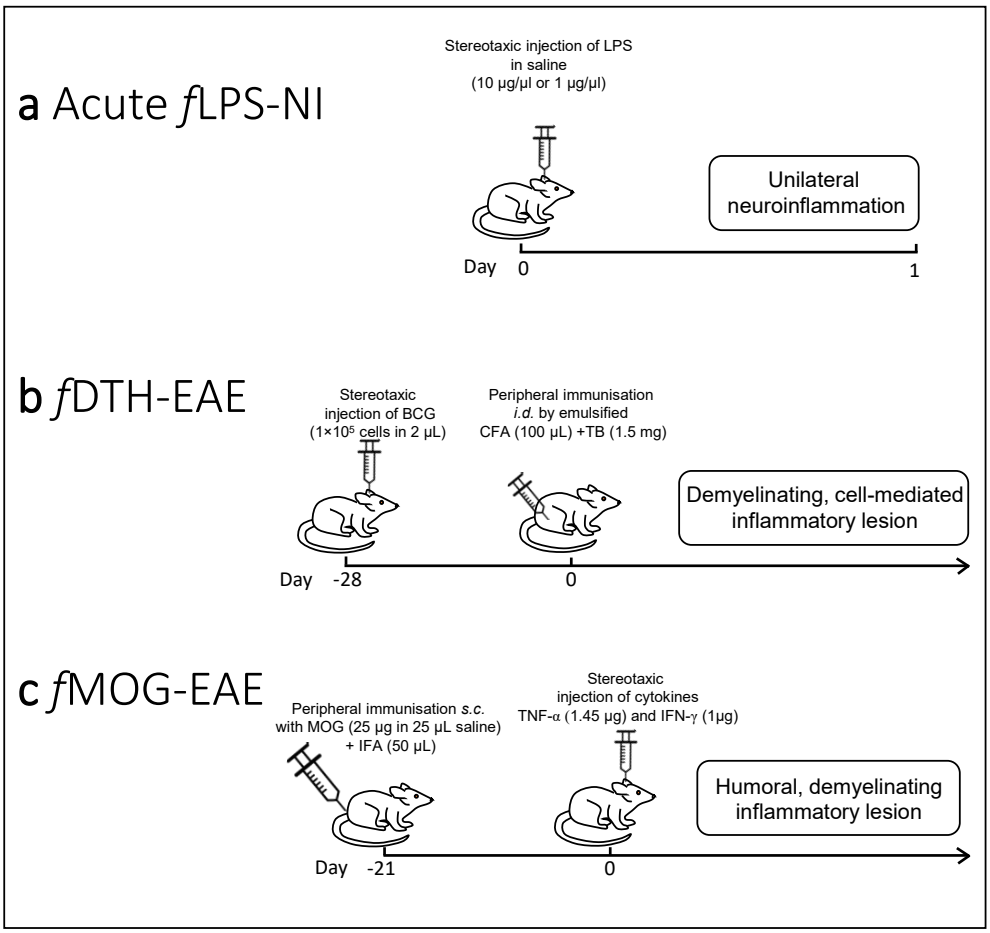

Figure 5. Timeline showing induction methods for the three different animal models used in this thesis. **a** The acute *f*LPS-NI model was induced by stereotaxic injection of 1 or 10 µg of LPS into Lewis rats, which causes widespread unilateral NI on the injected hemisphere within 16-24 h after the injection. **b** The *f*DTH-EAE was induced by first injecting the heat-killed BCG antigen intracerebrally into the right striatum and letting the BCG sequester behind the BBB (Matyszak and Perry, 1998), after which the lesion was activated by peripheral immunisation of the rat by injecting heat-killed TB in emulsified CFA intradermally. **c** The *f*MOG-EAE model was created by first immunising the animal peripherally with MOG in emulsified IFA, after which the lesion was created in a stereotaxic operation using the cytokines TNF-α and IFN-γ.

4.1.1 LPS model of acute neuroinflammation

For the induction of the acute LPS-NI model (Figure 5**a**), male Lewis rats (LEW/HanHsd) were acquired from Harlan Laboratories (Horst, Netherlands). Before the procedure, the rats were anaesthetised in a chamber using an isoflurane (Baxter Medical AB, Kista, Sweden) /oxygen mixture (3% of isoflurane with 700–800 mL/min of O_2 for induction, and 2.5% of isoflurane with 400–500 mL/min of

O_2 for maintenance during the procedure), and given as analgesic the opioid Temgesic *s.c.* (0.3 mg/ml, Reckitt-Benckiser Healthcare, Hull, UK; 0.05 mg/kg). Once asleep, the rats were placed in a stereotaxic frame (Kopf Instruments, Tujunga, California, USA) in a prone position on a heating pad. Oftagel (2.5 mg/g, Santen, Tampere, Finland) was applied to the eyes to avoid drying during the procedure. The head was shaved and disinfected using Betadine (Oy Leiras Takeda Pharmaceuticals Ab, Turku, Finland) after which a midline incision was made. A burr-hole (diameter 1.5–2 mm) was drilled on the skull with a dentist's drill to a determined position in the stereotaxic equipment (bregma: antero-posterior +1 mm; lateral -3 mm). The injection of LPS 1 µL (10 µg/µL or 1 µg/µL E. coli 026:B6, Sigma-Aldrich, St. Louis, Missouri, USA) in saline, or saline only for the controls, was made into the striatum (dorsal-ventral -4.0 mm). After the injection, the glass pipette was slowly pulled out and the incision sutured using 3/0 braided silk (Covidien, Dublin, Ireland).

A thin glass pipette was created from patch-clamp capillaries to minimize the mechanical damage and subsequent inflammation caused by the needle while injecting the toxin. Animals were used for imaging 16–24 h after the intrastriatal injection.

4.1.2 Focal models of MS

To induce the *f*DTH-EAE (Figure 5**b**) and *f*MOG-EAE (Figure 5**c**) models, male Lewis rats (LEW/Crl) were acquired from Charles River (Sulzfeld, Germany). The *f*DTH-EAE model was created by first injecting the antigen into the brain, letting the acute inflammation from the surgery subside, and the BCG sequester behind the BBB (Matyszak and Perry, 1998), after which the lesion was activated by peripheral immunisation by heat-killed TB in CFA. The *f*MOG-EAE model, on the other hand, was created by first immunising the animal peripherally with $MOG_{35–55}$ in IFA, after which the lesion was created in a stereotaxic operation using cytokines (Serres et al., 2009). Rats were anaesthetised similarly as the LPS-NI animals using isoflurane/oxygen (4–5% of isoflurane with 700–800 mL/min of O_2 for induction, and 2–3.0% of isoflurane with 400–500 mL/min of O_2 for maintenance during the procedure). Before the operation, the opioid drug Temgesic 0.3 mg/ml (*s.c.*, Reckitt-Benckiser Healthcare, Hull, UK; 0.05 mg/kg) was administered. The rats were placed in the stereotaxic frame (Kopf Instruments, Tujunga, California, USA) on a heating pad in a prone position.

To induce the *f*DTH-EAE model, heat-killed BCG (1×10^5 cells in 2 µL of PBS from the Pharmacology department in Oxford, United Kingdom) was injected into the right striatum by using a Hamilton syringe (10 µL; Sigma-Aldrich) with the coordinates (antero-posterior +1 mm; lateral -3 mm; dorsal-ventral -4.0 mm) (Paxinos and Watson, 1986). The injection was performed in four 0.5 µL volumes

within the dorsal-ventral depth -4.0–2.5 mm over 10 minutes. The incision was sutured by braided silk and the animals were allowed to recover under analgesia for 2 days (Temgesic 0.3 mg/ml: 0.05 mg/kg; Reckitt-Benckiser Healthcare, Hull, UK). 28 days after the intracerebral injection, the lesion was activated by an injection of TB (1.5 mg, Difco Laboratories, Detroit, MI, USA) emulsified in CFA (100 µL, Sigma Aldrich, Saint Louis, MO, USA) intradermally into the animal's flanks.

The *f*MOG-EAE model was created by first activating the peripheral immune system against MOG by injecting 100 µL of $MOG_{35–55}$ peptide (25 µg of diluted in 25 µL saline; Sigma-Aldrich, St. Louis, MO, USA) emulsified in IFA (50 µL; Sigma-Aldrich, St. Louis, MO, USA) subcutaneously into the base of the tail. After 21 days, the stereotaxic operation was performed using the same specifications as with the *f*DTH-EAE model, but the injected antigens were 1.45 µg of recombinant rat tumour necrosis factor α (TNF-α, Sigma-Aldrich, St. Louis, MO, USA) and 1 µg of recombinant rat interferon γ (IFN-γ, Sigma-Aldrich, St. Louis, MO, USA) dissolved in 2 µL of sterile saline.

4.2 Experimental design

The experimental design for the three different studies is illustrated in Figure 7. In Study I, the *f*LPS-NI model (n = 18) and control, sham-operated rats (n = 12) were applied 16 h after the intrastriatal injection of LPS or saline for comparison of the two radiotracers, [^{11}C]PK11195 and [^{18}F]GE-180. The methods that were applied in Study I were *in vivo* PET, *ex vivo* ARG, biodistribution measurements, as well as *in vitro* blocking and IHC against OX-42 and glial fibrillary acidic protein (GFAP). In Study II, the *f*DTH-EAE model (n = 17) was applied for efficacy assessment of anti-VLA-4 mAb treatment using *in vivo* PET and IHC for the ionised calcium-binding adapter molecule 1 (Iba1) staining. In Study III, both the *f*DTH-EAE (n = 24) and the *f*MOG-EAE (n = 8) models were applied to evaluate DMF therapy using *in vivo* PET and IHC for Iba1, CD4 and CD8. In addition, naïve S-D rats (n = 4) and the *f*LPS-NI model (n = 2) were applied for the evaluation of radiometabolites. Both treatment intervention specifications were based on previous literature (Schilling et al., 2006) and the rats were randomly chosen for the treatment or control groups so that littermates consisted of both.

In Study II, one group of animals was used for TSPO PET imaging until day 142 (n = 8). These were treated by VLA-4 mAb (GG5/3 Ab, ELAN Pharmaceuticals, USA) or the matched isotype control mAb (JH70 6F10, ELAN Pharmaceuticals, USA) starting 30 days after the peripheral activation of the lesion. Another group of rats (n = 4: anti-VLA-4 treated n = 2, control n = 2) was used for IHC evaluation of the chronic lesion on day 44, after 14 days of treatment with anti-VLA-4 mAb or the control Ab. Anti-VLA-4 or the control Ab was dosed *s.c.* 5 mg/kg every third day

during the days 30–61, and imaged on days 30, 44, 65, 86, and 142 after the peripheral activation of the lesion. The body weight was registered right before each of the PET scans.

In study III, the *f*DTH-EAE and *f*MOG-EAE rats were treated twice daily *per os* with 15 mg/kg of DMF (Sigma-Aldrich Chemie GmbH, Steinheim, Germany) diluted in 0.08% aqueous Methocel (Sigma-Aldrich Chemie GmbH, Steinheim, Germany), or vehicle (tap water with 0.08% Methocel) for controls, using an oral gavage starting on day 0. To aid the dissolution of DMF, Methocel was applied and the solution was sonicated for 15 min. The *f*DTH-EAE (n = 4 treated and n = 4 control) rats were imaged by PET (25–50 min) at baseline (d 0), at the acute phase of inflammation (at 1–2 weeks), chronic phase (at 4–8 weeks), and after halting the treatment for 10 weeks (at 18 weeks) to evaluate the potential rebound effect. Rats were euthanised for IHC after the last PET study. Furthermore, for IHC staining, there were two groups of *f*DTH-EAE animals: one euthanised after 2 weeks of treatment, and one after 4 weeks of treatment, to correspond with the time points of PET imaging. Also, weight gain was measured throughout the imaging period. The *f*MOG-EAE rats (n = 4 treated and n = 3 control) were imaged using only static PET (25–50 min).

Radiotracers for *in vivo, ex vivo*, and *in vitro* imaging (Figure 6) were produced at the Radiopharmaceutical Chemistry Laboratory of Turku PET Centre, or the Radiochemical laboratory in Gadolinia. Synthesis of [^{11}C]PK11195 ($logD_{7.4}$ = 4.58) (Pike, 2009; Shah et al., 1994) and [^{18}F]GE-180 ($logD_{7.4}$ = 2.95) (Wadsworth et al., 2012; Wickstrøm et al., 2014) was performed as previously described. The radionuclides, [^{11}C] ($T_{½}$ = 20.4 min) and [^{18}F] ($T_{½}$ = 109.8 min), were produced by a CC-18/9 or MGC-20 cyclotron (D.V. Efremov Research Institute, St. Petersburg, Russia) at the Accelerator Laboratory of the Åbo Akademi University.

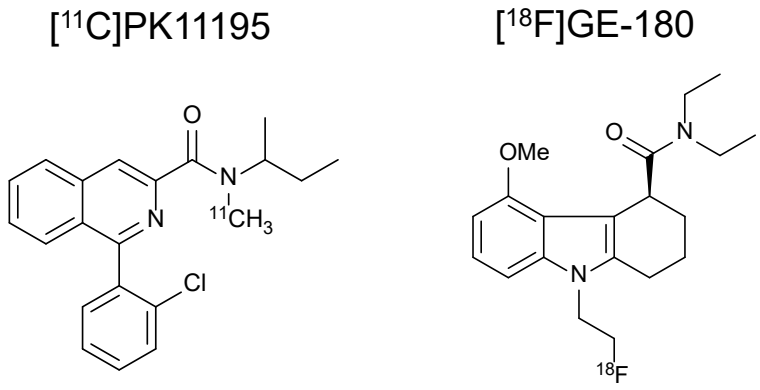

Figure 6. Chemical structures of **a** [^{11}C]PK11195 and **b** [^{18}F]GE-180 that were used in the PET imaging of this thesis.

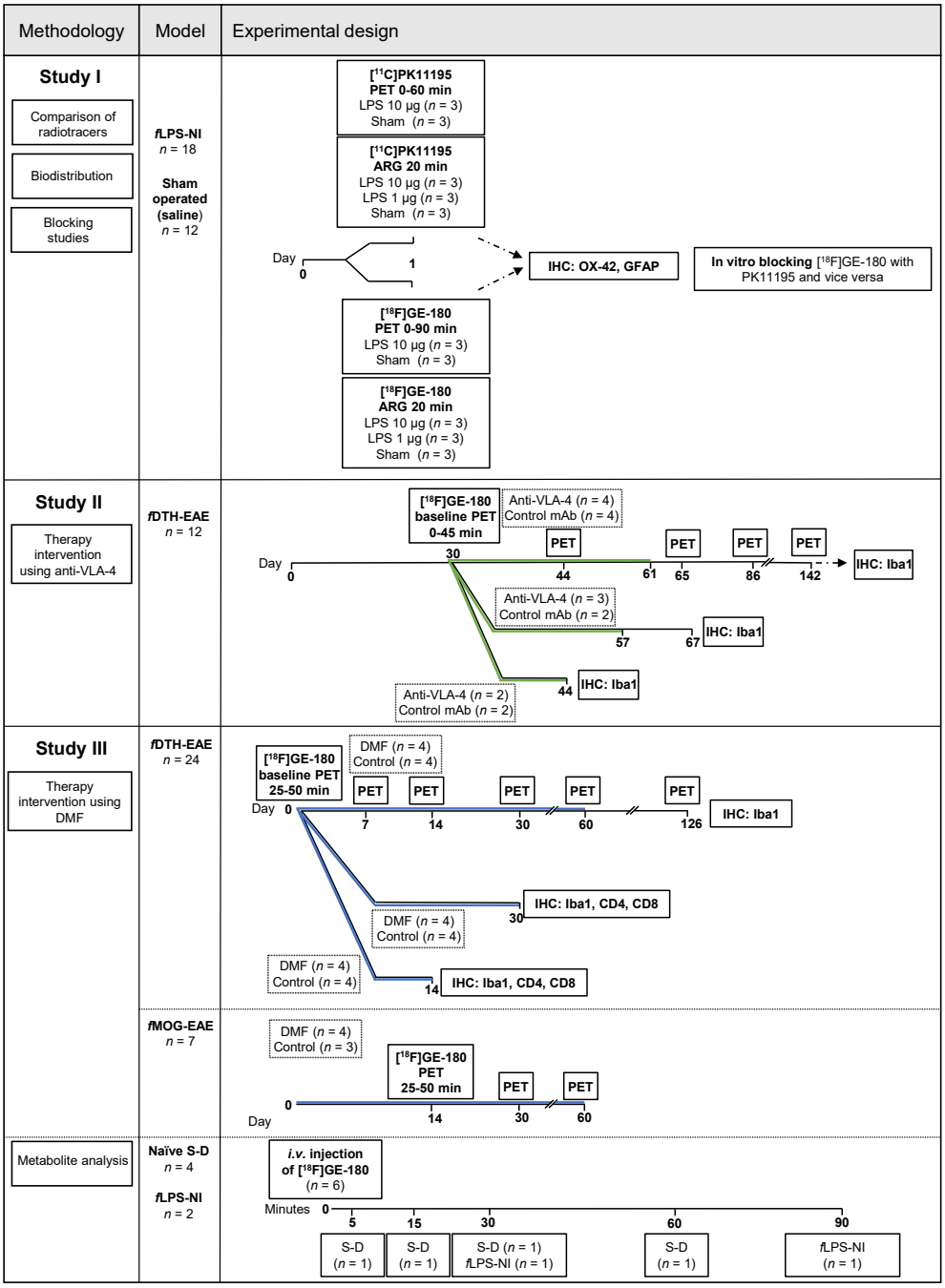

Figure 7. Timelines showing the experimental design of the different studies in this thesis. The green line indicates the treatment period with anti-VLA-4 5 mg/kg every third day. The blue line indicates the treatment period with DMF 15 mg/kg twice a day.

4.3 Small animal *in vivo* PET/CT imaging

PET/CT imaging of the rats was performed using a dedicated Inveon Siemens multimodality PET/CT scanner (Siemens Medical Solutions USA, Knoxville, TN) designed for small laboratory animals. All the rats were anaesthetised with isoflurane/oxygen (4–5% of isoflurane with 700–800 mL/min of O_2 for induction, and 2–3.0% of isoflurane with 400–500 mL/min of O_2 for maintenance) 20 min before the tracer ([^{11}C]PK11195 or [^{18}F]GE-180) injection. Body temperature during imaging was maintained using a heating pad and covering the rats with a piece of bubble wrap. Oftagel (2.5 mg/g, Santen) was applied to the eyes to avoid drying of the eyes during anaesthesia and imaging.

In study I, a CT scan was obtained for attenuation correction. Thereafter, an emission scan of 0–60 min (frames 30×10 s, 15×60 s, 4×300 s, 2×600 s) using [^{11}C]PK11195 or 0–90 min (frames 30×10 s, 15×60 s, 4×300 s, 1×600 s) using [^{18}F]GE-180 in list mode with an energy window of 350–650 keV was acquired. The dynamic scans were started immediately after the intravenous injection of the radiotracer. In study II, the CT scan was obtained after which a dynamic emission scan 0–45 min using [^{18}F]GE-180 was acquired (frames 30×10 s, 15×60 s, 5×300 s). In study III, following the CT transmission scan, a static PET image (frames 5×300 s) was obtained 25–50 min after the injection of [^{18}F]GE-180 at time point 0 min. In studies II and III, two rats were imaged at once due to the limited number of tracer syntheses to maximise the number of scans for each imaging date. The images were later divided to perform individual analysis on each animal.

PET images in Study I were reconstructed using FBP, but they were re-reconstructed later using OSEM3D, which had just become available in our facilities. All PET images in the other studies were reconstructed twice by OSEM3D and by 18 iterations of MAP with the target resolution of 1.5 mm.

4.4 *Ex vivo* methods

Three different *ex vivo* methods were applied in this thesis to validate the results obtained from *in vivo* imaging. First, the biodistribution of the radiotracer in the collected organs at the time of euthanasia was described (Study I). Second, the radio metabolite analysis showed dissociation of the radiotracer at different pre-determined time points, and their binding to plasma proteins (Study III). Third, digital autoradiography (ARG) analysis illustrated the tracer binding quantitatively with 25 μm^2 resolution (Study I).

4.4.1 Biodistribution studies

Biodistribution of radiotracers was studied in the acute *f*LPS-NI model (Study I) to evaluate tracer properties, control the normal biodistribution of the tracer, evaluate the success of the injection, and observe whether there is defluorination of [^{18}F]GE-180 in this model. The organs that were reported to have increased binding of [^{11}C]PK11195 or [^{18}F]GE180 were collected (Luoto et al., 2010). The predetermined organs were dissected from the carcass immediately after euthanisation of the rat. The organs were weighed and the radioactivity was measured in a NaI(Tl) well counter (3×3 in., Bicron, Newbury, Ohio, USA), or in a VDC-405 Dose Calibrator (Veenstra Instruments, Joure, The Netherlands).

The radioactivity of the [^{11}C]PK11195 and [^{18}F]GE-180 imaged animals was measured as injected activity per gram of tissue (%IA/g) for a blood sample, plasma sample, erythrocyte sample, kidneys, lungs, adrenals, a urine sample, heart, spleen, thyroids, a sample from the cerebellum, and the whole brain. In addition, a sample of the skull bone and olfactory bulb was measured from the [^{18}F]GE-180 imaged animals. To control the success of the tail vein injection, the tail radioactivity was measured for all animals to see if the tracer entered the systemic circulation.

4.4.2 Radiometabolite analysis

To understand the parent fraction characteristics of [^{18}F]GE-180, its radiometabolites were analysed by thin-layer chromatography (TLC) coupled with autoradiography digitation (radio TLC) from rat plasma and brain tissue at 5, 15, 30, and 60 min using 4 naïve S-D rats (n = 1 per time point) and 2 *f*LPS-NI Lewis rats (at 30 and 90 min). Blood samples were collected via cardiac puncture into heparinised Microtainer tubes (BD, Franklin Lakes, NJ, USA) and centrifuged (4 min, 3030 g). The separated plasma was mixed with methanol:plasma (3:2, vol/vol), vortexed, and proteins were precipitated with a centrifuge. Brain homogenate was mixed in methanol:water (9:1, vol/vol) using a glass homogeniser and centrifuged (4 min, 3030 g) to obtain a clear, protein-free homogenate. To determine the correct retardation factor (R_f-factor), a radioactive standard was prepared to distinguish the parent compound from the metabolites.

The supernatants from plasma and brain homogenates, and the radioactive standard were applied on a high-performance TLC plate (HPTLC, silica gel 60 RP-18, art no. 1.05914.0001, Merck KGaA, Darmstadt, Germany). The HPTLC plate was dried and eluted with methanol:water (9:1, vol/vol) in a Twin Trough Chamber (Camag, Muttenz, Switzerland) with a migration distance of 4 cm. The dried plate was exposed to an ARG plate (BAS-TR2025, Fuji Photo Film Co, Ltd, Tokyo, Japan) and scanned with a Bioimaging Analyzer Systems 5000 phosphor imager

(BAS-5000, Fuji, Tokyo, Japan). The percentage of parent fraction was calculated from the unchanged [^{18}F]GE-180 over the total radioactivity of the sample.

In addition, plasma protein binding was determined by ultrafiltration to characterize the plasma free fraction of the radioactivity. A plasma sample from each animal was applied on the TLC plate (silica gel 60, art no. 1.05554.0001, Merck KGaA, Darmstadt, Germany) and the remaining plasma was ultrafiltered using a 30-kDa cut-off ultrafilter (20 min, 1300 g) with regenerated cellulose membrane (Centrifree® Ultrafiltration Centrifugal Filters, Merck KGaA, Darmstadt, Germany). On the same TLC plate, a sample of the filtrate (5 µL) from each rat was applied. The TLC plate was dried and scanned using ARG similarly to the radiometabolite analysis. To obtain the free fraction of radioactivity in the plasma, the radioactivity concentration of the filtrate (protein-free analyte) was divided by the radioactivity concentration of the original plasma (protein-free + protein-bound analytes).

4.4.3 Autoradiography analysis

Ex vivo ARG imaging was performed in Study I using both [^{11}C]PK11195 and [^{18}F]GE-180. The animals were anaesthetised with isoflurane (Baxter Medical AB, Kista, Sweden) mixed with air (induction 4%, 700 ml/min, maintenance 2.5%, 400 ml/min). The tracer was injected *i.v.* into a lateral tail vein as a bolus followed by flushing with saline (~200 µl). At time point 20 min, the animal was killed by an overdose of anaesthesia. Blood was removed by doing a cardiac puncture and the animal was perfused with heparinised saline. The brain was immediately removed and frozen by immersing in isopentane (C_5H_{12}, Sigma Aldrich, St. Louis, Missouri, USA) that was cooled with dry ice to –40 °C.

The brain was mounted in Tissue-Tek® OCT™ Compound (Sakura Finetek Europe B.V., Alphen aan den Rijn, Netherlands) freezing medium and sectioned into 40 or 20 µm for [^{11}C]PK11195 and [^{18}F]GE-180 imaged rats, respectively, using a Leica CM 3050 S cryostat (Leica Microsystems, Germany). The sections were mounted on adhesion slides (Superfrost Ultra Plus®, Thermo Fisher Scientific, USA), and after drying with a hairdryer, the sections were exposed to the BAS-TR2025 imaging plates (Fuji Photo Film Co, Ltd., Tokyo, Japan) with the exposure time twice the $T_{½}$ of the isotope, i.e. some 40 min for [^{11}C]PK11195 and some 3.5 hours for [^{18}F]GE-180. The imaging plates were scanned using the Bioimaging Analyzer Systems 5000 (BAS-5000, Fuji Photo Film Co, Ltd., Tokyo, Japan) phosphor imager.

4.5 *In vitro* methods

The *in vitro* methods applied in this thesis were blocking studies of the radiotracers and IHC staining against specific tissue markers of interest. *In vitro* experiments were performed on tissue sections that were excised from the animals in the *in vivo* experiments.

4.5.1 Blocking studies

To detect whether [^{11}C]PK11195 and [^{18}F]GE-180 are binding to the identical target, an *in vitro* blocking assay was performed. Tracer binding can be evaluated *in vitro* using the radiotracer and its known competitor, a buffer system, and ARG for imaging purposes (Haubner and Decristoforo, 2011). The competitor is used in excess when compared to the radiotracer to ensure total blocking. Here, [^{11}C]PK11195 binding was blocked with unlabelled GE-180 and vice versa.

First, sections from *f*LPS-NI (10 µg) and vehicle-injected rats were defrosted and pre-incubated in 50 mM Tris-HCl (pH 7.4, room temperature RT) for 30 minutes. Then the sections were incubated with [^{11}C]-PK11195 (0.67 MBq, ~50 pM) or [^{18}F]GE-180 (0.42 MBq, ~50 pM,) after which non-specific binding of the tracers was determined by addition of the unlabelled compound, GE-180 (90 nM) or PK11195 (90 nM), respectively. Thereafter, the sections were washed in cold Tris-HCl (2 × 5 min) and to remove buffer salts, rinsed in ice-cold distilled water. After drying, the sections were exposed to the BAS-TR2025 phosphor imaging IPs (Fuji Photo Film Co, Ltd., Tokyo, Japan) for a period of two half-lives of the radiotracer in question. The imaging plates were scanned using the Bioimaging Analyzer Systems 5000 (BAS-5000, Raytest Isotopenmeßgeräte GmbH, Straubenhardt, Germany) and analysed using the AIDA 2D densitometry software 4.6 (Raytest Isotopenmeßgeräte GmbH, Straubenhardt, Germany) by drawing ROI's into the cortical and striatal areas and calculating the *ex vivo* binding potential using the formula:

$$\mathrm{BP}_{ex\ vivo} = \frac{(\mathrm{PSL/mm^2})_{lesion} - (\mathrm{PSL/mm^2})_{contralateral}}{(\mathrm{PSL/mm^2})_{contralateral}}$$

4.5.2 Immunohistochemistry

IHC in this thesis was partially performed at the Medicity Research lab and partially by HistoCore (University of Turku). In Study I, rats were euthanised immediately after the *in vivo* PET for ARG analysis, and therefore the rats were perfused rapidly using heparinized saline during the cardiac puncture after which the brain was snap-

frozen by immersion in isopentane at –40 ºC for further imaging. The same sections that were applied in ARG, were used for IHC in Study I.

In Studies II and III, *ex vivo* imaging was not applied, which allowed the more time-consuming perfusion fixation protocol. The rats were euthanised by an overdose of sodium pentobarbital (Mebunat vet 10 mg/100 g, *i.p.*, Orion Pharma, Turku, Finland) and perfused with heparinised saline and periodate-lysine-paraformaldehyde (PLP)-light-fixative containing 0.1% glutaraldehyde using a perfusion pump (Harvard Apparatus, Holliston, Massachusetts, United States). After this, the brain was excised and post-fixed in PLP light for 4 hours after which they were cryoprotected in a 30% (w/v) sucrose solution for 2 days. After this, the brain was mounted in Tissue-Tek® OCT™ Compound (Sakura Finetek Europe B.V., Alphen aan den Rijn, Netherlands) and snap-frozen in isopentane (Sigma Aldrich, St. Louis, Missouri, USA) chilled with dry ice (–40 °C) for later use. The brains were cut using a Leica CM 3050 S cryostat (Leica Microsystems, Germany) into 10 µm sections using a protocol allowing semi-quantitation after staining. Continuous cutting allowed staining with 100-µm intervals through the *f*DTH lesion area 750 µm from the lesion core on either side.

Given that a proper TSPO Ab was not available at our laboratory at the time of the studies, CD11b clone Ab recognising integrin alpha-M (OX-42; Serotec MCA275R, Mouse-anti-rat, Oxford, UK) and anti-Iba1 (Wako 019-19741, Rabbit-anti-rat, Wako Chemicals GmbH, Neuss, Germany), both CD11b markers, were chosen to depict microglial activation in the study subjects. In Study I, also GFAP (Millipore, Billerica, USA) staining was performed to detect astrocytes. The sections were first blocked using normal horse serum (10% in PBS) for 1 h, washed with PBS, and incubated with the primary Ab overnight at 4 °C. After this, the sections were incubated with a biotinylated secondary antibody (rat adsorbed horse-anti-mouse IgG for OX-42, horse-anti-goat IgG for GFAP; Vector, Peterborough, UK; or anti-rabbit IgG for Iba1, Invitrogen, Camarillo, CA, USA) for 1 h at RT. The immunostaining was then incubated with avidin-biotin-peroxidase complex (Vectastain Elite kits, Vector Laboratories, Burlingame, CA, USA), developed using 3,3′-diaminobenzidine (DAB; SIGMAFAST, Sigma-Aldrich, Saint Louis, MO, USA), and to stain the nuclei, counterstained with cresyl violet.

In Study III, staining was performed in a semiautomatic Labvision autostainer (Thermo-Fisher Scientific, Vantaa, Finland). The sections were pre-heated in citrate buffer (pH 6, Genmed), blocked with hydrogen peroxide and pre-protein block (Draco Ab diluent; WellMed), and incubated with either Iba1 (Wako, 1:2000 dilution, RT), anti-CD4 (Abcam, ab33775, dilution 1:50), or anti-CD8 (Abcam, ab33786, dilution 1:200) for 60 min at RT. For the anti-Iba1 staining, the Orion 1 step detection system (Goat anti-rabbit HRP; Wellmed) was used as a secondary Ab for 30 min at RT. For anti-CD4 and anti-CD8 staining, the Bright vision 1 step

detection system (Goat anti-mouse HRP) was used. The sections were stained with DAB (Taurus; Wellmed) and counterstained with Mayer's haematoxylin.

Different methodologies were applied in the quantification of the immunostainings of this thesis. In Study I, the number of OX-42$^+$ cells were calculated as an average count per area from three random locations in the cortex and striatum. In Studies II and III, the Iba1-immunopositive area was calculated semi-quantitatively. In Study II, the hypercellular lesion core volume was estimated by integrating the lesion areas with 300 µm intervals through the length of 1200 µm. In Study III both the perilesional area and the hypercellular core were evaluated with 100 µm intervals through the distance of 1500 µm by delineating the area of darker staining using CaseViewer 2.1 software (3DHISTECH Ltd., Budapest, Hungary). Integration of the volume using the trapezoidal rule was applied to each subinterval. The perilesional volume and the lesion core volume was estimated:

$$V = \frac{1}{2}\sum_{i=0}^{n-1}(x_{i+1} - x_i)(y_i + y_{i+1}),$$

where x = is the position of the cutting plane and y is the area of the region of interest (ROI).

Moreover, to detect T lymphocytes, brain sections adjacent to the lesion core that was detected by anti-Iba1 staining were selected for analysis. Because individual CD4$^+$ and CD8$^+$ T cells could not be detected, quantitation was performed by measuring the optical density (OD). The image was deconvolved to an 8-bit image representing the DAB staining (Fiji ImageJ v1.52p). A ROI was drawn on the coronal brain section in the lesion core, in the perilesional area, and to the contralateral side, which corresponds to the lesion core on the ipsilateral side. OD_{ROI} was calculated using the formula (NIH, 2021; Ruifrok and Johnston, 2001):

$$OD_{ROI} = \log\left(\frac{maximum\ intensity}{mean\ intensity_{ROI}}\right),$$

in which maximum intensity is 255 that corresponds white in an 8-bit image, and mean $intensity_{ROI}$ is the mean intensity from the lesional or perilesional area obtained from three brain sections within one individual. The final OD count was obtained by subtracting the contralateral OD_{ROI} from the lesional or perilesional OD_{ROI}, i.e. OD= $OD_{ROIlesion\ or\ perilesion}$– $OD_{ROIcontra}$.

4.6 *In vivo* image analysis

In Study I, image analysis was performed in Carimas (2.6, University of Turku) by calculating the binding potential (4.6.1) by drawing spherical VOI's in the ipsilateral and contralateral hemispheres. To increase spatial visualisation of the tracer binding,

the *f*LPS-NI rats were further modelled three-dimensionally (3D). Alignment of PET images was performed to the Schiffer template in PMOD (3.4) and pixel-wise calculation of the BP_{ND} was conducted based on values from a spherical contralateral reading (Matlab R2011a; The MathWorks). Averaging and subtraction of the processed images was completed in Statistical Parametric Mapping (SPM 8; Wellcome Trust Centre for Neuroimaging).

In Study II, image processing was performed in Pmod 3.4 (Pmod Technologies, Zurich, Switzerland) the analysis in MatLab 2011 (The MathWorks, Natick, MA, USA). The image analysis for Study II was optimised several times using different software, starting with Inveon Research Workplace, Carimas, and Pmod, and testing different methodologies for analysis before deciding the final analysis approach for the whole dataset, which was the simplified reference tissue model (SRTM; 4.6.2). For Study III, analysis was performed in Pmod 3.4.

First, in Study II, the preliminary analysis on day 14 data was performed using the image analysis software provided by the scanner manufacturer Inveon Research workplace (Inveon, Siemens) by applying a sphere of different sizes (ø 0.5–1 mm) on the lesion area. In this sphere approach, however, lesion delineation is only directional, because lesion shape varies between individuals. Thus, a hotspot was applied within the lesion with a visual inspection. This analysis was later confirmed using Carimas 2.6, to observe whether results vary between software.

Due to variance in the results, a thresholding approach was applied, where a percentage of the voxels with increased binding in reference to the contralateral binding is determined. Here, the threshold value was obtained by measuring the contralateral binding and considering values over the binding on the contralateral side and adding two standard deviations (SD). The threshold was set to 40% and 60% of the maximal binding within a specified volume of interest (VOI). Because we were interested in the perilesional binding of the tracer, we sought also to test a "donut"-method, in which the threshold was set to 40–85% or 60–85% of the maximal binding. However, setting the threshold seemed arbitrary, so finally, we decided to evaluate the SRTM approach, which is explained later. For this, normalised, parametric BP_{ND} maps were created to be able to compare images from different imaging sessions with each other. The lesion was first delineated using a small spherical VOI (1.5 mm^3), but delineation using the isocontour tool seemed to portray the lesion better. The decision was supported by calculating the coefficient of variation (anti-VLA-4 treated 40%; Control 45%), which expresses the precision and repeatability of an assay by determining the ratio of the SD to the mean.

Because imaging in Studies II and III was performed simultaneously for two rats, the images were divided before the analysis. Pre-processing of the images required alignment of the PET scan to the Schiffer MR template that was inbuilt into the PMOD software. First, the PET was aligned to the CT space, after which the CT was

aligned to the MR space. When the two transformations had been combined, the output was manually supervised and motion correction was applied whenever needed. Having the animals in the MR space allowed the contralateral input to be positioned in the same place within all animals in Study II. In Study III, the alignment allowed the use of a single VOI throughout the imaging time points.

4.6.1 Binding potential

In all three Studies, the binding potential was the outcome measure in the analysis of the *in vivo* imaging. Binding potential is the most commonly used output describing the specific binding of a radiotracer to its receptor (Sridharan et al., 2017). The non-displaceable binding potential (BP_{ND}) is a typical measurement in reference tissue methods, which describes the specifically bound radioligand in the ROI compared to the non-displaceable radioligand uptake within a reference region (Innis et al., 2007). However, in Study I, BP_{ND} was referred to as bound-to-free ratio due to inaccuracies in nomenclature.

In Study I, BP_{ND} was obtained by determining the window for maximal binding (25–50 min), drawing a spherical VOI on the ipsilateral side, mirroring the obtained VOI to the contralateral side, and applying the values to:

$$\mathrm{BP}_{ND} = \frac{(\int_{25}^{50} \mathrm{TAC})_{lesion} - (\int_{25}^{50} \mathrm{TAC})_{contralateral}}{(\int_{25}^{50} \mathrm{TAC})_{contralateral}}$$

In Study III, the images were first summed to create a standardised uptake value (SUV) map (25–50 min). The volume of interest (VOI) was drawn using the Automatic Isocontour Detection tool, by choosing the time point where the lesion is at its largest (varied between individuals from week 1 to week 2). This VOI was then applied to all other time points within one individual. To calculate the BP_{ND}, a value from a contralateral, spherical VOI was obtained:

$$\mathrm{BP}_{ND} = \frac{(\mathrm{SUV})_{lesion} - (\mathrm{SUV})_{contralateral}}{(\mathrm{SUV})_{contralateral}}$$

For the *f*DTH-EAE rats in Study III, the $BP_{ND}\Delta_{dayX-day0}$ was calculated from parametric BP_{ND}-maps (25-50 min) to increase comparability of individuals. This was performed by normalising the BP_{ND} from all imaging time points (days 7, 14, 30, 60, and 126) to the BP_{ND} of the baseline image at day 0. The *f*MOG-EAE rats were not imaged at day 0 because it is the day of the intracranial procedure and performing TSPO imaging is not reasonable. Thus, results are indicated as BP_{ND} for all the available imaging time points on days 14, 30, and 60.

4.6.2 Simplified reference tissue modelling

In Study II, parametric BP_{ND} maps were created using an in-house made basis function implementation of SRTM (Gunn et al., 1997) in MatLab 2011 (The MathWorks, Natick, MA, USA). Reference tissue input was obtained from a spherical VOI (1.4 mm^3) on the contralateral hemisphere. The θ parameter was limited to 0.05−0.4 min^{-1}. Estimation of the BP_{ND} was based on 100 basis functions.

The regional mean BP_{ND} was determined from the BP_{ND} map using the isocontour tool, where the threshold value was manually determined on the edge of the lesion area by visual inspection. The lesion size varied within individuals and time points between sizes 1–11 mm^3. The outcome measure, change in BP_{ND}, was calculated by normalising each time point (i.e. day 44, 65, 86, or 142) to the baseline (i.e. day 30) value by using the formula $BP_{ND}\Delta_{dayX/day30}=\Delta BP_{NDdayX}/BP_{NDday30}$. Because the images were parametric, they were visually comparable, even though some variation may result from the reference area.

4.7 Statistical analyses

All preliminary statistical analyses were conducted using GraphPad Prism (5.1 or 9; San Diego, CA, USA) using a two-tailed, unpaired Student's t-test and the results were considered significant if $p < 0.05$. All measures are reported as mean (SD).

Multivariate analyses for therapy interventions were performed in SAS (9.4 for Windows; SAS Institute Inc., Cary, NC, USA) using a linear mixed model with a compound symmetry covariance structure. It included a time factor, a group factor, and their interaction that was used to assess whether the change over time was significantly different in the treated groups compared to the control groups. *Post hoc* analysis was applied if the interaction term was significant, and the logarithm of the response was used instead of the original values for the model to fulfil the normality assumption. In *post hoc* analyses, *p*-values were adjusted using the Tukey-Kramer method and the normality assumption was checked using the studentised residuals.

5 Results

5.1 Effect of the procedures and pharmaceuticals on animal welfare

Animal weight gain was reported throughout the studies (Figure 8). In Study I, significant differences were detected between the [^{18}F]GE-180 imaged *ex vivo f*LPS (10 µg) and sham-operated rats ($p = 0.01$), *f*LPS (1 µg) and sham-operated rats ($p = 0.03$), as well as the [^{11}C]PK11195 *in vivo* imaged *f*LPS (10 µg) and sham-operated rats ($p = 0.04$). Bodyweight increased significantly during the conduct of Studies II and III within the control and treated groups, but no differences were detected between the studied groups. During the conduct of the studies, we did not observe any differences between the weights of the vehicle-treated rats to the rats treated with either anti-VLA-4 or DMF. The weight did not differ between the groups overall.

In Study I, all but two animals ($n = 32$) recovered from the stereotaxic procedure. In studies II and III, all animals ($n = 44$) recovered from the *f*DTH and *f*MOG-EAE model-induction procedures, but during the week 4 PET study, one control animal died in the PET scanner, possibly due to overdose of anaesthesia. During the course of the studies, we did not observe any adverse effects or clinical manifestation of NI as sickness behaviour or motor abnormalities.

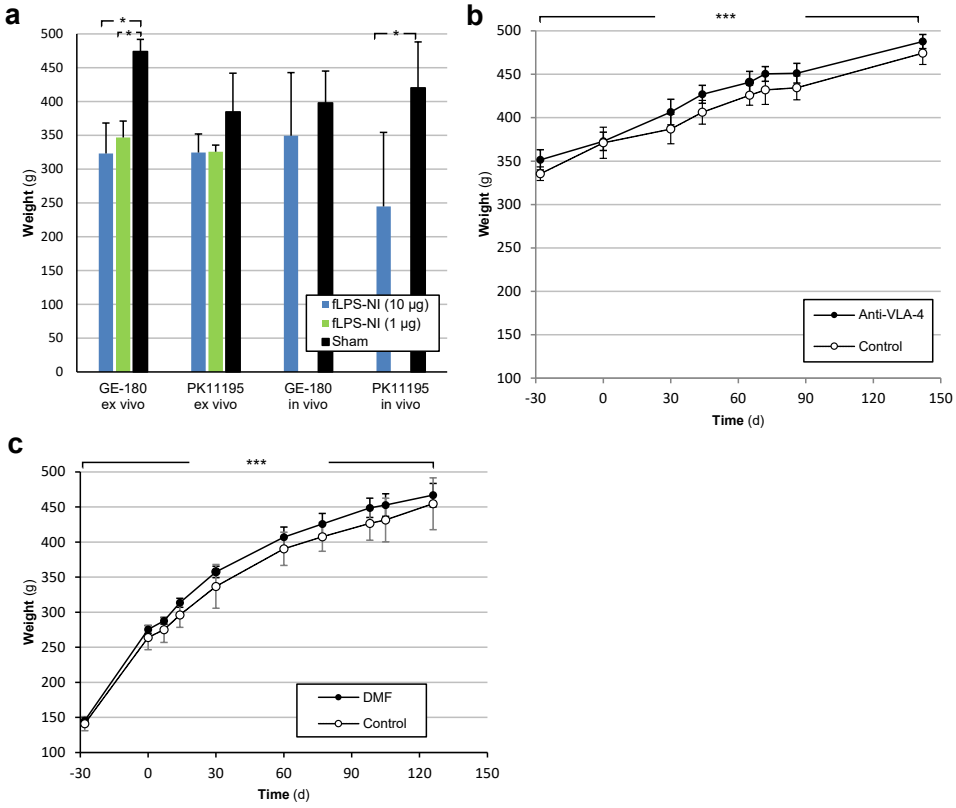

Figure 8. **Weight of rats**. **a** Weight of the *f*LPS-NI rats in Study I. **b** Weight gain of the *f*DTH-EAE rats during Study II. **c** Weight gain of the *f*DTH-EAE rats in Study III. * = p<0.05; *** = p<0.001.

5.2 Comparison of [^{18}F]GE-180 and [^{11}C]PK11195

Analysis of the biodistribution of the tracers in the *f*LPS-NI (1 µg or 10 µg) model and sham-operated animals (Figure 9) showed no differences between the studied tracers or groups. No overt defluorination of [^{18}F]GE-180, which would be expressed as skull bone binding, was detected. Overall tracer uptake in the brain was not increased, even though the intrastriatal injection of LPS unilaterally caused a diffuse inflammatory lesion in the injected hemisphere, which was detected by *ex vivo* ARG (Figure 10), *in vivo* PET imaging (Figure 11), and staining for OX-42 and GFAP (Study I). Increased TSPO binding in the injected hemisphere was detected using 10 µg and 1 µg injections of LPS, while the sham operated rats injected with saline, showed only a minor increase in uptake.

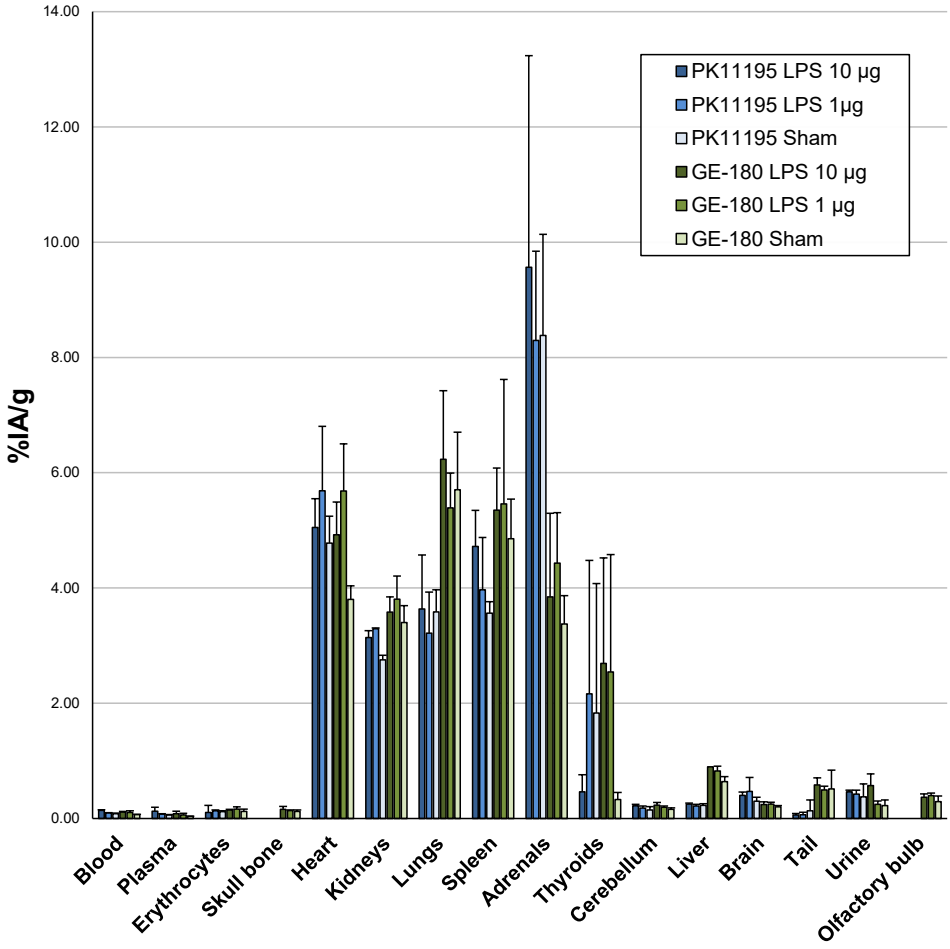

Figure 9. Biodistribution of [^{11}C]PK11195 and [^{18}F]GE-180 in the *f*LPS-NI (1 µg or 10 µg) and sham-operated rats (*n* = 3/group). No significant differences were observed between the studied tracers when analysed with one-way ANOVA. Skullbone and olfactory bulb samples were only collected from the [^{18}F]GE-180 imaged rats. No overt defluorination of [^{18}F]GE-180 was observed when looking at the skull bone biodistribution.

The properties of [^{18}F]GE-180 were further evaluated by radiometabolite analysis of [^{18}F]GE-180 using radio TLC. The method indicated five distinguishable radiometabolites in plasma, whereas previous studies using high-performance liquid chromatography (HPLC) showed up to three radiometabolites (Boutin et al., 2015). The parent fraction of [^{18}F]GE-180 in rat plasma followed a hill function, as expected. The unmetabolized fraction of [^{18}F]GE-180 in plasma was 0.81, 0.55, 0.31, and 0.23 at time points 5, 15, 30, and 60 minutes, respectively. The parent fraction of [^{18}F]GE-180 in the brain was 66–77% at all time points), which was slightly lower than previously reported (Boutin et al., 2015). Furthermore, Liu et al. (2015) have

reported slightly higher HPLC parent fraction in the mouse brain than what was found here (Liu et al., 2015).

By using the rapid ultrafiltration method for the plasma samples the fraction of radioactivity in plasma not bound to proteins was determined. The free fraction of radioactivity was 0.09, 0.31, 0.49, and 0.72 at time points 5, 15, 30, and 60 min, respectively, after the [^{18}F]GE-180 injection. Previously, the free fraction has been studied in human plasma using *in vitro* ultrafiltration methods and found to be 0.35 (0.011) (Zanotti-Fregonara et al., 2018).

The properties of [^{18}F]GE-180 were shown to be advantageous over those of [^{11}C]PK11195. Using *ex vivo* ARG imaging (Figure 10), increased uptake in the ipsilateral hemisphere was observed in the *f*LPS-NI (10 µg: 1.32 (0.13); 1 µg: 1.33 (0.17)) rats using [^{18}F]GE180 (p = 0.0004), but not with [^{11}C]PK11195. In the autoradiographs (Figure 10**c**), in addition to the NI that is visible on the injected hemisphere of the *f*LPS-NI rats, there is specific binding of both tracers, [^{11}C]PK11195 and [^{18}F]GE-180, in the ventricles, where the ependymal cells expressing TSPO are located, as well as the endothelial cells in the arteries and the venous sinuses. Therefore, no area in the brain is fully devoid of specific TSPO binding.

To assess the validity of the contralateral hemisphere as a reference area for calculation of the BP_{ND}, binding of [^{11}C]PK11195 in the contralateral hemisphere was compared to its binding in the cerebellum (Figure 10**b**). No differences were detected between the contralateral/cerebellum binding ratio of the *f*LPS-NI animals when compared to the sham-operated animals (p = 0.11).

Selectivity of [^{11}C]PK11195 and [^{18}F]GE-180 were shown in the *in vitro* binding studies, which indicated the reduced signal of the total binding of [^{11}C]PK11195 (Figure 11**a**; $p < 0.0001$) and [^{18}F]GE-180 (Figure 11**b**; $p < 0.001$) when blocked with GE-180 and PK11195, respectively.

In vivo imaging revealed that both tracers showed a difference in the *f*LPS-NI (10 µg) rats compared to the sham-operated rats ($p < 0.0001$), and additionally, [^{18}F]GE-180 showed increased uptake in the injected hemisphere ($p < 0.01$) compared to [^{11}C]PK11195 (Figure 12). Increased TSPO uptake was observed in the *f*LPS-NI (10 µg) rats ([^{11}C]PK11195 0.472 (0.057); [^{18}F]GE180 0.918 (0.068), but not in the controls ([^{11}C]PK11195 -0.002 (0.072), [^{18}F]GE180 0.000 (0.012) (Figure 12**b**). 3D pixel-wise modelling was performed to visually inspect tracer properties. Averaged and normalised BP_{ND} maps were modelled, using the time frame for maximal binding for both tracers (25–50 min), which was acquired from the bound-to-free TACs (Figure 12**a**). The resultant images indicate the larger segmented area when using [^{18}F]GE-180.

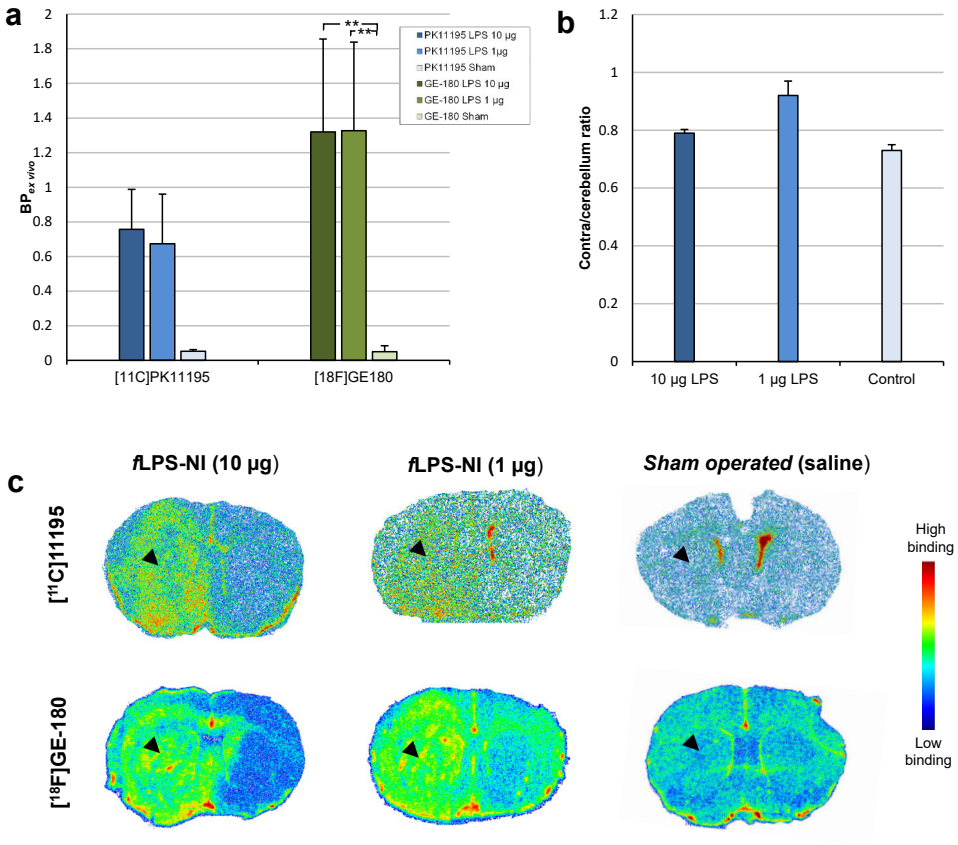

Figure 10. Comparison of [^{11}C]PK11195 and [^{18}F]GE-180 using *ex vivo* imaging of *f*LPS-NI. a ARG of [^{11}C]PK11195 and [^{18}F]GE-180 *f*LPS-NI (1 µg or 10 µg) and sham-operated rats (*n* = 3/group) showed an increase in the [^{18}F]GE-180 imaged *f*LPS-NI rats when compared to the sham-operated rats. **b** The use of the contralateral ROI as a reference area was evaluated by calculating the ratio between the contralateral ROI and the cerebellum from the *ex vivo* ARG by [^{11}C]PK11195. No differences were detected between the *f*LPS-NI and sham-operated animals. **c** Representative coronal autoradiographs from the *f*LPS-NI (1 µg or 10 µg) and sham-operated rats using [^{11}C]PK11195 and [^{18}F]GE-180. Arrowheads are pointing at the injection site.

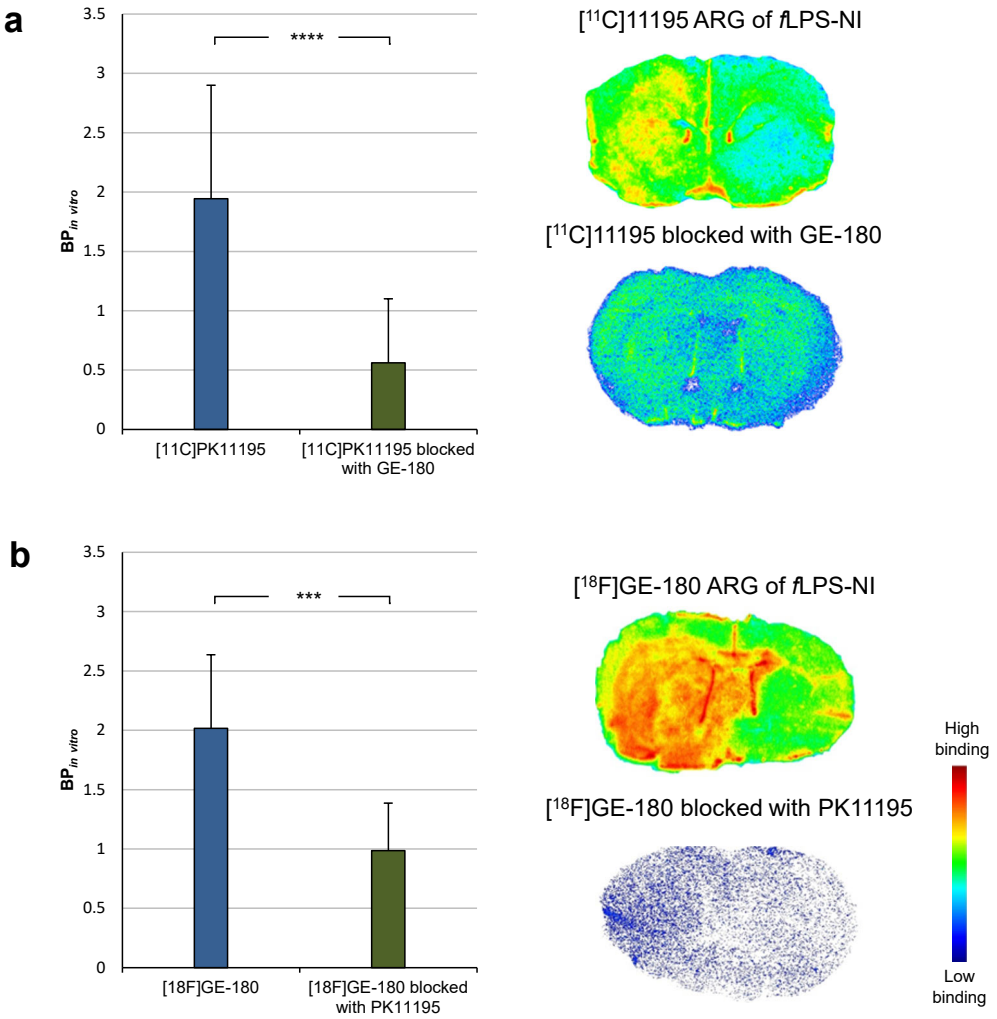

Figure 11. *In vitro* blocking studies demonstrating specificity of [^{11}C]PK11195 and [^{18}F]GE-180 with representative autoradiographs (colour scaling not comparable). **a** *In vitro* ARG indicated reduction of [^{11}C]PK11195 binding in a *f*LPS-NI (10 µg) rat when blocked with cold GE-180. **b** *In vitro* ARG indicated reduction of [^{18}F]GE-180 binding in a *f*LPS-NI (10 µg) rat when blocked with cold PK11195. *** = $p < 0.001$; **** = $p < 0.0001$.

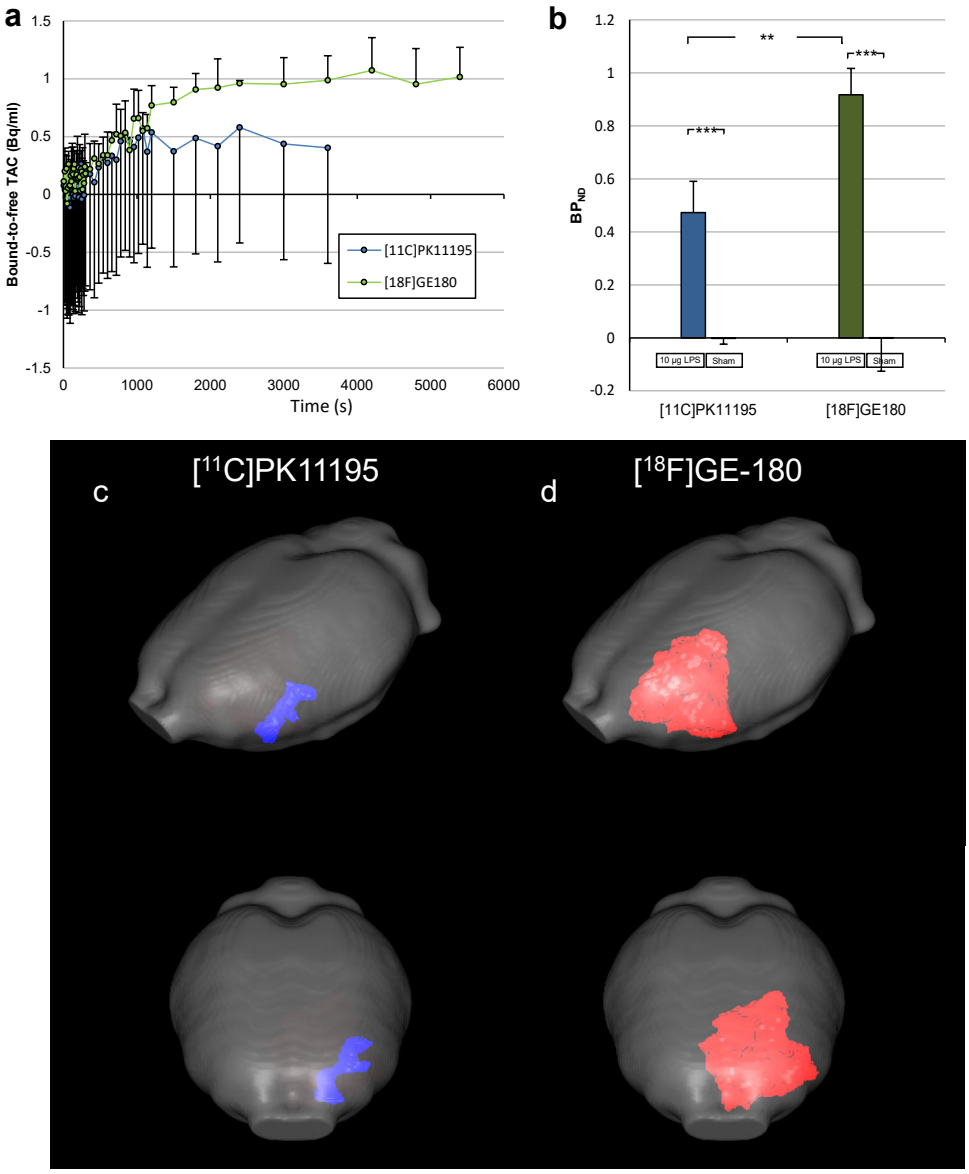

Figure 12. Comparison of [^{11}C]PK11195 and [^{18}F]GE-180 using *in vivo* imaging of *f*LPS-NI. **a** *In vivo* PET analysis of the bound-to-free activity counts were calculated by subtracting the contralateral ROI TAC from the lesion ROI TAC. Average counts of [^{18}F]GE-180 are shown in green and [^{11}C]PK11195 in blue (SD is shown one-sided to improve visualisation). **b** *In vivo* BP_{ND} of the *f*LPS-NI (10 µg) injected and sham-operated rats indicated a significant difference with both the tracers between the studied groups using [^{11}C]PK11195 (LPS: 0.472 (0.057); sham: –0.002 (0.072), $p < 0.0001$) and [^{18}F]GE180 (LPS: 0.918 (0.068), sham: 0.000 (0.012), $p < 0.0001$). A significant difference was also detected between the [^{18}F]GE-180 and [^{11}C]PK11195 imaged *f*LPS-NI rats. Error bars indicate the SD. ** = $p < 0.01$; ***= $p < 0.001$. 3D pixel-wise reconstruction of *f*LPS-NI (10 µg) rats demonstrated a larger VOI that can be segmented when imaged with [^{18}F]GE-180 (**d**) when compared to [^{11}C]PK11195 (**c**).

5.3 Effect of immunomodulatory treatment on the binding of [^{18}F]GE-180 in focal EAE-models

The *in vivo* PET image analysis for the anti-VLA-4 regimen was optimised for day 44 (i.e. 14 days of treatment) before analysing other time points of the study (Figure 13). A uniform spherical VOI was evidently neglecting parts of a lesion because the shape varies between individuals, so we sought to evaluate delineation of the lesion using a hotspot (Figure 13**b**), thresholding (Figure 13**c**), and 'the donut' analysis approach (Figure 13**d**). Finally, SRTM was chosen for analysis of the other time points (Figure 13**e**). Here, the parametric BP_{ND} maps were obtained using SRTM and a contralateral spherical VOI (constant volume 1.4 mm^3) as a reference region. The lesion was segmented using the isocontour tool by visual inspection, because of the previously mentioned issue with the spherical VOI. The decision was supported by calculating the coefficient of variation (anti-VLA-4 treated 40%; control 45%).

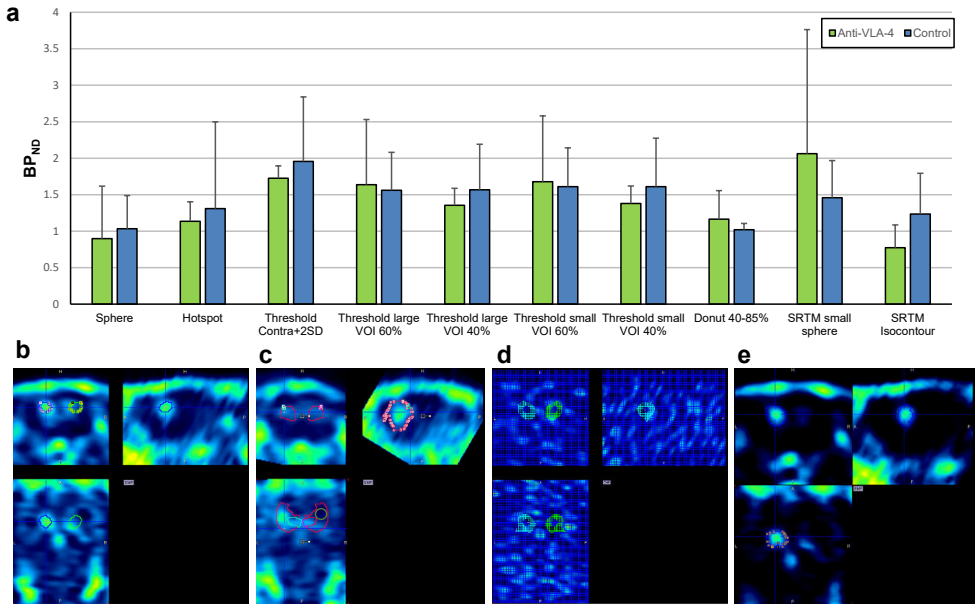

Figure 13. a Evaluation of the analysis methods for the anti-VLA-4 treatment regimen time point 44 days (after 14 days of treatment). **b** A representative image of a "Hotspot analysis", where a VOI was drawn on the lesion hotspot using the isocontour tool and then mirroring the VOI to the contralateral side. **c** Representative image of the "Threshold contra+2SD" analysis, in which the threshold was determined based on a count from a spherical VOI on the contralateral side, to which 2 SD's were added. This count was set as the delineation threshold, which was again mirrored to gain the contralateral reading. The specific binding from the ventricle was manually removed. **d** A representative image of the "donut" analysis, in which the threshold removed the highest 15% and the lowest 40% of the binding within a large spherical sphere. **e** A representative image of the "SRTM isocontour" analysis lesion was segmented using the isocontour tool by visual inspection.

To mimic a more progressive state of the *f*DTH-lesion, anti-VLA-4 treatment was started on day 30 after the lesion was activated, when the neuroinflammatory processes continue behind the resealed BBB. After two weeks of anti-VLA-4 treatment, between days 30 and 44, there was a trend towards decreased [^{18}F]GE-180 binding in the anti-VLA-4 treated rats compared to the controls (p = 0.067, Figure 14). However, after the treatment had been halted for four days, analysis of the day 65 images revealed a rebound increase in [^{18}F]GE-180 binding in the anti-VLA-4 treated rats when compared to the control rats (p = 0.0003). Additionally, a difference was detected between the treated and control animals in the binding on days 44–86 (p = 0.018). After the NI peak in [^{18}F]GE-180 binding on day 65, the [^{18}F]GE-180 binding of the animals treated with anti-VLA-4 returned to the level corresponding with the control animals on day 142 (p = 0.007).

While the anti-VLA-4 treatment was administered for 31 days at a chronic state of the lesion, the DMF therapy was started on the day of lesion induction in the acute stage of the lesion for both the *f*DTH- and *f*MOG-EAE rats and continued for 60 days twice daily. In the *f*DTH-EAE rats, the BP_{ND} of [^{18}F]GE-180 on day 7 ($BP_{ND}\Delta_{day7\text{-}day0}$) was reduced in the DMF-treated group compared to the control group (p = 0.031; Figure 15). However, when considering the longitudinal imaging time points, no significant differences were detected in the $BP_{ND}\Delta_{dayX\text{-}day0}$ over time between the DMF-treated group and control group (p = 0.142) on days 7, 14, 30, and 60. Furthermore, no rebound effect was detected on day 126 after halting the DMF treatment on day 60. The *f*MOG-EAE rats were not imaged at day 0 because it is the day of the intracranial procedure and thus, inflammation is increased because of the surgical procedure. Thus, results are indicated as BP_{ND}, since no baseline image was acquired at the start of treatment. PET imaging was performed on days 14, 30 and 60. No differences were detected between the DMF-treated and the control rats.

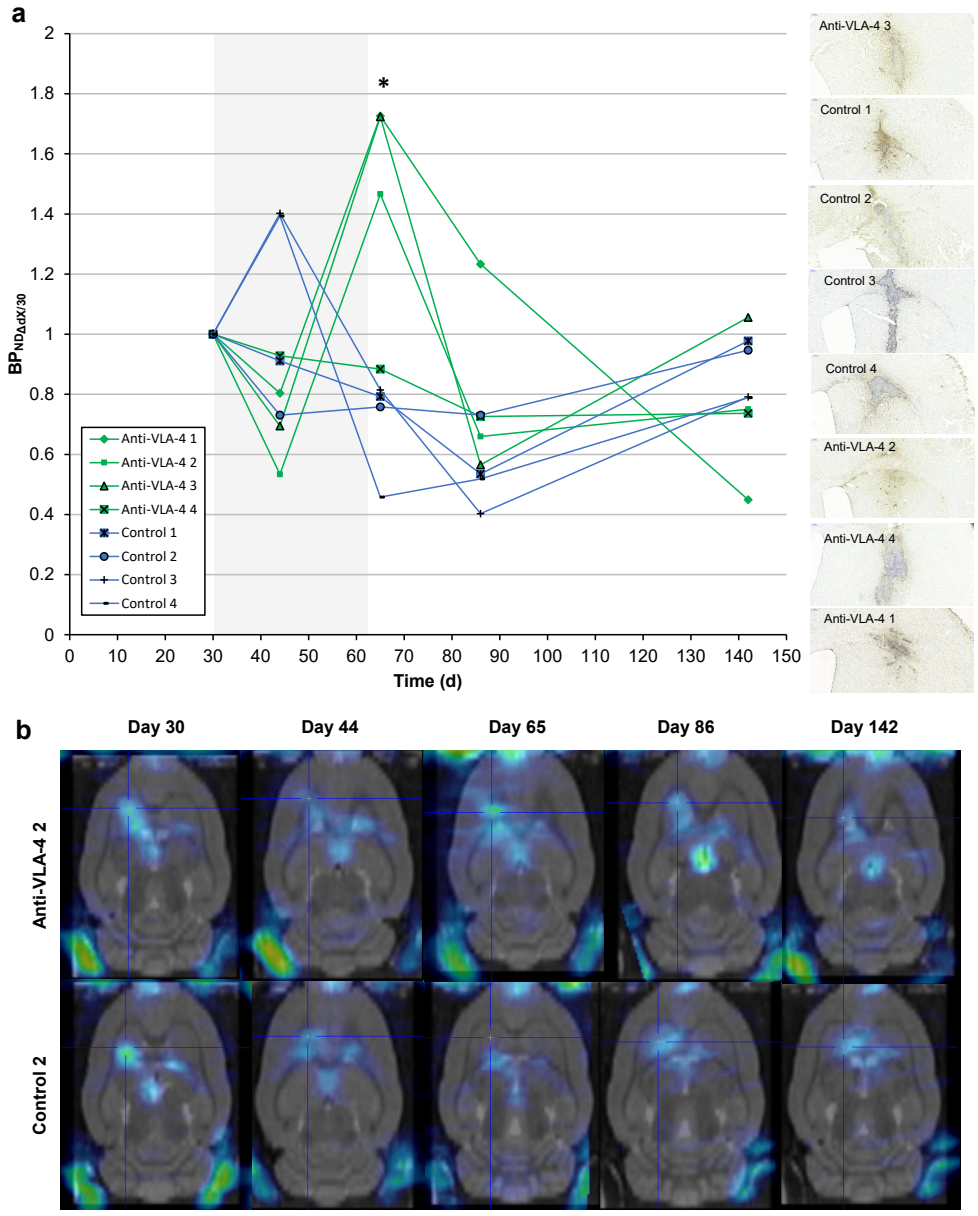

Figure 14. The SRTM analysis of the anti-VLA-4 treated (green) and control rats (blue) showing the individual course of lesions. **a** The BP_{ND} is calculated as a function of treatment from parametric SRTM-BP_{ND}-images by normalising the BP_{ND} value from all time points to the day 30 BP_{ND}. Treatment was started 30 days after the activation of the lesion, and a baseline PET/CT image was acquired. Animals were treated with anti-VLA-4 or an isotype-matched non-binding control mAb *s.c.* every 3rd day until day 61. The treatment period is visualised by the light grey background. On the right, the lesion cores stained for Iba1 are presented in the order in which they appear in the graph at day 142. **b** Representative *in vivo* BP_{ND} maps of an anti-VLA-4 treated (nr. 2) and control rat (nr. 2) from the axial plane from all the imaging time points.

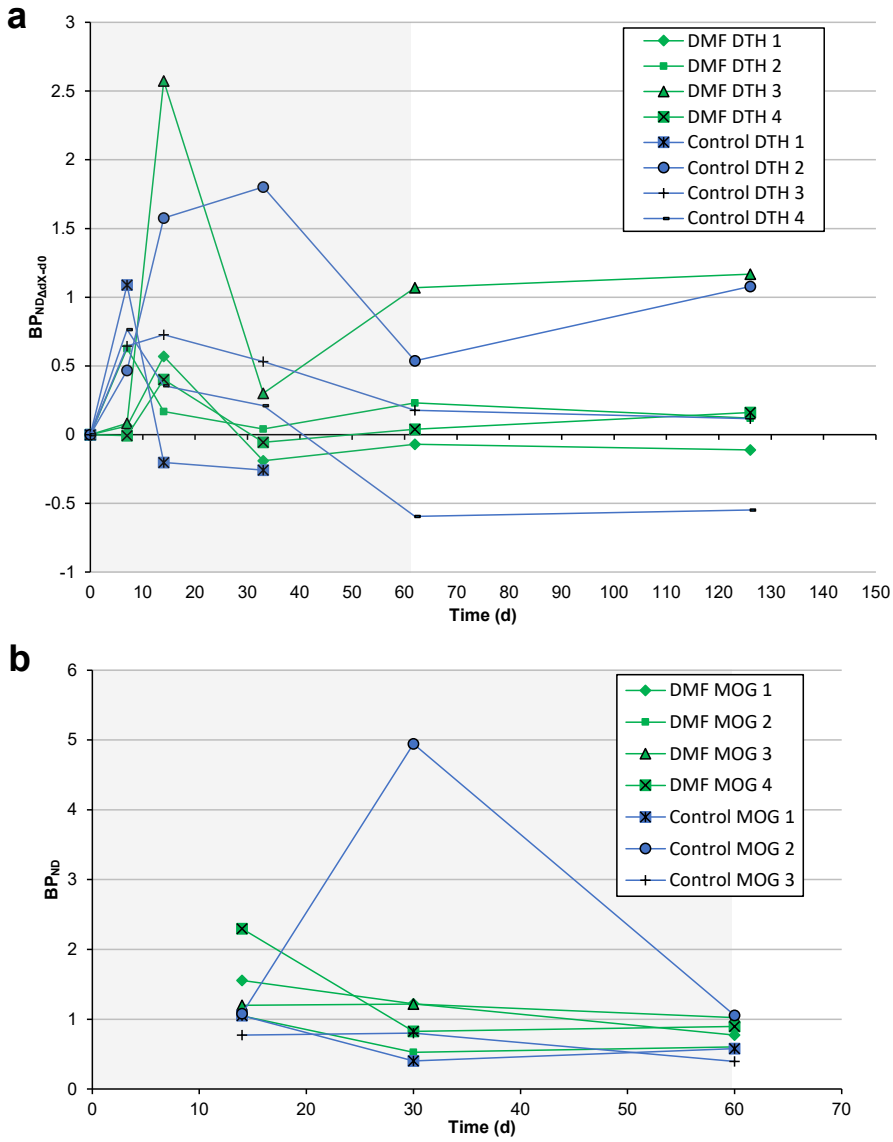

Figure 15. The BP_{ND} analysis of the DMF treated (green) and control rats (blue) showing the individual course of lesions. Animals were treated twice daily with oral DMF (15 mg/kg) in Methocel or with vehicle (tap water with 0.08% Methocel). The treatment period is visualised by the light grey background **a** The BP_{ND} for the *f*DTH-EAE rats was calculated as a function of treatment from parametric SUV-BP_{ND}-maps (25-50 min). The BP_{ND} values from all time points (days 7, 14, 30, 60, and 126) were normalised to the day 0 BP_{ND}. Treatment was started on the day of the activation of the lesion, and a baseline PET/CT image was acquired. Treatment effect was detected on day 7. **b** The *f*MOG-EAE rats were not imaged for baseline at day 0 because it is the day of the intracranial procedure and thus, results are indicated as BP_{ND}. PET imaging was instead performed on days 14, 30, and 60. No differences were detected between the DMF-treated and control rats.

5.4 The effect of immunomodulatory treatment on the histological composition in a focal EAE-model

The semi-quantitative analysis for Iba1 in Study II (Figure 16) and Study III (Figure 17), expressing microglial activation and infiltrated macrophages within the *f*DTH-lesion area, indicated no differences in the lesion size between the control and treated rats at the studied time points. In Study III, both the infiltrated core of the lesion and the perilesional activation were measured separately, but no differences were detected with either method.

In Study III, to detect changes in lymphocyte infiltration, staining was performed also for $CD4^+$ and $CD8^+$ T cells (Figure 18). Both the cell types were observed in the infiltrated lesion core and the perilesional area. Anti-CD4 staining showed significantly higher OD values at the lesion core of the control animals compared to the perilesional area ($p < 0.001$), but this was not observed in the DMF-treated group ($p = 1$). Additionally, the control rats showed higher OD of $CD4^+$ cells at the infiltrating lesion core compared to the DMF-treated rats ($p = 0.041$). No differences in anti-CD4 expression were observed between days 14 and 30 ($p = 0.3$), and no differences in OD were detected in the perilesional area.

Furthermore, the control rats had higher OD of $CD8^+$ cells in the lesion core compared to the perilesional area $p < 0.001$), whereas no such difference was detected in the DMF-treated group ($p = 0.2$). In addition, no difference was detected in the OD of $CD8^+$ cells between days 14 and 30 ($p = 0.9$), and no differences in the OD were detected in the perilesional area.

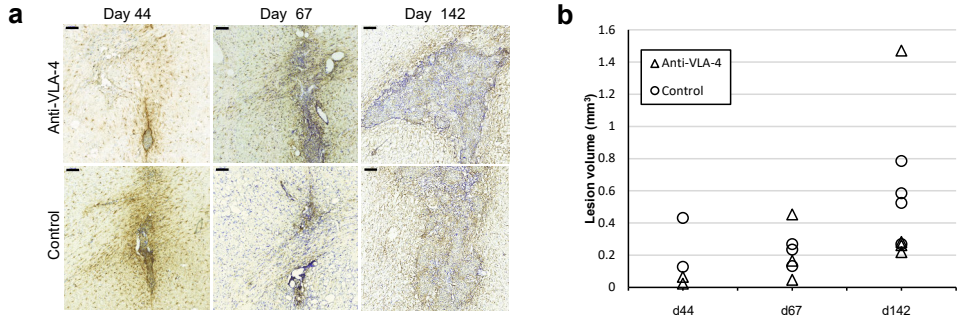

Figure 16. Anti-Iba1 staining of the anti-VLA-4 regimen at days 44, 67, and 142 in Study II. a Representative images of anti-Iba1 staining. Stereotaxic operation with heat-killed BCG was performed on day -28 ($n = 18$) and lesion activation was performed on day 0. Day 44 rats were treated every 3rd day during days 30–44 with anti-VLA-4 and the control animals with an isotype-matched control mAb. Day 67 rats were treated at days 30–57 with a 10 pause in treatment. Day 142 rats were treated during days 30–61 and euthanised for IHC at day 142. The scale bar in each figure is 100 µm. **b** Lesion volume was calculated by integrating lesion areas from 5 sections with 300 µm intervals from the lesion core. No differences in lesion volumes were detected between the studied groups.

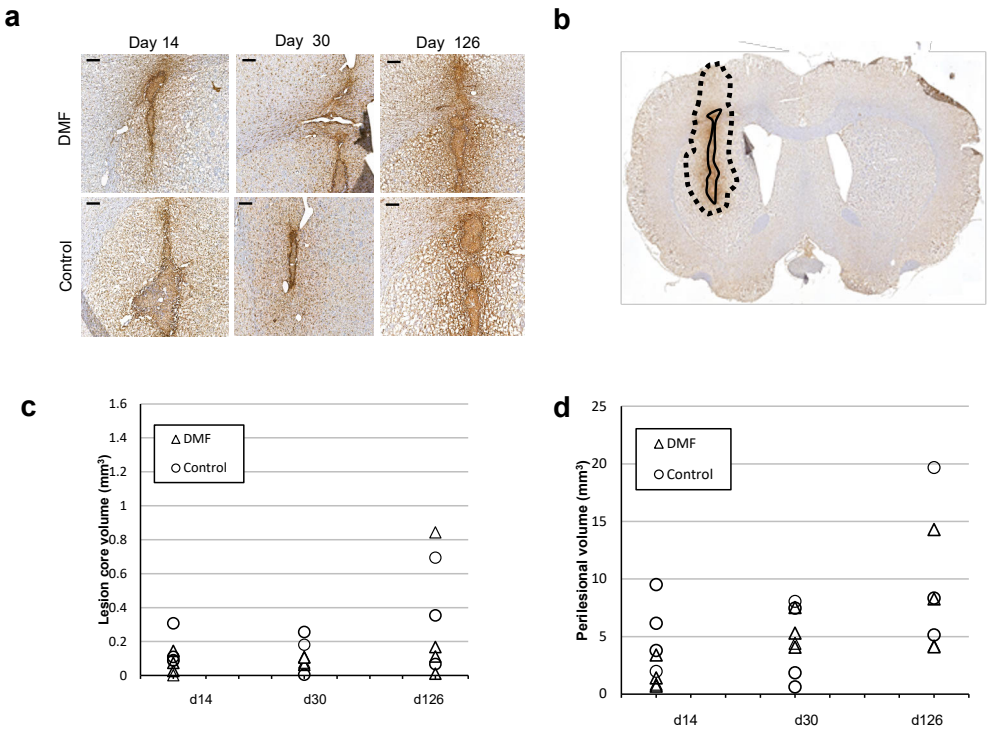

Figure 17. Anti-Iba1 staining of the DMF regimen on the *f*DTH-EAE rats at days 14, 30, and 126 in Study III. a Representative images of the anti-Iba1 staining. Stereotaxic operation with heat-killed BCG was performed on day -28 (*n* = 9) and lesion activation was performed on day 0. The day 14 and 30 rats were treated twice a day with DMF 15 mg/kg or vehicle. The day 126 rats were the same animals that were used for the PET regimen, treated with DMF 15 mg/kg or vehicle on days 0–60, and euthanised for IHC at day 126 after the last PET scan. The scale bar in each figure is 100 µm. **b** A representative image of the delineation of the lesion core (solid black line) and perilesional area (dotted black line) of a week 18 control animal. The lesion core is the infiltrative area of the lesion with high Iba1 expression and the perilesional area is a subjective estimate of the area of increased diffuse Iba1 expression that is higher from the contralateral Iba1 expression but less prominent as the lesion core. **c** Lesion core volume was calculated by integrating lesion areas from 15 sections with 100 µm intervals from the lesion core. **d** The perilesional volume was calculated similarly for the core volume. No differences in lesion volumes were detected between the studied groups.

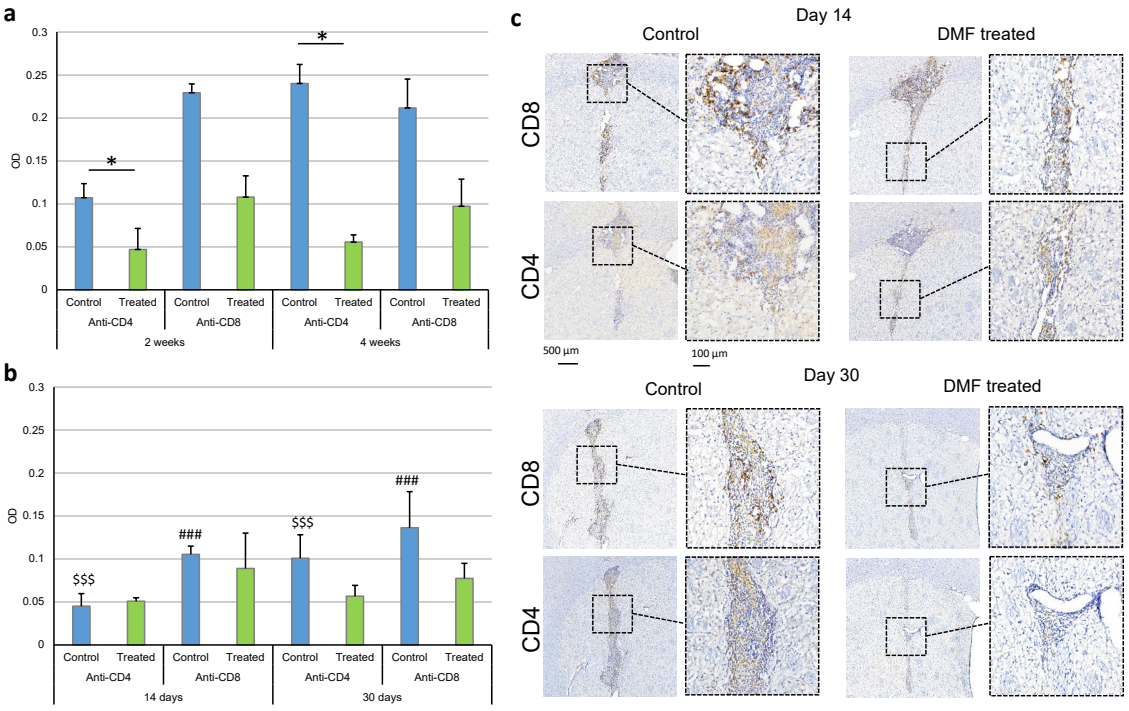

Figure 18. Anti-CD8 and anti-CD4 staining of the T lymphocytes in Study III. Staining was performed on the *f*DTH-EAE rats in the DMF regimen 14 (n = 8) and 30 (n = 8) days after treatment**. a** The OD of $CD4^+$ and $CD8^+$ T cells at the infiltrated *f*DTH-lesion core. The asterisk (*) is denoting the significant differences between DMF-treated and control rats. **b** The OD of the perilesional area, where microgliosis was also observed. The control group had significantly higher OD values of $CD4^+$ and $CD8^+$ staining at the lesion core when compared to the perilesional area ($p < 0.001$). Furthermore, the control rats had increased $CD4^+$ OD values at the lesion core (**a**) compared to the DMF-treated group ($p = 0.041$), which was not detected with CD8. The dollar sign ($) is indicating significant differences between the $CD4^+$ OD of the control animals at the focal *f*DTH-lesion core (**a**) compared to the perilesional area of the control rats (**b**) ($p < 0.001$). The number sign (#) indicates significant differences between the $CD8^+$ OD of the control animals at the lesion core (**a**) compared to the perilesional area of the control rats (**b**) ($p < 0.001$). The results are indicated as mean (SD). **c** Representative images of the IHC staining for $CD4^+$ and $CD8^+$ cells in the infiltrated *f*DTH-lesion core in the control and DMF-treated rats. Sections are counterstained with haematoxylin to detect the nuclei. Scale bar = 500 µm or 100 µm in the enlarged image.

6 Discussion

6.1 Animal models of neuroinflammation

It is often stated, that EAE is the most common animal model that is used for studying MS in animals (Burrows et al., 2018). It must be addressed, that models that are commonly referred to as EAE, can be induced in several different species and strains of animals, by using several different encephalitogens or toxins that can be administered in different anatomical locations, resulting in models that depict very different aspects of MS. Evidently, there are major challenges in the usability of animals for studying human diseases. EAE as a model has received criticism on the lack of resemblance with MS (Behan and Chaudhuri, 2014; Sriram and Steiner, 2005), while at the same time it has been praised for its capability to aid the research of MS (Kipp et al., 2017; Steinman and Zamvil, 2006).

In addition to EAE, there are purely inflammatory models of demyelination, which are induced by administering toxins in animals, such as the cuprizone model. Here, the focal models of NI were chosen as study subjects due to their applicability to imaging and longitudinal treatment studies. The model of acute NI induced by intrastriatal LPS injection has been applied in many PET studies since the publication of Study I (Berdyyeva et al., 2019; Ory et al., 2015; Sridharan et al., 2017). The model is relatively quick to induce because it can be applied to imaging studies already 16 h after the procedure. However, few clinical indications correspond with such inflammation. For this reason, the EAE models were applied in Studies II and III to evaluate the therapeutic effect of immunomodulatory drugs. By creating an individual lesion at a specific location in the CNS, assessment of lesion activity and the effect of drugs can be monitored longitudinally even after the BBB has resealed, i.e. the lesion is invisible to conventional MRI.

The question arises, how close a resemblance does EAE have with MS. The study by Höftberger and co-workers (2015) answers this question partially. When studying a patient *post mortem*, who had MS-like primary demyelination, and the diagnosis of demyelinating human autoimmune encephalitis (HAE), it was discovered that the direct immunisation of the subject using brain tissue can induce a disease fulfilling the pathological criteria of MS. However, HAE histopathology differs from EAE by the high number of $CD8^+$ T cells and B-lymphocytes, but lack

of $CD4^+$ T cells, which again are common in EAE and ADEM (Höftberger et al., 2015). Thus, histopathology does not directly describe the induction of the disease or the pathogenesis. In addition, it has been shown that the pathology of an EAE lesion is strongly site-dependent, since the outcome is different whether lesion initiation occurs in the WM vs. GM (Merkler et al., 2006).

There is no perfect model that would tell us the exact mechanism of how diseases, such as MS, emerge (Behan and Chaudhuri, 2014). Here, induced EAE was applied, which has been criticised for then non-spontaneous occurrence of the disease. In study I, the LPS-model was applied to create a massive unilateral inflammation in the whole hemisphere, which rarely occurs in disease states, like the rare disease Rasmussen's encephalitis (Varadkar et al., 2014). Such models may have lesser value in studies of pathology or therapeutic efficacy assessment because they are purely toxic induced models. However, they provide a rapid and reproducible tool for diagnostic assessment of NI. The *f*DTH- and *f*MOG-EAE models, on the other hand, provide a more pathophysiologically relevant model for studies of pharmaceuticals, even though the method of induction is non-spontaneous. The rationale for choosing these two models for evaluation of DMF was that they describe different aspects of MS: the *f*DTH-EAE model depicts a robust, Ab-independent cell-mediated lesion, while the *f*MOG-EAE represents a humoral demyelinating lesion (Anthony et al., 2014a).

6.1.1 Efficacy assessment of pharmaceuticals in animal models

EAE models are widely used in studies of pharmaceuticals. In a PubMed search, using the search terms "EAE/experimental autoimmune encephalomyelitis/ experimental allergic encephalomyelitis AND drug/pharmacotherapy/therapy/ treatment", more than 18 000 publications come out. Previously, several other studies have shown the applicability of the *f*DTH- and *f*MOG-EAE models in evaluation of the therapeutic effect of drugs (Airas et al., 2015a; Anthony et al., 2014a; Anthony et al., 2014b). In studies II and III, we applied the *f*DTH-EAE model, which depicts the MS pattern I lesion, where an active inflammation peak can be detected 1–2 weeks after the peripheral activation of the immune system. This has been observed as BBB breakdown using Gd-enhancement, followed by BBB resealing some 4 weeks after the intracerebral injection of heat-killed BCG (Matyszak and Perry, 1995). In Study II, in the chronic state of *f*DTH-EAE, 2-week treatment with anti-VLA-4 had a modest effect on NI, while withdrawal of treatment increased NI. This was detectable using TSPO PET.

Natalizumab was, in fact, first developed when studies with disseminated forms of EAE showed that anti-VLA-4 was able to slow down disease progression by

preventing entry of encephalitogenic T cells into the CNS (Yednock et al., 1992). In study II, despite the modest effect of anti-VLA-4 on the *f*DTH-lesion, discontinuation of the drug was causing a distinct increase of NI. To observe whether such a rebound would occur after discontinuation of DMF, which has been reported by others (Harmel et al., 2018), we sought to evaluate [^{18}F]GE-180 uptake 10 weeks after the discontinuation of DMF. Although no rebound effect was detected, we cannot rule out an increase in binding prior to study week 18.

In Study III, in addition to the *f*DTH-EAE, also the *f*MOG-EAE rat model depicting pattern II lesions in MS, was applied to evaluate the efficacy of DMF using the TSPO PET tracer [^{18}F]GE-180. Here, the *f*DTH-EAE was further analysed using IHC. The Student's t-test indicated reduced uptake of [^{18}F]GE-180 in the *f*DTH-EAE rats after 7 days of twice-a-day treatment with DMF compared to the vehicle-treated control group. However, in the longitudinal analysis, no therapeutic effect was detected. Likewise, no differences in [^{18}F]GE-180 binding were detected using the *f*MOG-EAE. Clearly, at most time points, more power would have been needed to confirm the results. In addition, the tracer may not have been specific enough to detect the inflammation in these models.

Moreover, we were not able to detect a reduced volume of the *f*DTH-EAE lesion neither in the anti-VLA-4 treated rats nor in the DMF-treated rats, using anti-Iba1 staining for activated microglia and macrophages. Burrows and colleagues (2018) state that timing of the therapeutic interventions is of critical value, highlighting the treatment schedule of natalizumab and fingolimod interventions, in which start of the treatment before symptoms or at the first relapse peak has apparent effects on the efficacy, being decreased or absent in the latter setting (Burrows et al., 2018). When using the focal EAE models, in which there is no apparent phenotype, the timing is evidently more conceptual.

Because DMF has been shown to reduce the number of $CD4^+$ and $CD8^+$ T lymphocytes in patients with RRMS (Mehta et al., 2019), we performed IHC also for $CD4^+$ and $CD8^+$ T lymphocytes in Study III. Interestingly, the staining for Iba1 as well as the $CD4^+$ and $CD8^+$ staining indicated a halo in the perilesional area outside the infiltrative *f*DTH-core. This indicates the expression of CD4 and CD8 in the activated microglia, in addition to the T lymphocytes. This could have been confirmed by doing a double-staining, but unfortunately there was no tissue left for the staining. Both markers have previously been shown to be expressed by microglial cells (Almolda et al., 2009; Boddaert et al., 2018; Sawada et al., 1992), because calculation of individual $CD4^+$ and $CD8^+$ cells was not possible due to observation of staining outside individual cells, the OD for both the lesion core and the perilesional area was calculated instead. OD values of CD4 staining were significantly higher in the lesion core of the control animals, which is possibly due to the lymphocytes with high expression of CD4 and CD8 when compared to the

perilesional area, in which the microglia with lower expression of these markers are located. Furthermore, DMF treatment reduced the staining of CD4 at the infiltrative lesion core, which indicates that DMF reduced infiltration of T cells at the lesion core but did not affect the cells in the perilesional area.

The use of DMF has previously been reported to induce gastrointestinal effects (Deeks, 2016), which would manifest as lesser weight gain in the DMF-treated group. However, this was not observed during the treatment period of 0–8 weeks using the *f*DTH-EAE rat model.

6.1.2 Ethical considerations of animal models in research

Undoubtedly, when using animals in scientific research, the question arises whether it is necessary or if it can be avoided. Institutions opposing animal experiments state that *in vitro* cell- and tissue cultures would be enough to avoid animal use, human volunteers can be recruited, or that already existing pharmaceuticals can be used for novel indications (Oikeutta eläimille, 2021). I believe that it is easy to state that animal experimentation needs to be discontinued, while not having a proper solution to replace them. By doing this, the individual is pushing not only the moral consideration of what is ethically acceptable in certain situations but also the scientific responsibility, on others' shoulders.

Indeed, great effort has been made to replace animal studies with *in vitro* or *in silico* models. The Organisation for Economic Co-operation and Development is promoting the validation of alternative testing worldwide (OECD, 2021). In Europe, the EU Reference Laboratory for alternatives to animal testing is promoting alternate methods (EURL-ECVAM, 2021), and in Finland, there was a special laboratory Finnish Centre for Alternative Methods (FICAM) that was supported by the Ministry of Agriculture and Forestry of Finland (MMM, 2013). Alternate methods are preferred whenever possible because it is required under the REACH Regulation (Registration, Evaluation, Authorization and Restriction of Chemicals, commission regulation (CE) n.1907/2006) within the EU.

However, when researching in fields such as NI, the complex nature of the physiological events and barriers cannot be fully replicated *in vitro*, and often there is limited access to human tissue samples (Bjelobaba et al., 2018), as is the case with MS patients who rarely die at an early stage of the disease. Furthermore, due to the legislation, prior to clinical studies of pharmaceuticals all substances, including radiopharmaceuticals, must be evaluated *in vivo* (EMA, 2018).

The use of animals in experiments is therefore operated under the legislation of the issuing country and the directives of the European Union (EU, 2010). An authorisation is required for all procedures involving animals and in Finland, it is issued by the Project Authorisation Board (AVI, 2021). All animal experiments must

to be performed following the principle of 3R's: *Replacement, Refinement and Reduction* (Kilkenny et al., 2012), which state that experiments need to be replaced whenever possible, the experiments need to be fine-tuned to maximise animal welfare, and the number of animals needs to be kept as low as possible. While animal experiments are under heavy legislative control, much of the responsibility of animal welfare relies on the operating researcher and the supervising institution.

6.2 PET as a tool for studying neuroinflammation

PET is a valuable tool for quantitative evaluation of inflammatory processes because it can visualise the physiological events during a disease state, not just the anatomy. Using PET, we can non-invasively monitor neuroinflammatory changes related to disease course, functionality of the brain, or individual therapeutic effect. However, some methods of PET data modelling require invasive arterial sampling, while there are methods, such as image-derived input function, which can be applied in many cases.

The limitation of the method is the spatial resolution of the camera, reflecting the physical boundary of the radiolabel (Moses, 2011). The applicability of PET imaging in the diagnosis of MS is also restricted by the high cost of the method that requires cyclotron and radiochemistry laboratories, PET scanners, and educated staff (Cheng et al., 2009; Niccolini et al., 2015). If the limitations can be overcome, PET can be applied in cases where a diagnosis is unclear or where treatment effect is ambiguous. In clinical settings, TSPO uptake has been shown to be a prognostic marker of disability in MS (Politis et al., 2012). In addition, increased [^{11}C]PK11195 BP_{ND} at baseline in the NAWM of patients with CIS has been shown to correlate with later diagnosis of MS and EDSS score (Giannetti et al., 2014).

6.2.1 TSPO imaging and efficacy assessment of pharmaceuticals

In this thesis, TSPO was used as a target to image inflammation. Interpreting TSPO imaging data is challenging, because firstly, TSPO is expressed by numerous cell types in the CNS, and secondly, it is expressed both in reparative and damaging processes of the CNS. Thus, the signal needs to be regarded as a sum of neuroinflammatory processes, where some events are detrimental and some restorative. Furthermore, targeting specifically the microglia by PET has confronted similar discussion: current ways of distinguishing between inflammatory and anti-inflammatory microglia *in vivo* are yet to be established (Ransohoff, 2016). The terminology, microglial polarisation into inflammatory (sometimes referred to as M1 or 'activated') and anti-inflammatory (sometimes referred to as M2 or 'resting state')

phenotypes, is derived from peripheral macrophage activation, and has not been established in microglia, and thus, these phenotypes cannot be distinguished using TSPO markers (Guerrero and Sicotte, 2020). Despite the common morphology and surface markers of reactive microglia and peripheral, blood-derived macrophages, the cells have strikingly different gene expression profiles and functions in a neuroinflammatory state (Yamasaki et al., 2014). Microglial phenotypes have been shown to be transient and demonstrate both temporal and spatial evolution and thus, the phenotypes of microglia can be better described as a spectrum of phenotypes rather than just "good" or "bad" (Guerrero and Sicotte, 2020; Jurga et al., 2020).

In addition to these inaccuracies as a target, TSPO can be detected in many cell types and the used tracer can have unwanted properties. In Study I, we showed, that the TSPO tracer, [^{18}F]GE-180 can detect NI in animal models having improved properties over [^{11}C]PK11195, and thus, [^{18}F]GE-180 was used as a marker of neuropathological changes in the focal EAE models. The higher BP_{ND} of [^{18}F]GE-180 over [^{11}C]PK11195 is largely due to the higher binding affinity of [^{18}F]GE-180 to TSPO (0.87 nM) (James et al., 2017) when compared to that of [^{11}C]PK11195 (< 20 nM) (Beurdeley-Thomas et al., 2000), but it does not necessarily indicate better ligand properties due to over-reporting and non-selectivity (Beurdeley-Thomas et al., 2000; Jones et al., 2011). Self-evidently, some of the superiority of [^{18}F]GE-180 results from the [^{18}F]-label. The shorter positron range of [^{18}F], ~0.6 mm, compared to that of ^{11}C, ~1.0 mm, results in better spatial resolution of the image (Sánchez-Crespo et al., 2004). In addition, nucleophilic synthesis of [^{18}F] results in a higher MA of the end-product [^{18}F]GE-180 (Bergström and Långström, 2005). The biodistribution of the applied tracers was similar, despite their different kinetics. This was in line with previous studies of these tracers (Jones et al., 2011).

We concluded that the detected signal of both [^{18}F]GE-180 and [^{11}C]PK11195 in the brain is originating from microglia, but also to a lesser extent, from astrocytes, which indicates the non-selectivity of TSPO as a biomarker. Disruption of the signal interpretation was further analysed in Study III, where we were unable to detect the changes that DMF was generating in the *f*DTH-model in the long term, partly because the radio metabolites are decreasing specificity of the signal from [^{18}F]GE-180 even further (Study III Supplemental data). Additional analysis showed that metabolites are readily transported through the BBB because the radio metabolites are less bound to plasma proteins than [^{18}F]GE-180. Additionally, a delay in TSPO expression has been previously reported, in which TSPO binding remained significantly above the baseline level for at least 3 weeks after insult to the CNS (Brackhan et al., 2016), making interpretation of the signal more complicated.

After the publication of Study I, and showing its beneficial properties over [^{11}C]PK11195 in the LPS-NI model, it was discovered that [^{18}F]GE-180 has low first-pass extraction in healthy humans (Feeney et al., 2016). Reasons for this can be

low BBB permeability, high plasma protein binding, or clearance by efflux pumps (Fan et al., 2016). According to Sridharan et al. (2016), the tracer showed high plasma-retention and low free fraction in human studies, which was not detected in studies with rodents. Therefore, its application to disease states where the BBB is sealed is seemingly low (Zanotti-Fregonara et al., 2020). Despite this, the tracer is applicable in preclinical studies and has been applied in clinical studies of MS (Unterrainer et al., 2018). The properties of [^{18}F]GE-180 as a tracer have been extensively evaluated and shown to be more sensitive than [^{11}C]PK11195. However, no significant improvement in the lesion-background ratio over other 2nd generation tracers, such as [^{18}F]DPA-714, was detected (Sridharan, 2016).

6.2.2 PET quantification

Commonly in neuro-PET studies, MRI atlases providing standard anatomical regions are applied for the segmentation of areas for quantification. In the focal NI-models, the lesion does not follow any standard brain region but can extend longitudinally from the striatum through the corpus callosum until the cortex, and thus, an atlas template cannot be applied as such. In addition, when applying the focal models of EAE, there is variation in the shape and size of the lesions due to the individual immunological response, even though the method of induction is standardised and performed in a similar manner between all rats. Therefore, in this thesis, several VOI delineation methods were applied and evaluated. In Study I, quantification was performed in Carimas 2.6 by calculating the BP_{ND} using a spherical VOI. After this, in Study II, the method of analysis was reassessed by testing various VOIs to evaluate the outcome differences within each of the methods stated in the methods section. The EAE lesion observed in a PET image can be seen as a tumour-like object. A spherical VOI, which was applied in Study I, has the shortcoming of the imbalance between the central high binding area and the low binding periphery, depending on the volume of the sphere. Manual ROI delineation is anyhow prone to inter-observer variation and due to the predefined areas, some out of target signals may not be detected (Schuitemaker et al., 2007). Another drawback here, with using the manual ROI method, is the assumption that the elementary kinetics within a ROI is equal in the tissue while covering areas of GM and WM brain areas. Voxel-wise analysis, however, may be too sensitive for image analysis of [^{11}C]PK11195, even though smoothing filters are applied (Sridharan, 2016).

In Study II SRTM was applied, which is a method that can be applied for dynamic images without the need for plasma input. Despite the advantages of SRTM, we were unable to apply this modelling approach in the following Study III, because the images were collected as static images with framing. Thus, we chose to apply SUV maps, from which a VOI was determined from the lesion at its largest

within one individual. The disadvantage of this approach was that when keeping the ROI identical to the one at its largest, the TSPO binding is likely underestimated in the other time points.

Due to the large number of rats imaged in Study III, we thought to image the rats semi-statically, i.e. collecting static images with five frames, from 25–50 min after the injection of the radiotracer. This decision was based on the Study I protocol of imaging, which indicated constant binding between 25-50 minutes. Research by other groups states that the optimal emission window for [^{18}F]GE-180 would be 40–60 minutes (Sridharan et al., 2017) or even 60–90 minutes after the injection to acquire stable SUV ratios in a transgenic model of AD (Brendel et al., 2016; Overhoff et al., 2016). While the aged AD-mice reached a plateau phase in the SUVr plots already after 20 min post-injection, the younger AD-mice attained a more delayed stabilisation of binding only after 50 minutes (Brendel et al., 2016) indicating variance between disease states.

To save time and to increase throughput in Studies II and III, we sought to image two animals simultaneously in the scanner. This can lead to a spatially varying point-spread-function, i.e. the resolution degrading phenomena is varying according to its position in the FOV (Cheng et al., 2009). The Inveon scanner can fit two rats under 500 g at a time, and this approach was applied here, because OSEM3D reconstruction was available. Application of OSEM3D reduces the effect of spatial variance outside the centre of the FOV (Disselhorst et al., 2010; Reilhac et al., 2016).

In this thesis, animal models having a lesion with a diameter of approximately 1–2 mm were applied. Given that the scanner spatial resolution, according to Teuho and colleagues is 1.8 mm, it is evident that we are operating on the detection limit of the camera (Teuho et al., 2020). The limited resolution of PET and the limited image sampling of heterogeneous tissue leads to a partial volume effect (PVE), which leads to significant depression of the isotope concentration, and could be corrected for (Hoffman et al., 1979). However, PVC is not widely applied in preclinical settings, due to the lack of validated methods, and due to the finding that it might, in fact, reduce the signal-to-noise ratio in models of low-level NI by amplifying noisy high-frequency signals (Sridharan, 2016).

6.2.3 Applicability of animal models in neuroinflammation PET studies

Rodent models are widely applied in studies of NI using PET and TSPO-tracers. It has been discovered, that the TSPO-genotype issue resulting in LAB, MAB, and HAB in humans, is not observed in animals (Feeney et al., 2016). In this thesis, we used different animal models to depict acute and more chronic NI. The acute LPS-induced unilateral inflammatory model provided a tool for imaging that was both

reliable and reproducible. Variation in both [^{11}C]PK11195 and [^{18}F]GE-180 between the LPS injected individuals was minimal.

Previously, finding a pathology free reference region with homogeneous binding in models with disseminated NI has been challenging (Brendel et al., 2016; Pedersen et al., 2006). In small animal studies generally, getting an arterial input function is complicated because it requires invasive femoral or jugular artery cannulations before imaging, and limited possibility for blood sample collection, while the animals are included in a longitudinal follow-up study. In addition, high binding of TSPO tracers in the myocardium prevents the use of the left heart ventricle to obtain an image derived input function in rodents. Here, the acute LPS-model provided unilateral inflammation, where the contralateral side is relatively intact and can be applied as a pseudoreference region, because the area is not fully clear of TSPO binding occurring in the endothelial cells of the vasculature. Likewise, the *f*DTH- and *f*MOG-models provide an intact contralateral reference region, because the lesion is induced unilaterally. Confirmation of the use of the contralateral side as reference region in similar NI models has been shown by Sridharan et al. (2017), suggesting simultaneously that the cerebellum is not an appropriate reference region due to specific binding.

In this work, a dedicated small animal PET scanner was used for imaging the animals. When applying a dedicated animal scanner instead of a human scanner, the image resolution is better due to the smaller transaxial FOV.

6.3 Study limitations

Currently, it has been discussed that the sex of the experimental animals (Hughes, 2003) should be paid attention to, because often in research, the findings are extrapolated and applied to both sexes without solid reasoning (Lee, 2018). Evidently, a milder disease course of EAE has been detected under the influence of oestrogens (Harbo et al., 2013). Here, in all studies, only male rats were applied, to minimise variability between individuals when having a low number of animals. This makes the extrapolation of the results inconclusive, since in MS sex has been identified as an individual risk factor.

When considering the therapy regimens, one limitation is the lack of plasma and tissue concentration analysis of the pharmaceuticals. Since this was considered only after the experiments, the experimental plan lacked some features, such as tissue samples from the brain as well as accurate documentation of the dosing and euthanasia time points, that would have been needed for proper analysis. For Study III, it would have been intriguing to know the availability of DMF and MMF in the different tissues.

In PET imaging generally, research needs to be planned well ahead, due to the complicated logistics chain that is needed to perform a study. Simultaneously, there

are variables and uncertainties such as the success of radiotracer production, which may affect the course of the study. In Study II, practical issues during the conduct of the study resulted in some illogical time points. Access to the drug was in this case challenging, which lead to the unfortunate change of protocol during the experiment, which is generally not recommended during the conduct of a study.

A limitation considering the applied imaging modalities is the lack of MR images, which would give a direct anatomical reference of the lesion and provide detailed knowledge of the lesion activity state. In addition to knowledge of the biological processes within a lesion, access to MRI would reduce workload from the analysis because PET scans could be directly aligned on the same individual's MR image and not a template. Furthermore, it would provide better soft-tissue contrast, better motion correction in case of a combined PET/MRI apparatus, allow use of contrast agents, and give a possibility to apply DWI or DTI (Ehman et al., 2017) to better characterise individual lesions. In these studies, alignment of images to the Schiffer MRI-space was performed by rigid matching with manual supervision. Furthermore, motion correction was applied in some cases. Given that there was an attempt to automate the alignment process to minimise human error, adjustment of the alignments was indeed needed in these studies. As spatial normalisations regularly fail, it is crucial to visually control post-processed images (Overhoff et al., 2016).

As we had previously shown in the *f*DTH-model, that treatment effect can be detected by *in vivo* PET and *ex vivo* ARG (Airas et al., 2015a), for practical reasons and to reduce the animal number, ARG-analysis was left out from the plan in Studies II and III. However, it would have been critical information in confirming the PET result from Study II and Study III, because some of the time points were showing a trend towards significance.

Another issue in these studies was the number of animals: the power is too low to draw concrete conclusions of some of the PET imaging time points. The single-time point measurements by the Student's T-test showed significance in the reported time points, but in the more powerful repeated measures analyses, the significance disappeared. In PET studies, due to the costliness of the method and workload on the staff, number of the animals are generally kept low. Burrows and colleagues (2018) state, that internal and external validity in preclinical studies are of uttermost importance. Randomisation, blinded analyses, and power calculations are performed in a small minority of EAE studies (Burrows et al., 2018). Here, blinding was not applied during the conduct of the analyses, due to the lack of staff.

As discussed in 6.2.2, different ways of analysing the data were applied in Study II. This was due to the inability to reproduce the first rapid analysis performed right after the day of imaging by using the Inveon RW software. A great issue in preclinical research is, indeed, the reproducibility of methods or results (Freedman et al., 2015). In fact, standardisation of analytical methods would be needed to allow

direct comparison of the results of small animal PET imaging studies performed at different locations using different equipment (Teuho et al., 2020), imaging protocols, and reconstruction parameters. Both animal handling and quality assurance of imaging modalities have an influence on the outcome (Mannheim et al., 2018). Standardisation relates to the use of valid animal models, the course of treatment, the imaging approach, as well as the method of analysis. Here, attempts to repeat the preliminary results led to optimisation of both the segmentation of the lesion and the analysis. In Study II, SRTM was decided to be the final method of analysis, because of the assumption that the non-specific binding in both lesion and contralateral areas are equal, and that there is no pathology in the contralateral side. In addition, the parametric BP_{ND} maps were applicable to visual reporting purposes. Despite the many efforts, the best method to analyse such lesions, is yet to be resolved.

In the biodistribution studies in Study I, the animals were of the same age during the procedure, and thus, they were expected to be of the same size. Nevertheless, the results should have been corrected for weights of the rats and calculated as SUVs.

6.4 Future prospects

Further characterisation of the animal models, that were applied in the efficacy assessment of therapeutics in this thesis, using multimodal imaging, could be of interest. Especially the formation of the lesions during the first days after lesion induction could be evaluated and validated in reference to emerging MS lesions.

Furthermore, with some results approaching significance, further validation of the results by evaluating the therapeutic effect of the immunomodulatory drugs could be performed. By adding up the number of subjects, a firmer conclusion of the effect of anti-VLA-4 and DMF in the applied models could be shown.

Molecular imaging using PET imaging is a valuable tool for studying pathological aspects of neuroinflammatory conditions as well as therapy interventions of these diseases. As there has been intensive research focusing on TSPO markers during recent years, the downsides of these tracers have become evident. Although several new targets, that were mentioned earlier in this thesis, have been evaluated, such as the P_2Y_{12}, novel targets for PET imaging with better selectivity are needed to predict disease progression in neuroinflammatory and neurodegenerative diseases.

While there are 1) high numbers of available animal models, 2) various approaches to visualise inflammation, and 3) numerous ways to analyse data, a challenge for future research will be standardisation and replicability of preclinical experimental settings. Common attempts to standardise the field of preclinical imaging from planning, executing, analysis, and reporting the studies would be of high importance.

7 Conclusions

The purpose of this thesis was to evaluate the usability of rat models of focal NI in the binding of TSPO PET radiopharmaceuticals. Rat models of focal acute and chronic NI were applied in the treatment regimens using immunomodulatory drugs. Based on the results that were presented in this thesis, the following conclusions can be drawn:

1. The 2nd generation TSPO PET tracer, [^{18}F]GE-180, indicated improved properties over the 1st generation tracer, [^{11}C]PK11195, in the *f*LPS-NI animal model of focal NI. The improved properties were higher binding potential values of [^{18}F]GE-180 compared to those of [^{11}C]PK11195, due to higher binding affinity, better specificity, and the properties of the [^{18}F]-label, such as higher molar activity, longer half-life, and the shorter positron range. The study also showed that the unilateral model of acute NI is suitable for the evaluation of novel PET tracers of NI (**Study I**).
2. Discontinuation of the immunomodulatory drug, anti-VLA-4, caused a rebound effect in the *f*DTH-EAE-rat model. However, the efficacy of anti-VLA-4 in short-term treatment was not detected using the *f*DTH-EAE-rat model (**Study II**).
3. The immunomodulatory drug, DMF, decreased uptake of [^{18}F]GE-180 after short term treatment in the *f*DTH-EAE rat model. However longitudinal analysis showed no decrease in TSPO binding, while drug effect on $CD4^+$ and $CD8^+$ positive cells was detected using IHC. In addition, no rebound effect was detected using TSPO PET after halting the treatment for 10 weeks. Furthermore, no treatment effect of DMF was detected using the *f*MOG-EAE model (**Study III**).

Acknowledgements

I want to start by thanking my supervisors. Merja Haaparanta-Solin, for a perseverant attitude towards this project, which did not always go as planned. By providing her knowledge in the preclinical imaging field and research in general, she encouraged me to continue and finish this work. Juha Rinne, who has provided important aspects to this project from the early meters and the connection to the EU 7th Framework Programme INMiND for this thesis and research to be conducted within. Laura Airas, who had the idea to start studying animal models of NI in Turku and has provided her vast experience in the clinics as well as within research of MS. An important supervisor for me, although not an official one, from the very beginning, was Alex Dickens, who thought me just about everything I know about the animal handling, procedures, tissue handling, and image analysis performed within this project.

I want to show my gratitude to the Turku PET Centre that has provided me with an excellent and fruitful environment to be working in. I also wish to thank Dr. Sylvie Chalon and Dr. Sandeep Golla for carefully reviewing my PhD thesis. I wish to thank Dr. Sabina Pappatà for accepting the invitation to be my opponent.

I wish to thank all my colleagues who have provided their knowledge for my project: Jouni Tuisku, who has always been willing to help with anything related to modelling of the data and other unrelated stuff as well. Jarkko Johansson, for who never got irritated for the non-stop questions about Pmod. Olof Solin, who has given valuable input to this work by implementing his long experience in the field and connections to GE Healthcare. Francisco Lopéz-Picòn, who has been an important link to getting the immunohistochemistry of this work in shape. Päivi Marjamäki, who was an important teacher at the beginning of my career at the PET Centre. Richard Aarnio for analysing the metabolite study in this thesis and many other fruitful discussions along the way. Thank you, Daniel C. Anthony, for providing extremely motivating input for both the reports of this project but also for my learning.

I acknowledge the technicians who have directly contributed to my work: Elisa Riuttala, who was an irreplaceable teacher at the beginning of my work, Aake Honkaniemi, who has had real trouble fitting all the numerous experiments in the schedule, and has had to be flexible many times to work late evenings for this project.

Marko Vehmanen, who has taken care of all the tissue measurements and Merja Tuomas for practical help in the lab.

The Radiochemistry staff: Olli Eskola, Paula Lehtiniemi, Piritta Saipa, and Johanna Rokka, who have produced the radiotracers for the project.

Biostatisticians Elisa Löyttyniemi and Markus Matilainen, who have provided their expertise in their complicated field of science.

My follow-up committee members: Veijo Hukkanen and Markku Koulu, who have been providing their know-how during the meetings. Thank you Veijo for showing personal interest in my project at the Doctoral School meetings and thank you Markku for fascinating meetings and parties during the early years at the DRDP.

Thank you Elnaz Fazeli and Laura Mairinoja from Turku Bioimaging, who have provided their expertise in image analysis and immunohistochemistry quantification.

Colleagues: Anniina Snellman, Kirsi Mikkola, Obada Alzghool, Diana Bocancea, Minna Yli-Karjanmaa, Jatta Helin, Päivi Kotitalo, Mira Eisala, Tove Grönroos, Anna Jalo, Saeka Shimochi, Sini Toppala, Laura Ekblad, and Petri Elo, who have provided their stimulating company during this thesis. A special thanks goes to Eero Rissanen, who has always been willing to help with anything related to clinical neurology or PET imaging.

Friends from the DRDP doctoral school: Noora Lindgren and Henriikka Salomäki with whom we also had an immemorable trip to Glasgow. Minttu Mattila, Helena Virtanen, Maria Grönman, Matias Knuuttila, Mia Ståhle, Riikka Viitanen, and Sanna Hellberg, who have been an enthusiastic group to study with.

Thank you University of Turku Central Animal Facility (UTUCAL) for taking superb care of the animals during the study. And the Histology core facility, Histocore, for processing the immunohistochemical staining for Study III.

I am grateful for the EU 7th Framework Programme INMiND (HEALTH-F2-2011-278850) that provided funding and a place to share my research in extremely rewarding meetings with talented researchers from all around Europe. The companies who have provided materials and knowledge to this project: GE Healthcare and Elan Pharmaceuticals. The private foundations that have supported both my salary and participation in conferences abroad: Turku University Foundation, The Cultural Foundation in Finland, The Swedish Cultural Foundation in Finland, The Finnish Concordia Fund, The European School of Neuroimmunology, The Finnish MS-foundation, The Brain Foundation in Finland, The Medical Radioisotope Society, the Drug Research Foundation, the Emil Niemelä Foundation, and the state funding for university level health research.

I want to acknowledge the DRDP doctoral school: for financial support and immense practical help especially from the coordinator Eeva Valve.

I want to show my gratitude to my dad Arto, who has always been encouraging and supportive with studies from the very first day I started pre-school until this day.

Also, thank you Leena for giving your time and support to our family life so that I've had the chance to finalise my thesis.

Finally, my three PhD-babies, who are not all babies anymore: Benjamin, Eveline, and Alfred. I am so proud to be the mother of such smart and lovely kids. You have enriched my life and shown the importance of concentrating on things with the limited time you have for certain tasks.

Last and most important: I owe my deepest gratitude to my husband Emil, who is my rock in life and has been giving his love and support during whole this time. Not only has he been working as my personal IT-support, but also a listener to all the ups and downs during this project. He has given smart tips and concrete help with anything I've ever needed. He has provided positive thoughts on difficult times with his never-ending optimistic attitude. Laughing helps.

"It is what it is." -*Kimi Rikkönen*

In Parainen, October 2021
Susanne Vainio

Susanne Vainio

MSc in Biomedical Imaging from Åbo Akademi University in 2013

BSc in Biosciences from Åbo Akademi University 2011

Physiotherapist from Turku University of Applied Sciences in 2008

References

Aarts, S. A., Seijkens, T. T., Kusters, P. J., van Tiel, C. M., Reiche, M. E., den Toom, M., Beckers, L., van Roomen, C. P., de Winther, M. P., Kooij, G. & Lutgens, E. (2019) Macrophage CD40 signaling drives experimental autoimmune encephalomyelitis. *J Pathol,* 247(4)**,** 471-480. 10.1002/path.5205.

Absinta, M., Sati, P., Masuzzo, F., Nair, G., Sethi, V., Kolb, H., Ohayon, J., Wu, T., Cortese, I. C. M. & Reich, D. S. (2019) Association of Chronic Active Multiple Sclerosis Lesions With Disability In Vivo. *JAMA Neurology,* 76(12)**,** 1474-1483. 10.1001/jamaneurol.2019.2399.

Airas, L., Dickens, A. M., Elo, P., Marjamäki, P., Johansson, J., Vainio, S., Eskola, O., Jones, P. A., Trigg, W., Solin, O., Haaparanta-Solin, M., Anthony, D. C. & Rinne, J. (2015a) In Vivo PET Imaging Demonstrates Diminished Microglial Activation After Fingolimod Treatment in an Animal Model of Multiple Sclerosis. *J Nucl Med,* 56**,** 305-310.

Airas, L., Rissanen, E. & Rinne, J. O. (2015b) Imaging neuroinflammation in multiple sclerosis using TSPO-PET. *Clin Transl Imaging,* 3**,** 461-473.

Al-Khishman, N. U., Qi, Q., Roseborough, A. D., Levit, A., Allman, B. L., Anazodo, U. C., Fox, M. S., Whitehead, S. N. & Thiessen, J. D. (2020) TSPO PET detects acute neuroinflammation but not diffuse chronically activated MHCII microglia in the rat. *EJNMMI Research,* 10(1)**,** 113. 10.1186/s13550-020-00699-x.

Alam, M. M., Lee, J. & Lee, S.-Y. (2017) Recent Progress in the Development of TSPO PET Ligands for Neuroinflammation Imaging in Neurological Diseases. *Nuclear medicine and molecular imaging,* 51(4)**,** 283-296. 10.1007/s13139-017-0475-8.

Alari-Pahissa, E., Moreira, A., Zabalza, A., Alvarez-Lafuente, R., Munteis, E., Vera, A., Arroyo, R., Alvarez-Cermeño, J. C., Villar, L. M., López-Botet, M. & Martínez-Rodríguez, J. E. (2018) Low cytomegalovirus seroprevalence in early multiple sclerosis: a case for the 'hygiene hypothesis'? *European Journal of Neurology,* 25(7)**,** 925-933. 10.1111/ene.13622.

Alberts, B., Johnson, A., Lewis, J., Raff, M., Roberts, K. & Walter, P. (2008) Molecular Biology of the Cell. In. New York, USA: Garland Science.

Alfredsson, L. & Olsson, T. (2019) Lifestyle and Environmental Factors in Multiple Sclerosis. *Cold Spring Harb Perspect Med,* 9(4). 10.1101/cshperspect.a028944.

Almolda, B., Costa, M., Montoya, M., González, B. & Castellano, B. (2009) CD4 microglial expression correlates with spontaneous clinical improvement in the acute Lewis rat EAE model. *J Neuroimmunol,* 209(1-2)**,** 65-80. 10.1016/j.jneuroim.2009.01.026.

Ambrosius, W., Michalak, S., Kozubski, W. & Kalinowska, A. (2020) Myelin Oligodendrocyte Glycoprotein Antibody-Associated Disease: Current Insights into the Disease Pathophysiology, Diagnosis and Management. *International journal of molecular sciences,* 22(1)**,** 100. 10.3390/ijms22010100.

Anthony, D. C., Dickens, A. M., Seneca, N., Couch, Y., Campbell, S., Checa, B., Kersemans, V., Warren, E. A., Tredwell, M., Sibson, N. R., Gouverneur, V. & Leppert, D. (2014a) Anti-CD20 inhibits T cell-mediated pathology and microgliosis in the rat brain. *Ann Clin Transl Neurol,* 1(9)**,** 659-69. 10.1002/acn3.94.

Anthony, D. C., Miller, K. M., Fearn, S., Townsend, M. J., Opdenakker, G., Wells, G. M. A., Clements, J. M., Chandler, S., Gearing, A. J. H. & Perry, V. H. (1998) Matrix metalloproteinase expression in an experimentally-induced DTH model of multiple sclerosis in the rat CNS. *Journal of Neuroimmunology,* 87(1)**,** 62-72. 10.1016/S0165-5728(98)00046-0.

Anthony, D. C., Sibson, N. R., Losey, P., Meier, D. P. & Leppert, D. (2014b) Investigation of immune and CNS-mediated effects of fingolimod in the focal delayed-type hypersensitivity multiple sclerosis model. *Neuropharmacology,* 79**,** 534-41. 10.1016/j.neuropharm.2013.12.022.

Aspelund, A., Antila, S., Proulx, S. T., Karlsen, T. V., Karaman, S., Detmar, M., Wiig, H. & Alitalo, K. (2015) A dural lymphatic vascular system that drains brain interstitial fluid and macromolecules. *J Exp Med,* 212(7)**,** 991-9. 10.1084/jem.20142290.

AVI (2021) *Laboratory animals: authorisations and enforcement*. Regional State Administrative Agency in Finland. Available at: https://avi.fi/en/services/individuals/licences-notices-and-applications/animals/laboratory-animals.

Babinski, J. A. d. t. (1885) *Étude anatomique et clinique sur la sclérose en plaques / par le Dr J. Babinski.* Paris.

Bailey, O. T., Pappenheimer, A. M., Cheever, F. S. & Daniels, J. B. (1949) A MURINE VIRUS (JHM) CAUSING DISSEMINATED ENCEPHALOMYELITIS WITH EXTENSIVE DESTRUCTION OF MYELIN : II. PATHOLOGY. *The Journal of experimental medicine,* 90(3)**,** 195-212.

Barkhof, F. (2002) The clinico-radiological paradox in multiple sclerosis revisited. *Curr Opin Neurol,* 15(3)**,** 239-245.

Baumgartner, A., Frings, L., Schiller, F., Stich, O., Mix, M., Egger, K., Schluh, G., Rauer, S. & Meyer, P. T. (2018) Regional neuronal activity in patients with relapsing remitting multiple sclerosis. *Acta Neurologica Scandinavica,* 138(6)**,** 466-474. 10.1111/ane.13012.

Beaino, W., Janssen, B., Kooij, G., van der Pol, S. M. A., van Het Hof, B., van Horssen, J., Windhorst, A. D. & de Vries, H. E. (2017) Purinergic receptors P2Y12R and P2X7R: potential targets for PET imaging of microglia phenotypes in multiple sclerosis. *J Neuroinflammation,* 14(1)**,** 259. 10.1186/s12974-017-1034-z.

Behan, P. O. & Chaudhuri, A. (2014) EAE is not a useful model for demyelinating disease. *Mult Scler Relat Disord,* 3(5)**,** 565-74. 10.1016/j.msard.2014.06.003.

Bell, J. S., Spencer, J. I., Yates, R. L., Yee, S. A., Jacobs, B. M. & DeLuca, G. C. (2018) Invited Review: From nose to gut – the role of the microbiome in neurological disease. *Neuropathology and Applied Neurobiology*. 10.1111/nan.12520.

Ben-Nun, A., Kaushansky, N., Kawakami, N., Krishnamoorthy, G., Berer, K., Liblau, R., Hohlfeld, R. & Wekerle, H. (2014) From classic to spontaneous and humanized models of multiple sclerosis: Impact on understanding pathogenesis and drug development. *Journal of autoimmunity,* 54**,** 33-50. 10.1016/j.jaut.2014.06.004.

Berdyyeva, T., Xia, C., Taylor, N., He, Y., Chen, G., Huang, C., Zhang, W., Kolb, H., Letavic, M., Bhattacharya, A. & Szardenings, A. K. (2019) PET Imaging of the P2X7 Ion Channel with a Novel Tracer [18F]JNJ-64413739 in a Rat Model of Neuroinflammation. *Molecular Imaging and Biology,* 21(5)**,** 871-878. 10.1007/s11307-018-01313-2.

Bergström, M. & Långström, B. (2005) Pharmacokinetic studies with PET. *Prog Drug Res,* 62**,** 280-317.

Best, L., Ghadery, C., Pavese, N., Tai, Y. F. & Strafella, A. P. (2019) New and Old TSPO PET Radioligands for Imaging Brain Microglial Activation in Neurodegenerative Disease. *Current Neurology and Neuroscience Reports,* 19(5)**,** 24. 10.1007/s11910-019-0934-y.

Beurdeley-Thomas, A., Miccoli, L., Oudard, S., Dutrillaux, B. & Poupon, M. F. (2000) The peripheral benzodiazepine receptors: a review. *JNO,* 46**,** 45-56.

Billiau, A. & Matthys, P. (2001) Modes of action of Freund's adjuvants in experimental models of autoimmune diseases. *J Leukoc Biol,* 70(6)**,** 849-60.

Bisht, K., Sharma, K., Lacoste, B. & Tremblay, M.-È. (2016) Dark microglia: Why are they dark? *Communicative & integrative biology,* 9(6)**,** e1230575-e1230575. 10.1080/19420889.2016.1230575.

Bjelobaba, I., Begovic-Kupresanin, V., Pekovic, S. & Lavrnja, I. (2018) Animal models of multiple sclerosis: Focus on experimental autoimmune encephalomyelitis. *J Neurosci Res,* 96(6)**,** 1021-1042. 10.1002/jnr.24224.

Bjornevik, K., Cortese, M., Healy Brian, C., Kuhle, J., Mina Michael, J., Leng, Y., Elledge Stephen, J., Niebuhr David, W., Scher Ann, I., Munger Kassandra, L. & Ascherio, A. (2022) Longitudinal analysis reveals high prevalence of Epstein-Barr virus associated with multiple sclerosis. *Science,* 375(6578)**,** 296-301. 10.1126/science.abj8222.

Boddaert, J., Bielen, K., s Jongers, B., Manocha, E., Yperzeele, L., Cras, P., Pirici, D. & Kumar-Singh, S. (2018) CD8 signaling in microglia/macrophage M1 polarization in a rat model of cerebral ischemia. *PLoS One,* 13(1)**,** e0186937. 10.1371/journal.pone.0186937.

Bodini, B., Veronese, M., García-Lorenzo, D., Battaglini, M., Poirion, E., Chardain, A., Freeman, L., Louapre, C., Tchikviladze, M., Papeix, C., Dollé, F., Zalc, B., Lubetzki, C., Bottlaender, M., Turkheimer, F. & Stankoff, B. (2016) Dynamic Imaging of Individual Remyelination Profiles in Multiple Sclerosis. *Annals of Neurology,* 79(5)**,** 726-738. 10.1002/ana.24620.

Boutin, H., Murray, K., Pradillo, J., Maroy, R., Smigova, A., Gerhard, A., Jones, P. A. & Trigg, W. (2015) 18F-GE-180: a novel TSPO radiotracer compared to 11C-R-PK11195 in a preclinical model of stroke. *European Journal of Nuclear Medicine and Molecular Imaging,* 42(3)**,** 503-511. 10.1007/s00259-014-2939-8.

Brackhan, M., Bascunana, P., Postema, J. M., Ross, T. L., Bengel, F. M., Bankstahl, M. & Bankstahl, J. P. (2016) Serial Quantitative TSPO-Targeted PET Reveals Peak Microglial Activation up to 2 Weeks After an Epileptogenic Brain Insult. *J Nucl Med,* 57(8)**,** 1302-8.

Brendel, M., Probst, F., Jaworska, A., Overhoff, F., Korzhova, V., Albert, N. L., Beck, R., Lindner, S., Gildehaus, F. J., Baumann, K., Bartenstein, P., Kleinberger, G., Haass, C., Herms, J. & Rominger, A. (2016) Glial Activation and Glucose Metabolism in a Transgenic Amyloid Mouse Model: A Triple-Tracer PET Study. *J Nucl Med,* 57(6)**,** 954-60. 10.2967/jnumed.115.167858.

Broom, K. A., Anthony, D. C., Blamire, A. M., Waters, S., Styles, P., Perry, V. H. & Sibson, N. R. (2005) MRI reveals that early changes in cerebral blood volume precede blood–brain barrier breakdown and overt pathology in MS-like lesions in rat brain. *J Cereb Blood Flow Metab,* 25**,** 204–216.

Brownlee, W. J., Hardy, T. A., Fazekas, F. & Miller, D. H. (2017) Diagnosis of multiple sclerosis: progress and challenges. *The Lancet,* 389(10076)**,** 1336-1346. https://doi.org/10.1016/S0140-6736(16)30959-X.

Burns, J. C., Cotleur, B., Walther, D. M., Bajrami, B., Rubino, S. J., Wei, R., Franchimont, N., Cotman, S. L., Ransohoff, R. M. & Mingueneau, M. (2020) Differential accumulation of storage bodies with aging defines discrete subsets of microglia in the healthy brain. *Elife,* 9. 10.7554/eLife.57495.

Burrows, D. J., McGown, A., Jain, S. A., De Felice, M., Ramesh, T. M., Sharrack, B. & Majid, A. (2018) Animal models of multiple sclerosis: From rodents to zebrafish. *Multiple Sclerosis Journal,* 25(3)**,** 306-324. 10.1177/1352458518805246.

Calder, P. C., Ahluwalia, N., Albers, R., Bosco, N., Bourdet-Sicard, R., Haller, D., Holgate, S. T., Jonsson, L. S., Latulippe, M. E., Marcos, A., Moreines, J., M'Rini, C., Muller, M., Pawelec, G., van Neerven, R. J., Watzl, B. & Zhao, J. (2013) A consideration of biomarkers to be used for evaluation of inflammation in human nutritional studies. *Br J Nutr,* 109 Suppl 1**,** S1-34. 10.1017/s0007114512005119.

Camsonne, R., Crouzel, C., Comar, D., Mazière, M., Prenant, C., Sastre, J., Moulin, M. A. & Syrota, A. (1984) Synthesis of N-[11C]methyl, N-(methyl-1 propyl), (chloro-2 phenyl)-1 isoquinoline carboxamide-3 (PK11195): a new ligand for peripheral benzodiazepine receptors. *J Labelled Compd. Radiopharm.,* 21**,** 985-991.

Carlstrom, K. E., Ewing, E., Granqvist, M., Gyllenberg, A., Aeinehband, S., Enoksson, S. L., Checa, A., Badam, T. V. S., Huang, J., Gomez-Cabrero, D., Gustafsson, M., Al Nimer, F., Wheelock, C. E., Kockum, I., Olsson, T., Jagodic, M. & Piehl, F. (2019) Therapeutic efficacy of dimethyl fumarate in relapsing-remitting multiple sclerosis associates with ROS pathway in monocytes. *Nat Commun,* 10(1)**,** 3081. 10.1038/s41467-019-11139-3.

Carrithers, M. D. (2014a) Innate immune viral recognition: relevance to CNS infections. *Handb Clin Neurol,* 123**,** 215-23. 10.1016/b978-0-444-53488-0.00009-2.

Carrithers, M. D. (2014b) Update on disease-modifying treatments for multiple sclerosis. *Clin Ther,* 36(12)**,** 1938-1945. 10.1016/j.clinthera.2014.08.006.

Cavalli, E., Mazzon, E., Basile, M. S., Mammana, S., Pennisi, M., Fagone, P., Kalfin, R., Martinovic, V., Ivanovic, J., Andabaka, M., Mesaros, S., Pekmezovic, T., Drulovic, J., Nicoletti, F. & Petralia, M. C. (2020) In Silico and In Vivo Analysis of IL37 in Multiple Sclerosis Reveals Its Probable Homeostatic Role on the Clinical Activity, Disability, and Treatment with Fingolimod. *Molecules,* 25(1). 10.3390/molecules25010020.

Charcot, J.-M. A. d. t. (1875) *Leçons sur les maladies du système nerveux : faites à la Salpêtrière. Tome 1 / par J.-M. Charcot,... ; recueillies et publ. par Bourneville.* Paris.

Chard, D. & Trip, S. A. (2017) Resolving the clinico-radiological paradox in multiple sclerosis. *F1000Research,* 6**,** 1828-1828. 10.12688/f1000research.11932.1.

CharlesRiver (2021) *Lewis rat*. Available at: https://www.criver.com/products-services/find-model/lewis-rat?region=3616 [Accessed 30.8.2021].

Cheng, J. C., Shoghi, K. & Laforest, R. (2012) Quantitative accuracy of MAP reconstruction for dynamic PET imaging in small animals. *Med Phys,* 39(2)**,** 1029-41. 10.1118/1.3678489.

Cheng, T. E., Yoder, K. K., Normandin, M. D., Risacher, S. L., Converse, A. K., Hampel, J. A., Miller, M. A. & Morris, E. D. (2009) A rat head holder for simultaneous scanning of two rats in small animal PET scanners: Design, construction, feasibility testing and kinetic validation. *Journal of Neuroscience Methods,* 176(1)**,** 24-33. https://doi.org/10.1016/j.jneumeth.2008.08.031.

Ching, A. S., Kuhnast, B., Damont, A., Roeda, D., Tavitian, B. & Dollé, F. (2012) Current paradigm of the 18-kDa translocator protein (TSPO) as a molecular target for PET imaging in neuroinflammation and neurodegenerative diseases. *Insights Imaging,* 3(1)**,** 111-9. 10.1007/s13244-011-0128-x.

Chunder, R., Weier, A., Mäurer, H., Luber, N., Enders, M., Luber, G., Heider, T., Spitzer, A., Tacke, S., Becker-Gotot, J., Kurts, C., Iyer, R., Ho Peggy, P., Robinson William, H., Lanz Tobias, V. & Kuerten, S. (2022) Antibody cross-reactivity between casein and myelin-associated glycoprotein results in central nervous system demyelination. *Proceedings of the National Academy of Sciences,* 119(10)**,** e2117034119. 10.1073/pnas.2117034119.

Chung, K. K., Altmann, D., Barkhof, F., Miszkiel, K., Brex, P. A., O'Riordan, J., Ebner, M., Prados, F., Cardoso, M. J., Vercauteren, T., Ourselin, S., Thompson, A., Ciccarelli, O. & Chard, D. T. (2020) A 30-Year Clinical and Magnetic Resonance Imaging Observational Study of Multiple Sclerosis and Clinically Isolated Syndromes. *Annals of Neurology,* 87(1)**,** 63-74. https://doi.org/10.1002/ana.25637.

Coda, A. R., Anzilotti, S., Boscia, F., Greco, A., Panico, M., Gargiulo, S., Gramanzini, M., Zannetti, A., Albanese, S., Pignataro, G., Annunziato, L., Salvatore, M., Brunetti, A., De Berardinis, P., Quarantelli, M., Palma, G. & Pappatà, S. (2021) In vivo imaging of CNS microglial activation/macrophage infiltration with combined [(18)F]DPA-714-PET and SPIO-MRI in a mouse model of relapsing remitting experimental autoimmune encephalomyelitis. *Eur J Nucl Med Mol Imaging,* 48(1)**,** 40-52. 10.1007/s00259-020-04842-7.

Compston, A. & Coles, A. (2008) Multiple Sclerosis. *Lancet,* 372(9648)**,** 1502-1517.

Conti, M. & Eriksson, L. (2016) Physics of pure and non-pure positron emitters for PET: a review and a discussion. *EJNMMI physics,* 3(1)**,** 1-17. 10.1186/s40658-016-0144-5.

Couch, Y., Alvarez-Erviti, L., Sibson, N. R., Wood, M. J. A. & Anthony, D. C. (2011) The inflammatory response to intranigral α-synuclein differs significantly from intranigral lipopolysaccharide and is exacerbated by peripheral inflammation. *J Neuroinflamm,* 8(166)**,** 1-14.

Cross, A. H. & Raine, C. S. (1990) Serial adoptive transfer of murine experimental allergic encephalomyelitis: successful transfer is dependent on active disease in the donor. *Journal of Neuroimmunology,* 28(1)**,** 27-37. https://doi.org/10.1016/0165-5728(90)90038-O.

Daugherty, D. J., Selvaraj, V., Chechneva, O. V., Liu, X.-B., Pleasure, D. E. & Deng, W. (2013) A TSPO ligand is protective in a mouse model of multiple sclerosis. *EMBO Molecular Medicine,* 5(6)**,** 891-903. https://doi.org/10.1002/emmm.201202124.

de Paula Faria, D., Copray, S., Buchpiguel, C., Dierckx, R. & de Vries, E. (2014) PET imaging in multiple sclerosis. *Journal of Neuroimmune Pharmacology,* 9(4)**,** 468-482. 10.1007/s11481-014-9544-2.

De Stefano, N. & Giorgio, A. (2017) Advanced MRI measures like DTI or fMRI should be outcome measures in future clinical trials - Commentary. *Mult Scler,* 23(11)**,** 1458-1460. 10.1177/1352458517717812.

Deeks, E. D. (2016) Dimethyl Fumarate: A Review in Relapsing-Remitting MS. *Drugs,* 76(2)**,** 243-54. 10.1007/s40265-015-0528-1.

Dienes, L. (1929) The Technic of Producing the Tuberculin Type of Sensitization with Eggwhite in Tuberculous Guinea Pigs. *The Journal of Immunology,* 17(6)**,** 531.

Disselhorst, J. A., Boerman, O. C., Oyen, W. J. G., Slump, C. H. & Visser, E. P. (2010) Spatial resolution of the Inveon small-animal PET scanner for the entire field of view. *Nuclear Instruments and Methods in Physics Research Section A: Accelerators, Spectrometers, Detectors and Associated Equipment,* 615(2)**,** 245-248. https://doi.org/10.1016/j.nima.2010.02.073.

Dobson, R. & Giovannoni, G. (2019) Multiple sclerosis - a review. *Eur J Neurol,* 26(1)**,** 27-40. 10.1111/ene.13819.

Dorward, D. A., Lucas, C. D., Rossi, A. G., Haslett, C. & Dhaliwal, K. (2012) Imaging inflammation: Molecular strategies to visualize key components of the inflammatory cascade, from initiation to resolution. *Pharmacol therapeut,* 135**,** 182-199.

Duncan, K. (1998) Radiopharmaceuticals in PET imaging. *J Nucl Med Technol,* 26(4)**,** 228-34; quiz 242.

Díaz, C., Zarco, L. A. & Rivera, D. M. (2019) Highly active multiple sclerosis: An update. *Mult Scler Relat Disord,* 30**,** 215-224. 10.1016/j.msard.2019.01.039.

Ehman, E. C., Johnson, G. B., Villanueva-Meyer, J. E., Cha, S., Leynes, A. P., Larson, P. E. Z. & Hope, T. A. (2017) PET/MRI: Where might it replace PET/CT? *Journal of magnetic resonance imaging : JMRI,* 46(5)**,** 1247-1262. 10.1002/jmri.25711.

EMA (2004) *TYSABRI® (natalizumab)*. European medicines agency. Available at: https://www.accessdata.fda.gov/drugsatfda_docs/label/2004/125104lbl.pdf [Accessed 10.8.2021].

EMA (2018) Reflection paper providing an overview of the current regulatory testing requirements for medicinal products for human use and opportunities for implementation of the 3Rs.

EMA (2021) *Medicines*. Available at: https://www.ema.europa.eu/en/medicines/human [Accessed 9.8.2021].

Endres, C. J., Pomper, M. G., James, M., Uzuner, O., Hammoud, D. A., Watkins, C. C., Reynolds, A., Hilton, J., Dannals, R. F. & Kassiou, M. (2009) Initial Evaluation of 11C-DPA-713, a Novel TSPO PET Ligand, in Humans. *J Nucl Med,* 50**,** 1276-1282.

Engelhardt, B., Vajkoczy, P. & Weller, R. O. (2017) The movers and shapers in immune privilege of the CNS. *Nat Immunol,* 18(2)**,** 123-131. 10.1038/ni.3666.

EU (2010) DIRECTIVE 2010/63/EU OF THE EUROPEAN PARLIAMENT AND OF THE COUNCIL of 22 September 2010 on the protection of animals used for scientific purposes.

EURL-ECVAM (2021) *EU Reference Laboratory for alternatives to animal testing*. EU Science Hub. [Accessed 27.8.2021].

Fan, Z., Calsolaro, V., Atkinson, R. A., Femminella, G. D., Waldman, A., Buckley, C., Trigg, W., Brooks, D. J., Hinz, R. & Edison, P. (2016) Flutriciclamide (18F-GE180) PET: First-in-Human PET Study of Novel Third-Generation In Vivo Marker of Human Translocator Protein. *J Nucl Med,* 57(11)**,** 1753-1759. 10.2967/jnumed.115.169078.

FDA (2020) *HIGHLIGHTS OF PRESCRIBING INFORMATION.* Available at: https://www.accessdata.fda.gov/drugsatfda_docs/label/2020/125104s968s969lbl.pdf.

FDA (2021) *Drugs@FDA: FDA-Approved Drugs*. U.S. Food and Drug Administration. Available at: https://www.accessdata.fda.gov/scripts/cder/daf/index.cfm?event=BasicSearch.process [Accessed 9.8.2021].

Feeney, C., Scott, G., Raffel, J., Roberts, S., Coello, C., Jolly, A., Searle, G., Goldstone, A. P., Brooks, D. J., Nicholas, R. S., Trigg, W., Gunn, R. N. & Sharp, D. J. (2016) Kinetic analysis of the translocator protein positron emission tomography ligand [(18)F]GE-180 in the human brain. *Eur J Nucl Med Mol Imaging,* 43(12)**,** 2201-2210. 10.1007/s00259-016-3444-z.

Ferrieri, R. (2003) Production and application of synthetic precursors labelled with carbon-11 and fluorine-18. In: Welch, M. J. & Redvanly, C. S. (eds.) *Handbook of radiopharmaceuticals, radiochemistry and applications.* Wiley.

Filippi, M., Rocca, M. A., Barkhof, F., Brück, W., Chen, J. T., Comi, G., DeLuca, G., De Stefano, N., Erickson, B. J., Evangelou, N., Fazekas, F., Geurts, J. J. G., Lucchinetti, C., Miller, D. H., Pelletier, D., Popescu, B. F. G. & Lassmann, H. (2012) Association between pathological and MRI findings in multiple sclerosis. *The Lancet Neurology,* 11(4)**,** 349-60.

Filippi, M., Rocca, M. A., Ciccarelli, O., De Stefano, N., Evangelou, N., Kappos, L., Rovira, A., Sastre-Garriga, J., Tintorè, M., Frederiksen, J. L., Gasperini, C., Palace, J., Reich, D. S., Banwell, B., Montalban, X. & Barkhof, F. (2016) MRI criteria for the diagnosis of multiple sclerosis: MAGNIMS consensus guidelines. *The Lancet Neurology,* 15(3)**,** 292-303. https://doi.org/10.1016/S1474-4422(15)00393-2.

Freedman, L. P., Cockburn, I. M. & Simcoe, T. S. (2015) The Economics of Reproducibility in Preclinical Research. *PLoS Biol,* 13(6)**,** e1002165. 10.1371/journal.pbio.1002165.

Freund, J., Stern, E. R. & Pisani, T. M. (1947) Isoallergic encephalomyelitis and radiculitis in guinea pigs after one injection of brain and Mycobacteria in water-in-oil emulsion. *J Immunol,* 57(2)**,** 179-94.

Frischer, J. M., Bramow, S., Dal-Bianco, A., Lucchinetti, C. F., Rauschka, H., Schmidbauer, M., Laursen, H., Sorensen, P. S. & Lassmann, H. (2009) The relation between inflammation and neurodegeneration in multiple sclerosis brains. *Brain (London, England : 1878),* 132(5)**,** 1175-1189. 10.1093/brain/awp070.

Galassi, S., Prosperini, L., Logoteta, A., Hirsch, M. N., Fanelli, F., De Giglio, L. & Pozzilli, C. (2016) A lesion topography-based approach to predict the outcomes of patients with multiple sclerosis treated with Interferon Beta. *Mult Scler Relat Disord,* 8**,** 99-106. 10.1016/j.msard.2016.05.012.

Giacomini, P. S. (2018) Rebound disease in multiple sclerosis. *Multiple sclerosis,* 24(8)**,** 1137-1138. 10.1177/1352458518772913.

Giannetti, P., Politis, M., Su, P., Turkheimer, F. E., Malik, O., Keihaninejad, S., Wu, K., Waldman, A., Reynolds, R., Nicholas, R. & Piccini, P. (2014) Increased PK11195-PET binding in normal-appearing white matter in clinically isolated syndrome.

Giovannoni, G., Popescu, V., Wuerfel, J., Hellwig, K., Iacobeus, E., Jensen, M. B., García-Domínguez, J. M., Sousa, L., De Rossi, N., Hupperts, R., Fenu, G., Bodini, B., Kuusisto, H.-M., Stankoff, B., Lycke, J., Airas, L., Granziera, C. & Scalfari, A. (2022) Smouldering multiple sclerosis: the 'real MS'. *Therapeutic Advances in Neurological Disorders,* 15**,** 17562864211066751. 10.1177/17562864211066751.

Glatigny, S. & Bettelli, E. (2018) Experimental Autoimmune Encephalomyelitis (EAE) as Animal Models of Multiple Sclerosis (MS). *Cold Spring Harb Perspect Med,* 8(11). 10.1101/cshperspect.a028977.

Goldschmidt, C. & McGinley, M. P. (2021) Advances in the Treatment of Multiple Sclerosis. *Neurologic Clinics,* 39(1)**,** 21-33. https://doi.org/10.1016/j.ncl.2020.09.002.

Goverman, J., Woods, A., Larson, L., Weiner, L. P., Hood, L. & Zaller, D. M. (1993) Transgenic mice that express a myelin basic protein-specific T cell receptor develop spontaneous autoimmunity. *Cell,* 72(4)**,** 551-60. 10.1016/0092-8674(93)90074-z.

Guerrero, B. L. & Sicotte, N. L. (2020) Microglia in Multiple Sclerosis: Friend or Foe? *Front Immunol,* 11**,** 374. 10.3389/fimmu.2020.00374.

Gunn, R. N., Lammertsma, A. A., Hume, S. P. & Cunningham, V. J. (1997) Parametric Imaging of Ligand-Receptor Binding in PET Using a Simplified Reference Region Model. *NeuroImage,* 6(4)**,** 279-287. https://doi.org/10.1006/nimg.1997.0303.

Hagens, M. H. J., Golla, S. S. V., Janssen, B., Vugts, D. J., Beaino, W., Windhorst, A. D., O'Brien-Brown, J., Kassiou, M., Schuit, R. C., Schwarte, L. A., de Vries, H. E., Killestein, J., Barkhof, F., van Berckel, B. N. M. & Lammertsma, A. A. (2020) The P2X(7) receptor tracer [(11)C]SMW139 as an in vivo marker of neuroinflammation in multiple sclerosis: a first-in man study. *Eur J Nucl Med Mol Imaging,* 47(2)**,** 379-389. 10.1007/s00259-019-04550-x.

Harbo, H. F., Gold, R. & Tintoré, M. (2013) Sex and gender issues in multiple sclerosis. *Therapeutic advances in neurological disorders,* 6(4)**,** 237-248. 10.1177/1756285613488434.

Harmel, P., Schlunk, F. & Harms, L. (2018) Fulminant rebound of relapsing–remitting multiple sclerosis after discontinuation of dimethyl fumarate: A case report. *Multiple Sclerosis Journal,* 24(8)**,** 1131-1133. 10.1177/1352458517741191.

Haubner, R. & Decristoforo, C. (2011) Radiotracer II: Peptide-Based Radiopharmaceuticals. In: Kiessling, F. & Pichler, B. J. (eds.) *Small Animal Imaging.* Heidelberg, Germany: Springer-Verlag.

Hauser, S. L. & Cree, B. A. C. (2020) Treatment of Multiple Sclerosis: A Review. *Am J Med,* 133(12)**,** 1380-1390.e2. 10.1016/j.amjmed.2020.05.049.

Hendee, W. R. & Morgan, C. J. (1984a) Magnetic resonance imaging. Part I--physical principles. *The Western journal of medicine,* 141(4)**,** 491-500.

Hendee, W. R. & Morgan, C. J. (1984b) Magnetic resonance imaging. Part II--Clinical applications. *West J Med,* 141(5)**,** 638-48.

Hershey, L. A., Gado, M. H. & Trotter, J. L. (1979) Computerized tomography in the diagnostic evaluation of multiple sclerosis. *Annals of Neurology,* 5(1)**,** 32-39. 10.1002/ana.410050106.

Hickman, S. E., Kingery, N. D., Ohsumi, T. K., Borowsky, M. L., Wang, L.-C., Means, T. K. & El Khoury, J. (2013) The microglial sensome revealed by direct RNA sequencing. *Nature neuroscience,* 16(12)**,** 1896-1905. 10.1038/nn.3554.

Hoffman, E. J., Huang, S. C. & Phelps, M. E. (1979) Quantitation in positron emission computed tomography: 1. Effect of object size. *Journal of computer assisted tomography,* 3(3)**,** 299-308. 10.1097/00004728-197906000-00001.

Holm Hansen, R., Højsgaard Chow, H., Christensen, J. R., Sellebjerg, F. & von Essen, M. R. (2020) Dimethyl fumarate therapy reduces memory T cells and the CNS migration potential in patients with multiple sclerosis. *Multiple Sclerosis and Related Disorders,* 37**,** 101451. https://doi.org/10.1016/j.msard.2019.101451.

Horti, A. G., Gao, Y., Ravert, H. T., Finley, P., Valentine, H., Wong, D. F., Endres, C. J., Savonenko, A. V. & Dannals, R. F. (2010) Synthesis and biodistribution of [11C]A-836339, a new potential radioligand for PET imaging of cannabinoid type 2 receptors (CB 2). *Bioorg Medicinal Chem,* 18(14)**,** 5202-5207.

Horti, A. G., Naik, R., Foss, C. A., Minn, I., Misheneva, V., Du, Y., Wang, Y., Mathews, W. B., Wu, Y., Hall, A., LaCourse, C., Ahn, H. H., Nam, H., Lesniak, W. G., Valentine, H., Pletnikova, O., Troncoso, J. C., Smith, M. D., Calabresi, P. A., Savonenko, A. V., Dannals, R. F., Pletnikov, M. V. & Pomper, M. G. (2019) PET imaging of microglia by targeting macrophage colony-stimulating factor 1 receptor (CSF1R). *Proc Natl Acad Sci U S A,* 116(5)**,** 1686-1691. 10.1073/pnas.1812155116.

Hughes, R. N. (2003) The categorisation of male and female laboratory animals in terms of "gender". *Brain Res Bull,* 60(3)**,** 189-90. 10.1016/s0361-9230(03)00037-6.

Hänninen, A. (2017) Infections in MS: An innate immunity perspective. *Acta Neurol Scand,* 136 Suppl 201**,** 10-14. 10.1111/ane.12838.

Höftberger, R., Leisser, M., Bauer, J. & Lassmann, H. (2015) Autoimmune encephalitis in humans: how closely does it reflect multiple sclerosis ? *Acta neuropathologica communications,* 3**,** 80-80. 10.1186/s40478-015-0260-9.

Innis, R. B., Cunningham, V. J., Delforge, J., Fujita, M., Gjedde, A., Gunn, R. N., Holden, J., Houle, S., Huang, S.-C., Ichise, M., Iida, H., Ito, H., Kimura, Y., Koeppe, R. A., Knudsen, G. M., Knuuti, J., Lammertsma, A. A., Laruelle, M., Logan, J., Maguire, R. P., Mintun, M. A., Morris, E. D., Parsey, R., Price, J. C., Slifstein, M., Sossi, V., Suhara, T., Votaw, J. R., Wong, D. F. & Carson, R. E. (2007) Consensus Nomenclature for in vivo Imaging of Reversibly Binding Radioligands. *Journal of Cerebral Blood Flow & Metabolism,* 27(9)**,** 1533-1539. doi:10.1038/sj.jcbfm.9600493.

Jain, P., Chaney, A. M., Carlson, M. L., Jackson, I. M., Rao, A. & James, M. L. (2020) Neuroinflammation PET Imaging: Current Opinion and Future Directions. *Journal of Nuclear Medicine,* 61(8)**,** 1107. 10.2967/jnumed.119.229443.

James, M. L., Belichenko, N. P., Shuhendler, A. J., Hoehne, A., Andrews, L. E., Condon, C., Nguyen, T. V., Reiser, V., Jones, P., Trigg, W., Rao, J., Gambhir, S. S. & Longo, F. M. (2017) [(18)F]GE-180 PET Detects Reduced Microglia Activation After LM11A-31 Therapy in a Mouse Model of Alzheimer's Disease. *Theranostics,* 7(6)**,** 1422-1436. 10.7150/thno.17666.

Jehna, M., Pirpamer, L., Khalil, M., Fuchs, S., Ropele, S., Langkammer, C., Pichler, A., Stulnig, F., Deutschmann, H., Fazekas, F. & Enzinger, C. (2015) Periventricular lesions correlate with cortical thinning in multiple sclerosis. *Annals of Neurology,* 78(4)**,** 530-539. 10.1002/ana.24461.

Jelcic, I., Al Nimer, F., Wang, J., Lentsch, V., Planas, R., Jelcic, I., Madjovski, A., Ruhrmann, S., Faigle, W., Frauenknecht, K., Pinilla, C., Santos, R., Hammer, C., Ortiz, Y., Opitz, L., Grönlund, H., Rogler, G., Boyman, O., Reynolds, R., Lutterotti, A., Khademi, M., Olsson, T., Piehl, F., Sospedra, M. & Martin, R. (2018) Memory B Cells Activate Brain-Homing, Autoreactive CD4(+) T Cells in Multiple Sclerosis. *Cell,* 175(1)**,** 85-100.e23. 10.1016/j.cell.2018.08.011.

Jones, P. A., Chau, W.-F., Fouladi, N., Khan, I., Morrison, M. S., Mantzilas, D. & Trigg, W. (2011). *Comparison of the novel TSPO (18kDa) targeting PET agent [18F]GE-180 with [18F]PBR06 and [11C]-(R)-PK 11195.* Unpublished paper presented at the The World Molecular Imaging Congress. San Diego, California.

Jurga, A. M., Paleczna, M. & Kuter, K. Z. (2020) Overview of General and Discriminating Markers of Differential Microglia Phenotypes. *Frontiers in Cellular Neuroscience,* 14**,** 198.

Kabat, E. A., Wolf, A. & Bezer, A. E. (1947) THE RAPID PRODUCTION OF ACUTE DISSEMINATED ENCEPHALOMYELITIS IN RHESUS MONKEYS BY INJECTION OF HETEROLOGOUS AND HOMOLOGOUS BRAIN TISSUE WITH ADJUVANTS. *J Exp Med,* 85(1)**,** 117-30. 10.1084/jem.85.1.117.

Kabat, E. A., Wolf, A., Bezer, A. E. & Murray, J. P. (1951) Studies on acute disseminated encephalomyelitis produced experimentally in rhesus monkeys. *The Journal of experimental medicine,* 93(6)**,** 615-633. 10.1084/jem.93.6.615.

Kemmerer, C. L., Pernpeintner, V., Ruschil, C., Abdelhak, A., Scholl, M., Ziemann, U., Krumbholz, M., Hemmer, B. & Kowarik, M. C. (2020) Differential effects of disease modifying drugs on peripheral blood B cell subsets: A cross sectional study in multiple sclerosis patients treated with interferon-β, glatiramer acetate, dimethyl fumarate, fingolimod or natalizumab. *PLOS ONE,* 15(7)**,** e0235449. 10.1371/journal.pone.0235449.

Kilkenny, C., Browne, W. J., Cuthill, I. C., Emerson, M. & Altman, D. G. (2012) Improving bioscience research reporting: the ARRIVE guidelines for reporting animal research. *Osteoarthr Cartil,* 20(4)**,** 256-260. http://dx.doi.org/10.1016/j.joca.2012.02.010.

Kipp, M., Clarner, T., Dang, J., Copray, S. & Beyer, C. (2009) The cuprizone animal model: new insights into an old story. *Acta neuropathologica,* 118(6)**,** 723-736. 10.1007/s00401-009-0591-3.

Kipp, M., Nyamoya, S., Hochstrasser, T. & Amor, S. (2017) Multiple sclerosis animal models: a clinical and histopathological perspective. *Brain Pathology,* 27(2)**,** 123-137. https://doi.org/10.1111/bpa.12454.

Kornek, B., Storch, M. K., Weissert, R., Wallstroem, E., Stefferl, A., Olsson, T., Linington, C., Schmidbauer, M. & Lassmann, H. (2000) Multiple sclerosis and chronic autoimmune encephalomyelitis: a comparative quantitative study of axonal injury in active, inactive, and remyelinated lesions. *Am J Pathol,* 157(1)**,** 267-76. 10.1016/s0002-9440(10)64537-3.

Kugler, E. C., Greenwood, J. & MacDonald, R. B. (2021) The "Neuro-Glial-Vascular" Unit: The Role of Glia in Neurovascular Unit Formation and Dysfunction. *Front Cell Dev Biol,* 9**,** 732820. 10.3389/fcell.2021.732820.

Kumar, D. R., Aslinia, F., Yale, S. H. & Mazza, J. J. (2011) Jean-Martin Charcot: The Father of Neurology. *Clin Med Res,* 9**,** 46-49.

Käypä hoito, X. (2020) *MS-tauti*. Available at: https://www.kaypahoito.fi/hoi36070#s8 [Accessed 09.06.2021 2021].

Lamport, A. C., Chedrawe, M., Nichols, M. & Robertson, G. S. (2019) Experimental autoimmune encephalomyelitis accelerates remyelination after lysophosphatidylcholine-induced demyelination in the corpus callosum. *J Neuroimmunol,* 334**,** 576995. 10.1016/j.jneuroim.2019.576995.

Landén, N. X., Li, D. & Ståhle, M. (2016) Transition from inflammation to proliferation: a critical step during wound healing. *Cellular and molecular life sciences : CMLS,* 73(20)**,** 3861-3885. 10.1007/s00018-016-2268-0.

Lassmann, H. (2018) Multiple Sclerosis Pathology. *Cold Spring Harbor perspectives in medicine*, 8(3). [Accessed 2018/03//].

Lassmann, H. (2019) Pathogenic Mechanisms Associated With Different Clinical Courses of Multiple Sclerosis. *Frontiers in Immunology,* 9**,** 3116.

Lassmann, H. & Bradl, M. (2017) Multiple sclerosis: experimental models and reality. *Acta Neuropathologica,* 133(2)**,** 223-244. 10.1007/s00401-016-1631-4.

Le Bihan, D., Mangin, J.-F., Poupon, C., Clark, C. A., Pappata, S., Molko, N. & Chabriat, H. (2001) Diffusion tensor imaging: Concepts and applications. *Journal of magnetic resonance imaging,* 13(4)**,** 534-546. 10.1002/jmri.1076.

Lee, S. K. (2018) Sex as an important biological variable in biomedical research. *BMB reports,* 51(4)**,** 167-173. 10.5483/bmbrep.2018.51.4.034.

Lee, Y., Park, Y., Nam, H., Lee, J.-W. & Yu, S.-W. (2020) Translocator protein (TSPO): the new story of the old protein in neuroinflammation. *BMB reports,* 53(1)**,** 20-27. 10.5483/BMBRep.2020.53.1.273.

Lehto, L. J., Albors, A. A., Sierra, A., Tolppanen, L., Eberly, L. E., Mangia, S., Nurmi, A., Michaeli, S. & Gröhn, O. (2017) Lysophosphatidyl Choline Induced Demyelination in Rat Probed by Relaxation along a Fictitious Field in High Rank Rotating Frame. *Frontiers in neuroscience,* 11**,** 433-433. 10.3389/fnins.2017.00433.

Levine, J. M. & Reynolds, R. (1999) Activation and Proliferation of Endogenous Oligodendrocyte Precursor Cells during Ethidium Bromide-Induced Demyelination. *Experimental Neurology,* 160(2)**,** 333-347. https://doi.org/10.1006/exnr.1999.7224.

Lewellen, T. K. (2008) Recent developments in PET detector technology. *Physics in medicine and biology,* 53(17)**,** R287-R317. 10.1088/0031-9155/53/17/R01.

Li, H., Hu, F., Zhang, Y. & Li, K. (2019) Comparative efficacy and acceptability of disease-modifying therapies in patients with relapsing-remitting multiple sclerosis: a systematic review and network meta-analysis. *J Neurol*. 10.1007/s00415-019-09395-w.

Liu, B., Le, K. X., Park, M. A., Wang, S., Belanger, A. P., Dubey, S., Frost, J. L., Holton, P., Reiser, V., Jones, P. A., Trigg, W., Di Carli, M. F. & Lemere, C. A. (2015) In Vivo Detection of Age- and Disease-Related Increases in Neuroinflammation by 18F-GE180 TSPO MicroPET Imaging in Wild-Type and Alzheimer's Transgenic Mice. *J Neurosci,* 35(47)**,** 15716-30. 10.1523/jneurosci.0996-15.2015.

Lorenzetti, S., Aquilina, G., Caloni, F., Coccia, E. M., Cozzini, P., Cruciani, G., Fouassier, A., Gissi, A., Goracci, L., Heinonen, T., Hubert, P., Madia, F., Nevelli, F., Rainer, A., Rovida, C., Vitale, A. & De Angelis, I. (2020) Non animal methodologies (NAMs): Research, testing, assessment and applications - ecopa Symposium 2019. *Altex,* 37(2)**,** 317-320. 10.14573/altex.2003041.

Louveau, A., Smirnov, I., Keyes, T. J., Eccles, J. D., Rouhani, S. J., Peske, J. D., Derecki, N. C., Castle, D., Mandell, J. W., Lee, K. S., Harris, T. H. & Kipnis, J. (2015) Structural and functional features of central nervous system lymphatic vessels. *Nature,* 523(7560)**,** 337-41. 10.1038/nature14432.

Lubetzki, C. (2018) 150 years since Charcot's lectures on multiple sclerosis. *Lancet Neurol,* 17(12)**,** 1041. 10.1016/s1474-4422(18)30410-1.

Lucchinetti, C. F., Parisi, J. & Bruck, W. (2005) The pathology of multiple sclerosis. *Neurol Clin,* 23(1)**,** 77-105.

Lunde, H. M. B., Assmus, J., Myhr, K.-M., Bø, L. & Grytten, N. (2017) Survival and cause of death in multiple sclerosis: a 60-year longitudinal population study. *Journal of Neurology, Neurosurgery & Psychiatry,* 88(8)**,** 621. 10.1136/jnnp-2016-315238.

Luoto, P., Laitinen, I., Suilamo, S., Någren, K. & Roivainen, A. (2010) Human Dosimetry of Carbon-11 Labeled N-butan-2-yl-1-(2-chlorophenyl)-Nmethylisoquinoline-3-carboxamide Extrapolated from Whole-body Distribution Kinetics and Radiometabolism in Rats. *Mol Imag Biol,* 12**,** 435-442.

Lyman, M., Lloyd, D. G., Ji, X., Vizcaychipi, M. P. & Ma, D. (2014) Neuroinflammation: The role and consequences. *Neuroscience Research,* 79**,** 1-12. https://doi.org/10.1016/j.neures.2013.10.004.

Magyari, M. & Sorensen, P. S. (2019) The changing course of multiple sclerosis: rising incidence, change in geographic distribution, disease course, and prognosis. *Current Opinion in Neurology,* 32(3).

Mammana, S., Bramanti, P., Mazzon, E., Cavalli, E., Basile, M. S., Fagone, P., Petralia, M. C., McCubrey, J. A., Nicoletti, F. & Mangano, K. (2018) Preclinical evaluation of the PI3K/Akt/mTOR pathway in animal models of multiple sclerosis. *Oncotarget,* 9(9)**,** 8263-8277. 10.18632/oncotarget.23862.

Mannheim, J. G., Kara, F., Doorduin, J., Fuchs, K., Reischl, G., Liang, S., Verhoye, M., Gremse, F., Mezzanotte, L. & Huisman, M. C. (2018) Standardization of Small Animal Imaging—Current Status and Future Prospects. *Molecular Imaging and Biology,* 20(5)**,** 716-731. 10.1007/s11307-017-1126-2.

Manni, A., Iaffaldano, A., Lucisano, G., D'Onghia, M., Mezzapesa, D. M., Felica, V., Iaffaldano, P., Trojano, M. & Paolicelli, D. (2019) Lymphocyte Count and Body Mass Index as Biomarkers of Early Treatment Response in a Multiple Sclerosis Dimethyl Fumarate-Treated Cohort. *Frontiers in Immunology,* 10**,** 1343.

Mar, S., Liang, S., Waltz, M., Casper, T. C., Goyal, M., Greenberg, B., Weinstock-Guttman, B., Rodriguez, M., Aaen, G., Belman, A., Barcellos, L. F., Rose, J., Gorman, M., Benson, L., Candee, M., Chitnis, T., Harris, Y., Kahn, I., Roalsted, S., Hart, J., Lotze, T., Moodley, M., Ness, J., Rensel, M., Rubin, J., Schreiner, T., Tillema, J. M., Waldman, A., Krupp, L., Graves, J. S., Waubant, E. & Centers, t. U. S. N. o. P. M. S. (2018) Several household chemical exposures are associated with pediatric-onset multiple sclerosis. *Annals of Clinical and Translational Neurology,* 5(12)**,** 1513-1521. 10.1002/acn3.663.

Massacesi, L., Parigi, A., Barilaro, A., Repice, A. M., Pellicanò, G., Konze, A., Siracusa, G., Taiuti, R. & Amaducci, L. (2005) Efficacy of Azathioprine on Multiple Sclerosis New Brain Lesions Evaluated Using Magnetic Resonance Imaging. *Archives of Neurology,* 62(12)**,** 1843-1847. 10.1001/archneur.62.12.1843.

Matejuk, A. & Ransohoff, R. M. (2020) Crosstalk Between Astrocytes and Microglia: An Overview. *Frontiers in Immunology,* 11**,** 1416.

Matyszak, M. K. & Perry, V. H. (1995) Demyelination in the central nervous system following a delayed-type hypersensitivity response to bacillus Calmette-Guerin. *Neuroscience,* 64(4)**,** 967-77. 030645229400448E.

Matyszak, M. K. & Perry, V. H. (1998) Bacillus Calmette–Guérin sequestered in the brain parenchyma escapes immune recognition. *Journal of neuroimmunology,* 82(1)**,** 73-80. http://dx.doi.org/10.1016/S0165-5728(97)00190-2.

Matyszak, M. K., Townsend, M. J. & Perry, V. H. (1997) Ultrastructural changes of an immune-mediated inflammatory response in the CNS parenchyma directed against a non-CNS antigen. *Neuroscience,* 78(2)**,** 549-560.

McGinley, M. P., Goldschmidt, C. H. & Rae-Grant, A. D. (2021) Diagnosis and Treatment of Multiple Sclerosis: A Review. *JAMA,* 325(8)**,** 765-779. 10.1001/jama.2020.26858.

Mehta, D., Miller, C., Arnold, D. L., Bame, E., Bar-Or, A., Gold, R., Hanna, J., Kappos, L., Liu, S., Matta, A., Phillips, J. T., Robertson, D., von Hehn, C. A., Campbell, J., Spach, K., Yang, L. & Fox, R. J. (2019) Effect of dimethyl fumarate on lymphocytes in RRMS: Implications for clinical practice. *Neurology,* 92(15)**,** e1724-e1738. 10.1212/wnl.0000000000007262.

Merkler, D., Ernsting, T., Kerschensteiner, M., Brück, W. & Stadelmann, C. (2006) A new focal EAE model of cortical demyelination: multiple sclerosis-like lesions with rapid resolution of inflammation and extensive remyelination. *Brain,* 129(Pt 8)**,** 1972-83. 10.1093/brain/awl135.

Mishina, M., Ishiwata, K., Kimura, Y., Naganawa, M., Oda, K., Kobayashi, S., Katayama, Y. & Ishii, K. (2007) Evaluation of distribution of adenosine A2A receptors in normal human brain measured with [11C]TMSX PET. *Synapse,* 61(9)**,** 778-84. 10.1002/syn.20423.

Mitterhauser, M. & Wadsak, W. (2014) Imaging biomarkers or biomarker imaging? *Pharmaceuticals (Basel, Switzerland),* 7(7)**,** 765-778. 10.3390/ph7070765.

MMM (2013) *KOLMIVUOTINEN OHJELMA FICAMILLE VUOSILLE 2014–2016: EU-DIREKTIIVIIN "TIETEELLISIIN TARKOITUKSIIN KÄYTETTÄVIEN ELÄINTEN SUOJELUSTA (2010/63/EU)" LIITTYVÄ MAA- JA METSÄTALOUSMINISTERIÖN OHJELMA*. Ministry of Agriculture and Forestry of Finland. Available at: https://mmm.fi/documents/1410837/1516643/MMM_ohjelma_FICAM_FINAL.PDF/8c46585f-698f-421a-b3fe-35fc29adfa6f/MMM_ohjelma_FICAM_FINAL.pdf/MMM_ohjelma_FICAM_FINAL.pdf [Accessed 27.8.2021].

Montero-Menei, C. N., Sindji, L., Pouplard-Barthelaix, A., Jehan, F., Denechaud, L. & Darcy, F. (1994) Lipopolysaccharide intracerebral administration induces minimal inflammatory reaction in rat brain. *Brain Res,* 653(1–2)**,** 101-111. http://dx.doi.org/10.1016/0006-8993(94)90377-8.

Morgan, I. M. (1947) ALLERGIC ENCEPHALOMYELITIS IN MONKEYS IN RESPONSE TO INJECTION OF NORMAL MONKEY NERVOUS TISSUE. *J Exp Med,* 85(1)**,** 131-40. 10.1084/jem.85.1.131.

Mori, Y., Kondziolka, D., Balzer, J., Fellows, W., Flickinger, J. C., Lunsford, L. D. & Thulborn, K. R. (2000) Effects of Stereotactic Radiosurgery on an Animal Model of Hippocampal Epilepsy. *Neurosurgery,* 46(1)**,** 157-168. 10.1093/neurosurgery/46.1.157.

Moses, W. W. (2011) Fundamental Limits of Spatial Resolution in PET. *Nucl Instrum Methods Phys Res A,* 648 Supplement 1**,** S236-s240. 10.1016/j.nima.2010.11.092.

Mrowietz, U., Morrison, P. J., Suhrkamp, I., Kumanova, M. & Clement, B. (2018) The Pharmacokinetics of Fumaric Acid Esters Reveal Their In Vivo Effects. *Trends in Pharmacological Sciences,* 39(1)**,** 1-12. https://doi.org/10.1016/j.tips.2017.11.002.

Munger, K. L., Zhang, S. M., O'Reilly, E., Hernán, M. A., Olek, M. J., Willett, W. C. & Ascherio, A. (2004) Vitamin D intake and incidence of multiple sclerosis. *Neurology,* 62(1)**,** 60-5. 10.1212/01.wnl.0000101723.79681.38.

Munoz, J. J., Bernard, C. C. & Mackay, I. R. (1984) Elicitation of experimental allergic encephalomyelitis (EAE) in mice with the aid of pertussigen. *Cell Immunol,* 83(1)**,** 92-100. 10.1016/0008-8749(84)90228-4.

Nack, A., Brendel, M., Nedelcu, J., Daerr, M., Nyamoya, S., Beyer, C., Focke, C., Deussing, M., Hoornaert, C., Ponsaerts, P., Schmitz, C., Bartenstein, P., Rominger, A. & Kipp, M. (2019)

Expression of Translocator Protein and [18F]-GE180 Ligand Uptake in Multiple Sclerosis Animal Models. *Cells,* 8(2). 10.3390/cells8020094.

Naegele, M. & Martin, R. (2014) Chapter 3 - The good and the bad of neuroinflammation in multiple sclerosis. In: Goodin, D. S. (ed.) *Handbook of Clinical Neurology.* Elsevier.

Nathoo, N., Yong, V. W. & Dunn, J. F. (2014) Understanding disease processes in multiple sclerosis through magnetic resonance imaging studies in animal models. *NeuroImage: Clinical,* 4**,** 743-756. https://doi.org/10.1016/j.nicl.2014.04.011.

NC3R^{S} (2021) *ARRIVE Guidelines*. National Centre for the Replacement, Refinement & Reduction of Animals in Research. Available at: https://arriveguidelines.org/ [Accessed 25.8.2021].

Negi, N. & Das, B. K. (2018) CNS: Not an immunoprivilaged site anymore but a virtual secondary lymphoid organ. *Int Rev Immunol,* 37(1)**,** 57-68. 10.1080/08830185.2017.1357719.

Neuhaus, O., Kieseier, B. C. & Hartung, H. P. (2007) Immunosuppressive agents in multiple sclerosis. *Neurotherapeutics,* 4(4)**,** 654-60. 10.1016/j.nurt.2007.08.003.

Niccolini, F., Su, P. & Politis, M. (2015) PET in Multiple Sclerosis. *Clinical Nuclear Medicine,* 40(1).

NIH (2021) *ImageJ*. NIH. Available at: https://imagej.nih.gov/ij/docs/menus/analyze.html#cal [Accessed 4.11.2021].

Nimmerjahn, A., Kirchhoff, F. & Helmchen, F. (2005) Resting microglial cells are highly dynamic surveillants of brain parenchyma in vivo. *Science,* 308.

Njenga, M. K., Marques, C. & Rodriguez, M. (2004) The role of cellular immune response in Theiler's virus-induced central nervous system demyelination. *Journal of neuroimmunology,* 147(1)**,** 73-77. 10.1016/j.jneuroim.2003.10.042.

Nutma, E., Stephenson, J. A., Gorter, R. P., de Bruin, J., Boucherie, D. M., Donat, C. K., Breur, M., van der Valk, P., Matthews, P. M., Owen, D. R. & Amor, S. (2019) A quantitative neuropathological assessment of translocator protein expression in multiple sclerosis. *Brain,* 142(11)**,** 3440-3455. 10.1093/brain/awz287.

OECD (2021) *Animal Welfare*. Organisation for Economic Co-operation and Development Available at: https://www.oecd.org/chemicalsafety/testing/animal-welfare.htm.

Oikeutta eläimille (2021) *Eläinkokeet*. Available at: https://oikeuttaelaimille.fi/muu-elainten-kaytto/elainkokeet.

Ory, D., Planas, A., Dresselaers, T., Gsell, W., Postnov, A., Celen, S., Casteels, C., Himmelreich, U., Debyser, Z., Van Laere, K., Verbruggen, A. & Bormans, G. (2015) PET imaging of TSPO in a rat model of local neuroinflammation induced by intracerebral injection of lipopolysaccharide. *Nuclear Medicine and Biology,* 42(10)**,** 753-761. https://doi.org/10.1016/j.nucmedbio.2015.06.010.

Overhoff, F., Brendel, M., Jaworska, A., Korzhova, V., Delker, A., Probst, F., Focke, C., Gildehaus, F.-J., Carlsen, J., Baumann, K., Haass, C., Bartenstein, P., Herms, J. & Rominger, A. (2016) Automated Spatial Brain Normalization and Hindbrain White Matter Reference Tissue Give Improved [(18)F]-Florbetaben PET Quantitation in Alzheimer's Model Mice. *Frontiers in neuroscience,* 10**,** 45-45. 10.3389/fnins.2016.00045.

Owen, D. R., Gunn, R. N., Wadsworth, G., Lewis, A., Rhodes, C., Bennacef, I., Parker, C. A., Matthews, P. M. & Rabiner, E. A. (2012) An 18 kDa translocator protein (TSPO) polymorphism (Ala147Thr) explains variation in PBR28 binding affinity between human subjects. *J Cereb Blood Flow Metab,* 32**,** 1-5.

Pappalardo, F., Russo, G., Pennisi, M., Parasiliti Palumbo, G. A., Sgroi, G., Motta, S. & Maimone, D. (2020) The Potential of Computational Modeling to Predict Disease Course and Treatment Response in Patients with Relapsing Multiple Sclerosis. *Cells,* 9(3)**,** 586. 10.3390/cells9030586.

Pappata, S., Levasseur, M., Gunn, R. N., Myers, R., Crouzel, C., Syrota, A., Jones, T., Kreutzberg, G. W. & Banati, R. B. (2000) Thalamic microglial activation in ischemic stroke detected in vivo by PET and [11C]PK1195. *Neurology,* 55(7)**,** 1052-4. 10.1212/wnl.55.7.1052.

Parravicini, C., Lecca, D., Marangon, D., Coppolino, G. T., Daniele, S., Bonfanti, E., Fumagalli, M., Raveglia, L., Martini, C., Gianazza, E., Trincavelli, M. L., Abbracchio, M. P. & Eberini, I. (2020)

Development of the first in vivo GPR17 ligand through an iterative drug discovery pipeline: A novel disease-modifying strategy for multiple sclerosis. *PloS one,* 15(4)**,** e0231483-e0231483. 10.1371/journal.pone.0231483.

Patel, S. & Gibson, R. (2008) In vivo site directed radiotracers: a mini-review. *Nucl Med Biol,* 35**,** 805-815.

Paxinos, G. & Watson, C. (1986) *The Rat Brain in Stereotaxic Coordinates.* San Diego: Hartcourt Brace Jovanovich.

Pedersen, M. D., Minuzzi, L., Wirenfeldt, M., Meldgaard, M., Slidsborg, C., Cumming, P. & Finsen, B. (2006) Up-regulation of PK11195 binding in areas of axonal degeneration coincides with early microglial activation in mouse brain. *The European journal of neuroscience,* 24(4)**,** 991-1000. 10.1111/j.1460-9568.2006.04975.x.

Percie du Sert, N., Hurst, V., Ahluwalia, A., Alam, S., Avey, M. T., Baker, M., Browne, W. J., Clark, A., Cuthill, I. C., Dirnagl, U., Emerson, M., Garner, P., Holgate, S. T., Howells, D. W., Karp, N. A., Lazic, S. E., Lidster, K., MacCallum, C. J., Macleod, M., Pearl, E. J., Petersen, O. H., Rawle, F., Reynolds, P., Rooney, K., Sena, E. S., Silberberg, S. D., Steckler, T. & Würbel, H. (2020) The ARRIVE guidelines 2.0: Updated guidelines for reporting animal research. *Exp Physiol.* 10.1113/ep088870.

Phelps, M. E., Hoffman, E. J., Mullani, N. A. & Ter-Pogossian, M. M. (1975) Application of annihilation coincidence detection to transaxial reconstruction tomography. *J Nucl Med,* 16(3)**,** 210-24.

Pike, V. W. (2009) PET radiotracers: crossing the blood-brain barrier and surviving metabolism. *Trends Pharmacol Sci,* 30**,** 431-440.

Pirttisalo, A. L., Soilu-Hänninen, M. & Sipilä, J. O. T. (2019) Multiple sclerosis epidemiology in Finland: Regional differences and high incidence. *Acta Neurologica Scandinavica.* 10.1111/ane.13057.

Politis, M., Giannetti, P., Su, P., Turkheimer, F., Keihaninejad, S., Wu, K., Waldman, A., Malik, O., Matthews, P. M., Reynolds, R., Nicholas, R. & Piccini, P. (2012) Increased PK11195 PET binding in the cortex of patients with MS correlates with disability. *Neurology,* 79(6)**,** 523-530. 10.1212/WNL.0b013e3182635645.

Pomeroy, I. M., Matthews, P. M., Frank, J. A., Jordan, E. K. & Esiri, M. M. (2005) Demyelinated neocortical lesions in marmoset autoimmune encephalomyelitis mimic those in multiple sclerosis. *Brain,* 128(11)**,** 2713-2721. 10.1093/brain/awh626.

Portnow, L. H., Vaillancourt, D. E. & Okun, M. S. (2013) The history of cerebral PET scanning: From physiology to cutting-edge technology. *Neurology,* 80(10)**,** 952-956. 10.1212/WNL.0b013e318285c135.

Pozzilli, C., Passafiume, D., Bernardi, S., Pantano, P., Incoccia, C., Bastianello, S., Bozzao, L., Lenzi, G. L. & Fieschi, C. (1991) SPECT, MRI and cognitive functions in multiple sclerosis. *Journal of Neurology, Neurosurgery & Psychiatry,* 54(2)**,** 110. 10.1136/jnnp.54.2.110.

Procaccini, C., De Rosa, V., Pucino, V., Formisano, L. & Matarese, G. (2015) Animal models of Multiple Sclerosis. *European Journal of Pharmacology,* 759**,** 182-191. https://doi.org/10.1016/j.ejphar.2015.03.042.

Prosperini, L. & Pontecorvo, S. (2016) Dimethyl fumarate in the management of multiple sclerosis: appropriate patient selection and special considerations. *Ther Clin Risk Manag,* 12**,** 339-50. 10.2147/tcrm.s85099.

Pöllinger, B., Krishnamoorthy, G., Berer, K., Lassmann, H., Bösl, M. R., Dunn, R., Domingues, H. S., Holz, A., Kurschus, F. C. & Wekerle, H. (2009) Spontaneous relapsing-remitting EAE in the SJL/J mouse: MOG-reactive transgenic T cells recruit endogenous MOG-specific B cells. *J Exp Med,* 206(6)**,** 1303-16. 10.1084/jem.20090299.

Qiao, L., Fisher, E., McMurray, L., Milicevic Sephton, S., Hird, M., Kuzhuppilly-Ramakrishnan, N., Williamson, D. J., Zhou, X., Werry, E., Kassiou, M., Luthra, S., Trigg, W. & Aigbirhio, F. I. (2019) Radiosynthesis of (R,S)-[18F]GE387: A Potential PET Radiotracer for Imaging Translocator

Protein 18 kDa (TSPO) with Low Binding Sensitivity to the Human Gene Polymorphism rs6971. *ChemMedChem,* 14(9)**,** 982-993. https://doi.org/10.1002/cmdc.201900023.

Raffel, J., Wakerley, B. & Nicholas, R. (2016) Multiple sclerosis. *Medicine,* 44(9)**,** 537-541. https://doi.org/10.1016/j.mpmed.2016.06.005.

Ransohoff, R. M. (2016) A polarizing question: do M1 and M2 microglia exist? *Nat Neurosci,* 19(8)**,** 987-91. 10.1038/nn.4338.

Ransohoff, R. M. (2018) Immune-cell crosstalk in multiple sclerosis. *Nature (London),* 563(7730)**,** 194-195. 10.1038/d41586-018-07063-z.

Ratchford, J. N., Endres, C. J., Hammoud, D. A., Pomper, M. G., Shiee, N., McGready, J., Pham, D. L. & Calabresi, P. A. (2012) Decreased microglial activation in MS patients treated with glatiramer acetate. *Journal of neurology,* 259(6)**,** 1199-1205. 10.1007/s00415-011-6337-x.

Reilhac, A., Boisson, F., Wimberley, C., Parmar, A., Zahra, D., Hamze, H., Davis, E., Arthur, A., Bouillot, C., Charil, A. & Grégoire, M. C. (2016) Simultaneous scanning of two mice in a small-animal PET scanner: a simulation-based assessment of the signal degradation. *Phys Med Biol,* 61(3)**,** 1371-88. 10.1088/0031-9155/61/3/1371.

Rissanen, E., Tuisku, J., Rokka, J., Paavilainen, T., Parkkola, R., Rinne, J. O. & Airas, L. (2014) In Vivo Detection of Diffuse Inflammation in Secondary Progressive Multiple Sclerosis Using PET Imaging and the Radioligand 11C-PK11195. *J Nucl Med,* 55(6)**,** 939-44.

Rissanen, E., Virta, J. R., Paavilainen, T., Tuisku, J., Helin, S., Luoto, P., Parkkola, R., Rinne, J. O. & Airas, L. (2013) Adenosine A2A receptors in secondary progressive multiple sclerosis: a [(11)C]TMSX brain PET study. *J Cereb Blood Flow Metab,* 33(9)**,** 1394-401. 10.1038/jcbfm.2013.85.

Ritzel, R. M., Doran, S. J., Glaser, E. P., Meadows, V. E., Faden, A. I., Stoica, B. A. & Loane, D. J. (2019) Old age increases microglial senescence, exacerbates secondary neuroinflammation, and worsens neurological outcomes after acute traumatic brain injury in mice. *Neurobiology of Aging,* 77**,** 194-206. https://doi.org/10.1016/j.neurobiolaging.2019.02.010.

Rivers, T. M. & Schwentker, F. F. (1935) ENCEPHALOMYELITIS ACCOMPANIED BY MYELIN DESTRUCTION EXPERIMENTALLY PRODUCED IN MONKEYS. *J Exp Med,* 61(5)**,** 689-702. 10.1084/jem.61.5.689.

Rivers, T. M., Sprunt, D. H. & Berry, G. P. (1933) OBSERVATIONS ON ATTEMPTS TO PRODUCE ACUTE DISSEMINATED ENCEPHALOMYELITIS IN MONKEYS. *The Journal of experimental medicine,* 58(1)**,** 39-53. 10.1084/jem.58.1.39.

Rocca, M. A. & Filippi, M. (2007) Functional MRI in Multiple Sclerosis. *Journal of Neuroimaging,* 17(s1)**,** 36S-41S. https://doi.org/10.1111/j.1552-6569.2007.00135.x.

Rudin, M. (2009) Noninvasive structural, functional, and molecular imaging in drug development. *Curr Opin Chem Biol,* 13**,** 360-371.

Ruifrok, A. C. & Johnston, D. A. (2001) Quantification of histochemical staining by color deconvolution. *Anal Quant Cytol Histol,* 23(4)**,** 291-9.

Sawada, M., Suzumura, A. & Marunouchi, T. (1992) Down regulation of CD4 expression in cultured microglia by immunosuppressants and lipopolysaccharide. *Biochem Biophys Res Commun,* 189(2)**,** 869-76. 10.1016/0006-291x(92)92284-5.

Schilling, S., Goelz, S., Linker, R., Luehder, F. & Gold, R. (2006) Fumaric acid esters are effective in chronic experimental autoimmune encephalomyelitis and suppress macrophage infiltration. *Clin Exp Immunol,* 145(1)**,** 101-7. 10.1111/j.1365-2249.2006.03094.x.

Schuitemaker, A., van Berckel, B. N. M., Kropholler, M. A., Veltman, D. J., Scheltens, P., Jonker, C., Lammertsma, A. A. & Boellaard, R. (2007) SPM analysis of parametric (R)-[11C]PK11195 binding images: Plasma input versus reference tissue parametric methods. *NeuroImage,* 35(4)**,** 1473-1479. https://doi.org/10.1016/j.neuroimage.2007.02.013.

Sengupta, P. (2013) The Laboratory Rat: Relating Its Age With Human's. *International journal of preventive medicine,* 4(6)**,** 624-630.

Serres, S., Anthony, D. C., Jiabg, Y., Broom, K. A., Campbell, S. J., Tyler, D. J., van Kasteren, S. I., Davis, B. G. & Sibson, N. R. (2009) Systemic Inflammatory Response Reactivates Immune-Mediated Lesions in Rat Brain. *J Neurosci,* 29**,** 4820-4828.

Serres, S., Anthony, D. C., Jiang, Y. Y., Campbell, S. J., Broom, K. A., Khrapitchev, A. & Sibson, N. R. (2009a) Comparison of MRI signatures in pattern I and II multiple sclerosis models. *NMR Biomed,* 22(10)**,** 1014-1024.

Shah, F., Hume, S. P., Pike, V. W., Ashworth, S. & McDermott, J. (1994) Synthesis of the enantiomers of [N-methyl-11C]PK 11195 and comparison of their behaviours as radioligands for PK binding sites in rats. *Nucl Med Biol,* 21(4)**,** 573-81. 10.1016/0969-8051(94)90022-1.

Siemens (2014) Inveon™ Operator Manual - Inveon Scanners and Iveon Acquisition Workplace 2.0. Siemens Medical Solutions USA, Inc.

Silvin, A. & Ginhoux, F. (2018) Microglia heterogeneity along a spatio-temporal axis: More questions than answers. *Glia,* 66(10)**,** 2045-2057. 10.1002/glia.23458.

Sridharan, S. (2016) *Quantitative analysis of positron emission tomography (PET) with the second generation translocator protein (TSPO) ligand [18F]GE-180.* Doctor of Philosophy (PhD) University of Manchester.

Sridharan, S., Lepelletier, F.-X., Trigg, W., Banister, S., Reekie, T., Kassiou, M., Gerhard, A., Hinz, R. & Boutin, H. (2017) Comparative Evaluation of Three TSPO PET Radiotracers in a LPS-Induced Model of Mild Neuroinflammation in Rats. *Mol Imaging Biol,* 19(1)**,** 77-89. 10.1007/s11307-016-0984-3.

Sriram, S. & Steiner, I. (2005) Experimental allergic encephalomyelitis: A misleading model of multiple sclerosis. *Annals of Neurology,* 58(6)**,** 939-945. 10.1002/ana.20743.

Steinman, L. & Zamvil, S. S. (2006) How to successfully apply animal studies in experimental allergic encephalomyelitis to research on multiple sclerosis. *Annals of Neurology,* 60(1)**,** 12-21. 10.1002/ana.20913.

Stephenson, J., Nutma, E., van der Valk, P. & Amor, S. (2018) Inflammation in CNS neurodegenerative diseases. *Immunology,* 154(2)**,** 204-219. 10.1111/imm.12922.

Storch, M. K., Stefferl, A., Brehm, U., Weissert, R., Wallström, E., Kerschensteiner, M., Olsson, T., Linington, C. & Lassmann, H. (1998) Autoimmunity to Myelin Oligodendrocyte Glycoprotein in Rats Mimics the Spectrum of Multiple Sclerosis Pathology. *Brain pathology (Zurich, Switzerland),* 8(4)**,** 681-694. 10.1111/j.1750-3639.1998.tb00194.x.

Summers, B. A., Greisen, H. A. & Appel, M. J. G. (1984) Canine distemper and experimental allergic encephalomyelitis in the dog: Comparative patterns of demyelination. *Journal of Comparative Pathology,* 94(4)**,** 575-589. https://doi.org/10.1016/0021-9975(84)90062-8.

Sánchez-Crespo, A., Andreo, P. & Larsson, S. A. (2004) Positron flight in human tissues and its influence on PET image spatial resolution. *Eur J Nucl Med Mol Imaging,* 31**,** 44-51.

Takata, K., Kato, H., Shimosegawa, E., Okuno, T., Koda, T., Sugimoto, T., Mochizuki, H., Hatazawa, J. & Nakatsuji, Y. (2014) 11C-acetate PET imaging in patients with multiple sclerosis. *PLoS One,* 9(11)**,** e111598. 10.1371/journal.pone.0111598.

Ter-Pogossian, M. M., Phelps, M. E., Hoffman, E. J. & Mullani, N. A. (1975) A positron-emission transaxial tomograph for nuclear imaging (PETT). *Radiology,* 114(1)**,** 89-98. 10.1148/114.1.89.

Tetard, M.-C., Vermandel, M., Leroy, H.-A., Leroux, B., Maurage, C.-A., Lejeune, J.-P., Mordon, S. & Reyns, N. (2016) Interstitial 5-ALA photodynamic therapy and glioblastoma: Preclinical model development and preliminary results. *Photodiagnosis and Photodynamic Therapy,* 13**,** 218-224. https://doi.org/10.1016/j.pdpdt.2015.07.169.

Teuho, J., Riehakainen, L., Honkaniemi, A., Moisio, O., Han, C., Tirri, M., Liu, S., Grönroos, T. J., Liu, J., Wan, L., Liang, X., Ling, Y., Hua, Y., Roivainen, A., Knuuti, J., Xie, Q., Teräs, M., D'Ascenzo, N. & Klén, R. (2020) Evaluation of image quality with four positron emitters and three preclinical PET/CT systems. *EJNMMI Research,* 10(1)**,** 155. 10.1186/s13550-020-00724-z.

Thompson, A. J., Banwell, B. L., Barkhof, F., Carroll, W. M., Coetzee, T., Comi, G., Correale, J., Fazekas, F., Filippi, M., Freedman, M. S., Fujihara, K., Galetta, S. L., Hartung, H. P., Kappos, L.,

Lublin, F. D., Marrie, R. A., Miller, A. E., Miller, D. H., Montalban, X., Mowry, E. M., Sorensen, P. S., Tintoré, M., Traboulsee, A. L., Trojano, M., Uitdehaag, B. M. J., Vukusic, S., Waubant, E., Weinshenker, B. G., Reingold, S. C. & Cohen, J. A. (2018a) Diagnosis of multiple sclerosis: 2017 revisions of the McDonald criteria. *Lancet Neurol,* 17(2)**,** 162-173. 10.1016/S1474-4422(17)30470-2.

Thompson, A. J., Baranzini, S. E., Geurts, J., Hemmer, B. & Ciccarelli, O. (2018b) Multiple sclerosis. *Lancet,* 391(10130)**,** 1622-1636. 10.1016/s0140-6736(18)30481-1.

Tompkins, S. M., Padilla, J., Dal Canto, M. C., Ting, J. P. Y., Van Kaer, L. & Miller, S. D. (2002) De Novo Central Nervous System Processing of Myelin Antigen Is Required for the Initiation of Experimental Autoimmune Encephalomyelitis. *The Journal of immunology (1950),* 168(8)**,** 4173-4183. 10.4049/jimmunol.168.8.4173.

Trapp, B. D. & Nave, K.-A. (2008) Multiple Sclerosis : An Immune or Neurodegenerative Disorder? *Annual review of neuroscience,* 31(1)**,** 247-269. 10.1146/annurev.neuro.30.051606.094313.

Tremblay, M.-È. (2021) Microglial functional alteration and increased diversity in the challenged brain: Insights into novel targets for intervention. *Brain, behavior, & immunity - health,* 16**,** 100301-100301. 10.1016/j.bbih.2021.100301.

Unterrainer, M., Mahler, C., Vomacka, L., Lindner, S., Havla, J., Brendel, M., Böning, G., Ertl-Wagner, B., Kümpfel, T., Milenkovic, V. M., Rupprecht, R., Kerschensteiner, M., Bartenstein, P. & Albert, N. L. (2018) TSPO PET with [(18)F]GE-180 sensitively detects focal neuroinflammation in patients with relapsing-remitting multiple sclerosis. *Eur J Nucl Med Mol Imaging,* 45(8)**,** 1423-1431. 10.1007/s00259-018-3974-7.

Valencia-Sanchez, C. & Carter, J. L. (2020) An evaluation of dimethyl fumarate for the treatment of relapsing remitting multiple sclerosis. *Expert Opin Pharmacother,* 21(12)**,** 1399-1405. 10.1080/14656566.2020.1763304.

van der Weijden, C. W. J., Meilof, J. F. & de Vries, E. F. J. (2021) PET Imaging in Multiple Sclerosis. In: Dierckx, R. A. J. O., Otte, A., de Vries, E. F. J., van Waarde, A. & Leenders, K. L. (eds.) *PET and SPECT in Neurology.* Cham: Springer International Publishing.

Varadkar, S., Bien, C. G., Kruse, C. A., Jensen, F. E., Bauer, J., Pardo, C. A., Vincent, A., Mathern, G. W. & Cross, J. H. (2014) Rasmussen's encephalitis: clinical features, pathobiology, and treatment advances. *The Lancet. Neurology,* 13(2)**,** 195-205. 10.1016/S1474-4422(13)70260-6.

Varrone, A., Oikonen, V., Forsberg, A., Joutsa, J., Takano, A., Solin, O., Haaparanta-Solin, M., Nag, S., Nakao, R., Al-Tawil, N., Wells, L. A., Rabiner, E. A., Valencia, R., Schultze-Mosgau, M., Thiele, A., Vollmer, S., Dyrks, T., Lehmann, L., Heinrich, T., Hoffmann, A., Nordberg, A., Halldin, C. & Rinne, J. O. (2015) Positron emission tomography imaging of the 18-kDa translocator protein (TSPO) with [18F]FEMPA in Alzheimer's disease patients and control subjects. *European Journal of Nuclear Medicine and Molecular Imaging,* 42(3)**,** 438-446. 10.1007/s00259-014-2955-8.

Vicidomini, C., Panico, M., Greco, A., Gargiulo, S., Coda, A. R., Zannetti, A., Gramanzini, M., Roviello, G. N., Quarantelli, M., Alfano, B., Tavitian, B., Dollé, F., Salvatore, M., Brunetti, A. & Pappatà, S. (2015) In vivo imaging and characterization of [(18)F]DPA-714, a potential new TSPO ligand, in mouse brain and peripheral tissues using small-animal PET. *Nucl Med Biol,* 42(3)**,** 309-16. 10.1016/j.nucmedbio.2014.11.009.

Villa, A., Klein, B., Janssen, B., Pedragosa, J., Pepe, G., Zinnhardt, B., Vugts, D. J., Gelosa, P., Sironi, L., Beaino, W., Damont, A., Dollé, F., Jego, B., Winkeler, A., Ory, D., Solin, O., Vercouillie, J., Funke, U., Laner-Plamberger, S., Blomster, L. V., Christophersen, P., Vegeto, E., Aigner, L., Jacobs, A., Planas, A. M., Maggi, A. & Windhorst, A. D. (2018) Identification of new molecular targets for PET imaging of the microglial anti-inflammatory activation state. *Theranostics,* 8(19)**,** 5400-5418. 10.7150/thno.25572.

Visser, E. P., Disselhorst, J. A., Brom, M., Laverman, P., Gotthardt, M., Oyen, W. J. G. & Boerman, O. C. (2009) Spatial Resolution and Sensitivity of the Inveon Small-Animal PET Scanner. *Journal of Nuclear Medicine,* 50(1)**,** 139. 10.2967/jnumed.108.055152.

Visser, L. A., Louapre, C., Uyl-de Groot, C. A. & Redekop, W. K. (2020) Patient needs and preferences in relapsing-remitting multiple sclerosis: A systematic review. *Multiple Sclerosis and Related Disorders,* 39**,** 101929. https://doi.org/10.1016/j.msard.2020.101929.

Wadsworth, H., Jones, P. A., Chau, W.-F., Durrant, C., Fouladi, N., Passmore, J., O'Shea, D., Wynn, D., Morisson-Iveson, V., Ewan, A., Thaning, M., Mantzilas, D., Gausemel, I., Khan, I., Black, A., Avory, M. & Trigg, W. (2012) [18F]GE-180: A novel fluorine-18 labelled PET tracer for imaging Translocator protein 18 kDa (TSPO). *Bioorg Medicinal Chem,* 22(3)**,** 1308-1313. http://dx.doi.org/10.1016/j.bmcl.2011.12.084.

Werry, E. L., Bright, F. M., Piguet, O., Ittner, L. M., Halliday, G. M., Hodges, J. R., Kiernan, M. C., Loy, C. T., Kril, J. J. & Kassiou, M. (2019) Recent Developments in TSPO PET Imaging as A Biomarker of Neuroinflammation in Neurodegenerative Disorders. *International journal of molecular sciences,* 20(13)**,** 3161. 10.3390/ijms20133161.

Westerlind, H., Boström, I., Stawiarz, L., Landtblom, A.-M., Almqvist, C. & Hillert, J. (2014) New data identify an increasing sex ratio of multiple sclerosis in Sweden. *Multiple sclerosis (Houndmills, Basingstoke, England),* 20(12)**,** 1578-1583. 10.1177/1352458514530021.

White, R. G. (1967) ROLE OF ADJUVANTS IN THE PRODUCTION OF DELAYED HYPERSENSITIVITY. *British Medical Bulletin,* 23(1)**,** 39-45. 10.1093/oxfordjournals.bmb.a070514.

Wickstrøm, T., Clarke, A., Gausemel, I., Horn, E., Jørgensen, K., Khan, I., Mantzilas, D., Rajanayagam, T., In 't Veld, D.-J. & Trigg, W. (2014) The development of an automated and GMP compliant FASTlab™ Synthesis of 18-F-GE-180; a radiotracer for imaging translocator protein (TSPO). *J Label Compd Radiopharm,* 57(1)**,** 42-48.

Wu, M. & Shu, J. (2018) Multimodal Molecular Imaging: Current Status and Future Directions. *Contrast media & molecular imaging,* 2018**,** 1382183-1382183. 10.1155/2018/1382183.

Xi, W., Tian, M. & Zhang, H. (2011) Molecular imaging in neuroscience research with small-animal PET in rodents. *Neurosci Res,* 70(2)**,** 133-143. 10.1016/j.neures.2010.12.017.

Xie, L., Yamasaki, T., Ichimaru, N., Yui, J., Kawamura, K., Kumata, K., Hatori, A., Nonomura, N., Zhang, M.-R., Li, X.-K. & Takahara, S. (2012) [11C]DAC-PET for Noninvasively Monitoring Neuroinflammation and Immunosuppressive Therapy Efficacy in Rat Experimental Autoimmune Encephalomyelitis Model. *Journal of Neuroimmune Pharmacology,* 7(1)**,** 231-242. 10.1007/s11481-011-9322-3.

Xu, J., Wang, T., Wu, Y., Jin, W. & Wen, Z. (2016) Microglia Colonization of Developing Zebrafish Midbrain Is Promoted by Apoptotic Neuron and Lysophosphatidylcholine. *Developmental Cell,* 38(2)**,** 214-222. https://doi.org/10.1016/j.devcel.2016.06.018.

Yadav, S. K., Soin, D., Ito, K. & Dhib-Jalbut, S. (2019) Insight into the mechanism of action of dimethyl fumarate in multiple sclerosis. *Journal of Molecular Medicine,* 97(4)**,** 463-472. 10.1007/s00109-019-01761-5.

Yamasaki, R., Lu, H., Butovsky, O., Ohno, N., Rietsch, A. M., Cialic, R., Wu, P. M., Doykan, C. E., Lin, J., Cotleur, A. C., Kidd, G., Zorlu, M. M., Sun, N., Hu, W., Liu, L., Lee, J. C., Taylor, S. E., Uehlein, L., Dixon, D., Gu, J., Floruta, C. M., Zhu, M., Charo, I. F., Weiner, H. L. & Ransohoff, R. M. (2014) Differential roles of microglia and monocytes in the inflamed central nervous system. *J Exp Med,* 211(8)**,** 1533-49. 10.1084/jem.20132477.

Yang, Q. q. & Zhou, J. w. (2018) Neuroinflammation in the central nervous system: Symphony of glial cells. *Glia*. 10.1002/glia.23571.

Yednock, T. A., Cannon, C., Fritz, L. C., Sanchez-Madrid, F., Steinman, L. & Karin, N. (1992) Prevention of experimental autoimmune encephalomyelitis by antibodies against [alpha]4[beta]l integrin. *Nature,* 356(6364)**,** 63-66.

Zanotti-Fregonara, P., Pascual, B., Rizzo, G., Yu, M., Pal, N., Beers, D., Carter, R., Appel, S. H., Atassi, N. & Masdeu, J. C. (2018) Head-to-Head Comparison of (11)C-PBR28 and (18)F-GE180 for Quantification of the Translocator Protein in the Human Brain. *J Nucl Med,* 59(8)**,** 1260-1266. 10.2967/jnumed.117.203109.

Zanotti-Fregonara, P., Pascual, B., Rostomily, R. C., Rizzo, G., Veronese, M., Masdeu, J. C. & Turkheimer, F. (2020) Anatomy of 18F-GE180, a failed radioligand for the TSPO protein. *European Journal of Nuclear Medicine and Molecular Imaging,* 47(10)**,** 2233-2236. 10.1007/s00259-020-04732-y.

Zhang, L., Hu, K., Shao, T., Hou, L., Zhang, S., Ye, W., Josephson, L., Meyer, J. H., Zhang, M.-R., Vasdev, N., Wang, J., Xu, H., Wang, L. & Liang, S. H. (2021) Recent developments on PET radiotracers for TSPO and their applications in neuroimaging. *Acta Pharmaceutica Sinica B,* 11(2)**,** 373-393. https://doi.org/10.1016/j.apsb.2020.08.006.

Zhang, Y., Chen, K., Sloan, S. A., Bennett, M. L., Scholze, A. R., O'Keeffe, S., Phatnani, H. P., Guarnieri, P., Caneda, C., Ruderisch, N., Deng, S., Liddelow, S. A., Zhang, C., Daneman, R., Maniatis, T., Barres, B. A. & Wu, J. Q. (2014) An RNA-sequencing transcriptome and splicing database of glia, neurons, and vascular cells of the cerebral cortex. *The Journal of neuroscience,* 34(36)**,** 11929-11947. 10.1523/JNEUROSCI.1860-14.2014.

Ziegler, S. I. (2011) PET and SPECT. In: Kiessling, F. & Pichler, B. J. (eds.) *Small Animal Imaging.* Heidelberg, Germany: Springer-Verlag.

TURUN
YLIOPISTO
UNIVERSITY
OF TURKU

Painosalama, Turku, Finland 2022

ISBN 978-951-29-8799-3 (PRINT)
ISBN 978-951-29-8800-6 (PDF)
ISSN 0355-9483 (Print)
ISSN 2343-3213 (Online)